SRR-CWDA-2021-00034
Revision 0

Chemical and Physical Evolution of Tank Closure Cementitious Materials

April 2021

Prepared by: Savannah River Remediation LLC
Waste Disposal Authority
Aiken, SC 29808

Prepared for U.S. Department of Energy Under Contract No. DE-AC09-09SR22505

APPROVALS

Author:

GREGORY FLACH (Affiliate) Digitally signed by GREGORY FLACH (Affiliate) Date: 2021.04.26 10:39:20 -04'00'

Greg Flach — Date
WDA Closure & Disposal Assessment
Savannah River Remediation, LLC

Technical Review per S4-ENG.51:

Steven Hommel Digitally signed by Steven Hommel Date: 2021.04.26 10:46:40 -04'00'

Steve Hommel — Date
WDA Closure & Disposal Assessment
Savannah River Remediation, LLC

Technical Review per S4-ENG.51:

r2465 Digitally signed by r2465 Date: 2021.04.26 18:48:14 -04'00'

David Watkins — Date
WDA Closure & Disposal Assessment
Savannah River Remediation, LLC

Management Review:

KENT ROSENBERGER (Affiliate) Digitally signed by KENT ROSENBERGER (Affiliate) Date: 2021.04.26 12:28:04 -04'00'

Kent Rosenberger — Date
WDA Closure & Disposal Assessment, Manager
Savannah River Remediation, LLC

TABLE OF CONTENTS

LIST OF FIGURES

LIST OF TABLES

ACKNOWLEDGEMENT

Dr. Miles Denham (Inspection Experts Inc.) provided invaluable consulting advice on geochemistry and using *The Geochemist's Workbench* software that is acknowledged and appreciated.

ACRONYMS/ABBREVIATIONS

atm	Atmosphere
C-A-S-H	Calcium-Aluminum-Silicate-Hydrate
C-S-H	Calcium-Silicate-Hydrate
CLSM	Controlled Low Strength Material
DB	Database
DIC	Dissolved Inorganic Carbon
ET	Evapotranspiration
FTF	F-Area Tank Farm
GWB	The Geochemist's Workbench®
HTF	H-Area Tank Farm
IBM	International Business Machines
K_d	Solid-Solute Distribution Coefficient
LMA	Law of Mass Action
LWO	Liquid Waste Organization
mil	0.001 inches
NBFS	No Blast Furnace Slag
NEA	Nuclear Energy Agency
PA	Performance Assessment
ppm	Parts Per Million
PV	Pore Volume
QA	Quality Assurance
SREL	Savannah River Ecology Laboratory
SRNL	Savannah River National Laboratory
SRR	Savannah River Remediation LLC
SRS	Savannah River Site
TFG	Tank Fill Grout
WT	Water Table
XRD	X-Ray Diffraction

1.0 INTRODUCTION

Liquid waste storage structures at the Savannah River Site (SRS) incorporate concrete barriers that enclose steel tanks containing radioactive and chemical waste, and operational closure of these structures includes filling void space within and surrounding the emptied steel tanks with grout. The long-term performance of concrete and grout is an important consideration for Performance Assessment (PA) of closed tanks in F-Area Tank Farm (FTF) and H-Area Tank Farm (HTF). Over PA timeframes of hundreds, thousands, to tens of thousands of years, the chemical and physical properties of these cementitious materials will slowly evolve due to environmental exposure and material aging. Evolving chemical properties of concrete and grout will affect solid-solute distribution coefficients (K_d), solubility controls, steel corrosion rates, and physical degradation within containment barriers and adjoining materials. Evolving physical properties of cementitious materials, such as permeability and effective diffusion coefficient, will influence advective and diffusive transport, which may in turn affect chemical evolution through feedback mechanisms.

The current FTF and HTF PAs (SRS-REG-2007-00002, SRR-CWDA-2010-00128) are based on multiple studies that consider the chemical and/or physical degradation of cementitious materials, either directly or indirectly: SRNL-STI-2012-00404, WSRC-STI-2007-00607, SRNL-STI-2010-00035, WSRC-STI-2007-00061, and SRNL-STI-2010-00047. The current study updates relevant portions of these previous works and is designed to support an imminent revision to the HTF PA and a future update to the FTF PA. The current work draws upon the cited studies, SRNL-STI-2018-00077 developed for the Saltstone Disposal Facility PA, new methods and data, and the recommendations of Denham (2020).

Much of the chemical evolution analysis is performed with equilibrium chemistry simulation software, namely The Geochemist's Workbench® (GWB) and PHREEQC. Custom thermodynamic databases formatted for these codes are developed from SRNL-STI-2012-00404, CEMDATA18.1 (Lothenbach et al. 2019), and ThermoChimie (Giffaut et al. 2014). Initial simulations define the equilibrium chemical state of SRS rainwater, soil moisture, groundwater, and hydrated grouts and concrete. Subsequent simulations predict the chemical evolution of the initially cured cementitious materials when subjected to long-term 1) successive pore volume flushes (advective transport) and 2) leaching to adjoining soil/sediment (diffusive transport). The principal results are pH and Eh variations in cement pore solutions as a function of pore volumes (advection) or time (diffusion).

The physical evolution analysis is based on simplified conceptual models (abstractions) that facilitate analytic mathematical solutions. A feedback mechanism is provided whereby physical damage to concrete predicted by reactive transport in turn affects species transport rates. Results for penetration depth in concrete as a function of time are generated for 1) carbonation and physical damage fronts, 2) decalcification and damage fronts, and 3) combined carbonation + decalcification and damage fronts. Methods for estimating 1) oxygen flux and cumulative mass transported, and 2) chloride concentration are developed for potential use in separate corrosion studies. Grout degradation via advective decalcification is also predicted.

Methods, input values, and assumptions in this study generally represent a varying blend of best-estimate and pessimistic settings. Selected sensitivity cases are provided in the chemical evolution analysis to provide a sense of model biases and uncertainties. For physical evolution, three cases

representing varying conservatism are considered: Realistic, Compliance, and Pessimistic. The Realistic Case assumes an evolution and input values that best reflect expected conditions based on current understanding of cementitious materials. In general, input values for the Realistic Case represent mean or median values. The Compliance Case reflects an intermediate case that is more defensible than the Realistic Case but not as conservative as the Pessimistic Case. In general, key input values and assumptions for the Compliance Case are modestly conservative. Finally, the Pessimistic Case is designed to approach bounding conditions and thus strongly biased towards faster degradation rates. In general, input values and assumptions for the Pessimistic Case are selected to be bounding or highly defensible.

2.0 EQUILIBRIUM CHEMISTRY SIMULATION SOFTWARE

The "software" used to generate equilibrium chemistry results in this report refers to the set of

1) a simulation code (GWB or PHREEQC),
2) a cement mineral set, and
3) a thermodynamic database.

Quality Assurance (QA) for software used in engineering calculations may be achieved through (E7, 2.31A):

1) "Pre-Verification" following Manual 1Q, Procedure 20-1, *Software Quality Assurance* and Manual E7, Procedure 5.01, *Software Engineering and Control*, or
2) "Verification at Each Use" following Manual E7, Procedure 2.31A, *LW Engineering Calculations*, Section 5.5.2.

The second option is chosen for this study. Specifically, independent results are typically generated for each analysis case by performing the simulation with both GWB and PHREEQC. Results are accepted if the two independent software simulations produce equivalent outcomes.

2.1 Simulation Codes

The Geochemist's Workbench (GWB 2021, https://www.gwb.com/) and PHREEQC (version 3.6.2, https://www.usgs.gov/software/phreeqc-version-3) are used to independently simulate equilibrium chemistry states, advective reactive transport (reaction paths), and diffusive reactive transport. Although the two codes have similar capabilities in relation to the needs of this study, GWB 2021 is generally chosen as the lead simulator with PHREEQC serving the verification role from a QA perspective. This decision is motivated by a desire to maintain continuity with previously utilized analyses documented in SRNL-STI-2012-00404 and to take advantage of more aesthetically pleasing graphics built into the GWB graphical user interface. However, PHREEQC is the primary software used for diffusive transport because GWB exhibited numerical problems with this class of simulations.

2.2 Mineral Set

Table 2.2-1 compares the mineral set selected for the current study to the SRNL-STI-2012-00404 model and Savannah River Ecology Laboratory (SREL) observations for candidate tank-fill grouts reported in SREL Doc. R-21-0001 (Tables 14 through 16). X-Ray Diffraction (XRD) Rietveld Refinement is an experimental technique for quantifying the kind and mass of crystalline solids present in a sample material. The current mineral set is a perturbation of SRNL-STI-2012-00404 based on the following rationale:

1) The CEMDATA18.1 thermodynamic database (Lothenbach et al. 2019, https://www.empa.ch/web/s308/thermodynamic-data) is judged to be the best consolidated information available for cement-based systems and generally used to update the mineral set (and equilibrium constants, next section) representing cementitious materials. In a few instances, information from the ThermoChimie version 10a database (Giffaut et al. 2014, https://www.thermochimie-tdb.com/) is also used.

2) SRNL-STI-2012-00404 used a solid solution model based on Lothenbach and Winnefeld (2006) and Kulik (2011) to represent $C\text{-}S\text{-}H$ (calcium-silicate-hydrate) gel. This model was updated to the CSHQ (Quaternary solid solution model for C-S-H of tobermorite–jennite-like structure) model in CEMDATA18.1 by revising the stoichiometry of TobH (and revising its equilibrium constant). TobH refers to the "Tobermorite-like endmember with H+ (without Ca2+) in the interlayer", Kulik (2011).

3) The grouts of interest contain significant amounts of fly ash and/or ground blast furnace slag, which lowers the Ca/Si ratio in $C\text{-}S\text{-}H$ gel. While the CSHQ model is well adapted for Portland cement (high Ca/Si) systems, for blended cements / alkali activated systems which have lower Ca/Si ratios, Lothenbach et al. (2019) recommend the CNASH solid solution model, which considers the uptake of aluminum and sodium in low Ca/Si $C\text{-}S\text{-}H$. Thus, the five non-sodium bearing components of the CNASH model were added to the mineral set, and these minerals collectively supersede the original CSHQ model. In addition to $C\text{-}S\text{-}H$ minerals, the CNASH solid solution model includes $C\text{-}A\text{-}S\text{-}H$ (calcium-aluminum-silicate-hydrate) minerals: INFCA_CNASHss and 5CA_CNASHss (defined in Section 2.3). Portland cement concrete initially has a high Ca/Si ratio and the CSHQ model would be preferred for near-term simulations. However, as concrete ages over PA timeframes it will develop a low Ca/Si ratio and be better simulated with the CNASH model. Thus, the latter is suitable for both cementitious materials in the context of this study.

4) Gibbsite is replaced by microcrystalline $Al(OH)_3$, a polymorph, based on Lothenbach et al. (2019) who state the latter forms at ambient temperatures, outside of very short timeframes (minutes to hour) when amorphous $Al(OH)_3$ might initially be observed. However, if curing temperatures exceed 60°C, Gibbsite will likely form instead of microcrystalline $Al(OH)_3$ (Lothenbach et al. 2019) and be the preferred polymorph in that case. Similarly, amorphous $Fe(OH)_3$ is replaced with the more crystalline ferrihydrite, consistent with selection of microcrystalline $Al(OH)_3$ rather its amorphous polymorph. Selection of microcrystalline polymorphs is a middle-ground between amorphous phases likely to form in the near-term versus more ordered/stable crystalline phases likely to develop over the long-term.

5) Hemicarboaluminate was added to the current mineral set based on 4.1 wt% being observed by SREL in initially cured grout mix LP#8-16. However, hemicarboaluminate was not observed in subsequently aged/leached samples and may be a transient phase not reflective of long-term equilibrium conditions.

6) Other minerals observed by SREL were either already in the mineral set (e.g., portlandite, calcite), represented by a polymorph (e.g., hematite) or otherwise similar mineral (e.g., hydrotalcite), not present in significant quantities (e.g., kuzelite, strätlingite), or presumed to be unreacted components of the dry mix (e.g., mullite in fly ash) which can be accounted for through partial hydration assumptions.

7) Amorphous phases (presumably $C\text{-}S\text{-}H$ / $C\text{-}A\text{-}S\text{-}H$ gel) and unreacted minerals constitute roughly 90% of the solid mass tested by SREL, leaving much of the hydrated mineral/gel mass undefined and precluding further refinement of the selected mineral set.

Although the CNASH solid solution model supersedes CSHQ, the latter is still available as an alternative for model sensitivity study and used in Section 4.1.

Table 2.2-1: Minerals Associated with Cementitious Materials.

SRNL-STI-2012-00404 Model	Current Model	SREL R-21-0001 X-Ray Diffraction Rietveld Refinement		
		Match or Other	Polymorph	Similar
Portlandite	Portlandite	Portlandite		
Calcite	Calcite	Calcite		
JenD	*JenD*			
JenH	*JenH*			
TobD	*TobD*			
TobH	*TobH (revised)*			
Gypsum	Gypsum			
C4AH13	C4AH13			
Monocarboaluminate	Monocarboaluminate	Monocarboaluminate		
Ettringite	Ettringite	Ettringite		Kuzelite
Fe-Ettringite	Fe-Ettringite			
Gibbsite	Al(OH)3(mic)			
Brucite	Brucite			
OH-Hydrotalcite	OH-Hydrotalcite			Hydrotalcite
Fe(OH)3(am)	Ferrihydrite			
Maghemite	Maghemite	Maghemite		
Magnetite	Magnetite		Hematite	
SiO2(a)	SiO2(a)		Quartz	
Pyrite	Pyrite			
	Hemicarboaluminate	Hemicarboaluminate		
	5CA_CNASHss			Strätlingite
	INFCA_CNASHss			Strätlingite
	T2C_CNASHss			
	T5C_CNASHss			
	TobH_CNASHss			
		Mullite (unreacted)		
		Amorphous		

Notes: *Italics* = C-S-H solid solution components; gray text = "CSHQ" model; _CNASHss = "CNASH" model; yellow highlight = different or added minerals compared to SRNL-STI-2012-00404.

2.3 Thermodynamic Databases

Four existing thermodynamic databases (DBs) were used to develop two new databases customized for this study that are equivalent for simulating cement chemistry, one formatted for GWB and the other for PHREEQC. The existing DBs are

1) SRNL-STI-2012-00404: `thermocement.v2.radNEA_5-7-2012.txt` is formatted for GWB and was previously used to simulate the chemical evolution of tank fill grout. An electronic copy resides in project archive folder \\pitstop\pitdata2\C&WDA\Folks\Layton-Mark\HTF NRC\HTF PA RAI Working\RAI Response Clarification\Response Folders\CQ-4 and in the IBM Notes *Liquid Waste Organization (LWO) Document Library* under SRR-CWDA-2013-00144 (the electronic file was transmitted to the Nuclear Regulatory Commission as noted in SRR-CWDA-2013-00144 Appendix B-1.1). This database started with the "thermo_phreeqc.dat" DB supplied with GWB circa 2011. Cement mineral data from Lothenbach and Winnefeld (2006) and Kulik (2011) and radionuclide data from a Nuclear Energy Agency (NEA) DB and other DBs were then added.
2) CEMDATA18.1: `CEMDATA18.1-16-01-2019-phaseVol.dat` formatted for PHREEQC (Lothenbach et al. 2019, https://www.empa.ch/web/s308/thermodynamic-data) is the default DB for making cement mineral updates within this study as previously stated.
3) ThermoChimie: Version 10a available in multiple GWB and PHREEQC formats (Giffaut et al. 2014, https://www.thermochimie-tdb.com/) is used as an alternative to CEMDATA18.1 in a few instances.
4) Thermoddem: This online DB (https://thermoddem.brgm.fr/data) was accessed December 21, 2020 for the molar volumes of ferrihydrite, chalcedony, and maghemite, which are not available or outdated in the preceding DBs.

The custom database for GWB simulations, `thermocement.v2.radNEA_12Jan2021.tdat`, was developed from `thermocement.v2.radNEA_5-7-2012.txt` through these modifications:

1) Using `ThermoChimie_GWB_electron.v10a.dat` dated November 22, 2018,
    a. Added cement mineral
        i. Ferrihydrite ("Ferryhydrite" in ThermoChimie)
    b. Revised the equilibrium constant at 25°C (logK25) for
        i. Maghemite ("Maghemite(ord)" in ThermoChimie)
2) Using `CEMDATA18.1-16-01-2019-phaseVol.dat` dated 16Jan2019,
    a. Added cement minerals
        i. Al(OH)3(mic) ("AlOHmic" in CEMDATA18.1)
        ii. Hemicarboaluminate ("hemicarbonat10.5" in CEMDATA18.1)
        iii. 5CA_CNASHss ("5CA" in CEMDATA18.1)

iv. INFCA_CNASHss ("INFCA" in CEMDATA18.1)
v. T2C_CNASHss ("T2C-CNASHss" in CEMDATA18.1)
vi. T5C_CNASHss ("T5C-CNASHss" in CEMDATA18.1)
vii. TobH_CNASHss ("TobH-CNASHs" in CEMDATA18.1)

b. Revised logK25 for ("name" in CEMDATA18.1 if different)
i. Portlandite
ii. Calcite ("Cal")
iii. JenD ("CSHQ-JenD")
iv. JenH ("CSHQ-JenH")
v. TobD ("CSHQ-TobD")
vi. TobH ("CSHQ-TobH", different mineral)
vii. Gypsum ("Gp")
viii. C4AH13
ix. Monocarboaluminate ("monocarbonate")
x. Ettringite ("ettringite")
xi. Fe-Ettringite ("Fe-ettringite")
xii. Brucite ("Brc")
xiii. OH-Hydrotalcite ("M4A-OH-LDH")
xiv. Magnetite ("Mag")
xv. SiO2(a) ("Amor-Sl")
xvi. Pyrite ("Py")

c. Added molar volumes for several cement minerals (see in-line comments in electronic files)

3) Using online Thermoddem DB on December 21, 2020,
a. Added molar volumes for
i. Ferrihydrite (https://thermoddem.brgm.fr/data?title=ferrihydrite)
ii. Chalcedony (https://thermoddem.brgm.fr/data?title=chalcedony)
iii. Maghemite (https://thermoddem.brgm.fr/data?title=maghemite, "Maghemite(disordered)")

4) Added several “oxides” to support initial hydration reactions (e.g., CaO, MgO, FeO).

Many of the logK25 updates using CEMDATA18.1 data were insignificant but performed nonetheless to ensure strict equivalence with CEMDATA18.1 and parallel PHREEQC simulations.

The custom database for PHREEQC simulations, `CEMDATA18.1-16-01-2019-phaseVol_21Dec2020.dat`, was developed from `CEMDATA18.1-16-01-2019-phaseVol.dat` through these modifications:

1) Using `ThermoChimie_GWB_electron.v10a.dat` dated November 22, 2018,
    a. Added cement minerals and associated logK25 values
        i. Ferrihydrite ("Ferryhydrite" in ThermoChimie)
        ii. Maghemite ("Maghemite(ord)" in ThermoChimie)
2) Using online Thermoddem DB on December 21, 2020,
    a. Added molar volumes for
        i. Ferrihydrite (https://thermoddem.brgm.fr/data?title=ferrihydrite)
        ii. Maghemite (https://thermoddem.brgm.fr/data?title=maghemite, "Maghemite(disordered)")
3) Replaced `O2(g)` and `CO2(g)` phases with alternative reactions involving only aqueous O_2 and CO_2 respectively per https://phreeqcusers.org/index.php?topic=1604.0;wap2
4) Corrected the `NH3` reaction per https://phreeqcusers.org/index.php?topic=1604.0;wap2
5) Commented-out (removed) the `CO3-2 + NO3- + 10e- + 13H+ = HCN + 6H2O` reaction because the HCN species is commented-out under the SOLUTION_MASTER_SPECIES heading

No edits were made to common aqueous species reactions and logK25 values (equilibrium constants) in either custom DB because the associated thermodynamic data are well-established, and any potential updates are not likely to be significant. The two custom DBs are equivalent for the chosen mineral set and produce nearly the same cement chemistry results, as will be shown later. The radionuclide (e.g., NEA) data in the custom GWB DB is legacy content from the SRNL-STI-2012-00404 study, used then for radionuclide solubility analysis. Because radionuclide information is not needed within the scope of this study, no attempt was made to update this data or add it to the custom PHREEQC (modified CEMDATA18.1) DB.

Table 2.3-1 compares the labels given to each mineral in the custom GWB and PHREEQC databases. For example, OH-Hydrotalcite in GWB and M4A-OH-LDH in PHREEQC refer to the identical mineral $Mg_4Al_2(OH)_{14}(H_2O)_3$.

Table 2.3-1: Mineral Names Used in the Custom GWB and PHREEQC Databases.

Chemical Formula as Expressed in CEMDATA18.1 DB	Custom GWB DB	Custom PHREEQC DB
Ca(OH)2	Portlandite	Portlandite
CaCO3	Calcite	Cal
(CaO)1.5(SiO2)0.6667(H2O)2.5	JenD	CSHQ-JenD
(CaO)1.3333(SiO2)1(H2O)2.1667	JenH	CSHQ-JenH
((CaO)1.25(SiO2)1(H2O)2.75)0.6667	TobD	CSHQ-TobD
(CaO)0.6667(SiO2)1(H2O)1.5	TobH (revised)	CSHQ-TobH
CaSO4(H2O)2	Gypsum	Gp
Ca4Al2(OH)14(H2O)6	C4AH13	C4AH13
Ca4Al2CO9(H2O)11	Monocarboaluminate	monocarbonate
((H2O)2)Ca6Al2(SO4)3(OH)12(H2O)24	Ettringite	ettringite
Ca6Fe2(SO4)3(OH)12(H2O)26	Fe-Ettringite	Fe-ettringite
Al(OH)3	Al(OH)3(mic)	AlOHmic
Mg(OH)2	Brucite	Brc
Mg4Al2(OH)14(H2O)3	OH-Hydrotalcite	M4A-OH-LDH
Fe(OH)3	Ferrihydrite	Ferrihydrite
Fe2O3	Maghemite	Maghemite
FeFe2O4	Magnetite	Mag
SiO2	SiO2(a)	Amor-Sl
FeSS	Pyrite	Py
(CaO)3Al2O3(CaCO3)0.5(CaO2H2)0.5(H2O)10	Hemicarboaluminate	hemicarbonat10.5
(CaO)1.25(SiO2)1(Al2O3)0.125(H2O)1.625	5CA_CNASHss	5CA
(CaO)1(SiO2)1.1875(Al2O3)0.15625(H2O)1.65625	INFCA_CNASHss	INFCA
(CaO)1.5(SiO2)1(H2O)2.5	T2C_CNASHss	T2C-CNASHss
(CaO)1.25(SiO2)1.25(H2O)2.5	T5C_CNASHss	T5C-CNASHss
(CaO)1(SiO2)1.5(H2O)2.5	TobH_CNASHss	TobH-CNASHss

2.4 Equilibrium constants

All equilibrium calculations in this study were conducted at 25°C. Transfer of thermodynamic information at 25°C from one database to another is a simple transcription process for identical reactions in the DBs. This convenience is often not the case when some of the Basis (GWB) species and/or Master Species (PHREEQC) differ between DBs. Table 2.4-1 compares the GWB Basis species in the reference SRNL-STI-2012-00404 DB to the Master Species in the PHREEQC-formatted CEMDATA18.1 DB. Note that AlO_2^- replaces Al^{+++} and FeO_2^- replaces Fe^{++} in CEMDATA18.1. This leads to different (although equivalent) sets of mineral dissolution and aqueous species reactions in the DBs, and the associated equilibrium constants at 25°C (logK25) are not the same numerically. This section discusses calculation of the logK25 values needed in the custom GWB DB from CEMDATA18.1 and ThermoChimie logK25 values.

Table 2.4-1: GWB Basis and PHREEQC Master Species.

SRNL-STI-2012-00404 / GWB Basis Species	CEMDATA18.1 / PHREEQC Master Species
Al+++	AlO2-
CO3--	CO3--
Ca++	Ca++
H+	H+
H4SiO4	SiO2
Fe++	FeO2-
Mg++	Mg++
O2(aq)	O2
SO4--	SO4--

Note: yellow highlight = difference compared to SRNL-STI-2012-00404.

In CEMDATA18.1 the dissolution/ionization reaction for microcrystalline $Al(OH)_3$ is written

$$Al(OH)_3 \rightleftharpoons AlO_2^- + H^+ + H_2O \tag{2-1}$$

with Law of Mass Action (LMA) equilibrium constant (e.g., Pilar 1979) given by

$$K_1 = \frac{[AlO_2^-][H^+][H_2O]}{[Al(OH)_3]} \tag{2-2}$$

where brackets denote the activity of the indicated species and

$$logK_1 = log[H^+] + log[H_2O] + log[AlO_2^-] - log[Al(OH)_3] = -14.670074 \tag{2-3}$$

at 25°C. Also in CEMDATA18.1

$$AlO_2^- \rightleftharpoons Al^{+++} + 2H_2O - 4H^+ \tag{2-4}$$

where

$$K_2 = \frac{[Al^{+++}][H_2O]^2}{[AlO_2{}^-][H^+]^4} \tag{2-5}$$

and

$$logK_2 = log[Al^{+++}] + 2log[H_2O] - log[AlO_2{}^-] - 4log[H^+] = +22.879124 \tag{2-6}$$

at 25°C. In the custom GWB DB based on SRNL-STI-2012-00404 the dissolution/ionization reaction for microcrystalline $Al(OH)_3$ is alternatively written

$$Al(OH)_3 \rightleftharpoons Al^{+++} + 3H_2O - 3H^+ \tag{2-7}$$

Thus, the associated LMA equilibrium constant is

$$K_3 = \frac{[Al^{+++}][H_2O]^3}{[Al(OH)_3][H^+]^3} \tag{2-8}$$

or equivalently

$$logK_3 = log[Al^{+++}] + 3log[H_2O] - log[Al(OH)_3] - 3log[H^+] \tag{2-9}$$

Note that Equations (2-1) and (2-4) can be combined to yield Equation (2-7):

$$\begin{gathered} Al(OH)_3 \rightleftharpoons AlO_2{}^- + H^+ + H_2O \\ Al(OH)_3 \rightleftharpoons \{Al^{+++} + 2H_2O - 4H^+\} + H^+ + H_2O \\ Al(OH)_3 \rightleftharpoons Al^{+++} + 3H_2O - 3H^+ \end{gathered} \tag{2-10}$$

In analogous fashion, Equations (2-3) and (2-6) can be added to yield Equation (2-9):

$$\begin{gathered} logK_1 = log[H^+] + log[H_2O] + log[AlO_2{}^-] - log[Al(OH)_3] \\ \underline{+\ \ logK_2 = log[Al^{+++}] + 2log[H_2O] - log[AlO_2{}^-] - 4log[H^+]} \\ logK_1 + \ logK_2 = log[H^+] + log[H_2O] + log[AlO_2{}^-] - log[Al(OH)_3] \\ + log[Al^{+++}] + 2log[H_2O] - log[AlO_2{}^-] - 4log[H^+] \\ logK_1 + \ logK_2 = +log[Al^{+++}] + 3log[H_2O] - log[Al(OH)_3] \ - 3log[H^+] \\ logK_1 + \ logK_2 = logK_3 \end{gathered} \tag{2-11}$$

Rearranging terms and evaluating the expression using CEMDATA18.1 LMA values from Equations (2-3) and (2-6) produces the required LMA constant for the custom GWB DB:

$$logK_3 = logK_1 + \ logK_2 = -14.670074 + 22.879124 = +8.209050 \tag{2-12}$$

Several calculations of this nature were performed in creating the custom GWB DB. Table 2.4-2 summarizes the key mineral and aqueous species reactions and associated logK25 values in the custom PHREEQC DB based on CEMDATA18.1 (principally) and ThermoChimie. These data have either been transcribed to the custom GWB DB based on SRNL-STI-2012-00404 or used to calculate the required logK25 values for alternative reactions. Table 2.4-3 summarizes the results of that process.

Table 2.4-2: Reactions and Equilibrium Constants in the Custom PHREEQC DB.

Mineral	Reaction	logK25
Portlandite	Ca(OH)2 + 2H+ = Ca+2 + 2H2O	22.799937
Cal	CaCO3 = CO3-2 + Ca+2	-8.479966
CSHQ-JenD	(CaO)1.5(SiO2)0.6667(H2O)2.5 + 3H+ = 1.5Ca+2 + 4H2O + 0.6667SiO2	28.730362
CSHQ-JenH	(CaO)1.3333(SiO2)1(H2O)2.1667 + 2.6666H+ = 1.3333Ca+2 + 3.5H2O + SiO2	22.179305
CSHQ-TobD	((CaO)1.25(SiO2)1(H2O)2.75)0.6667 + 1.66675H+ = 0.833375Ca+2 + 2.6668H2O + 0.6667SiO2	13.655314
CSHQ-TobH	(CaO)0.6667(SiO2)1(H2O)1.5 + 1.3334H+ = 0.6667Ca+2 + 2.1667H2O + SiO2	8.286642
Gp	CaSO4(H2O)2 = Ca+2 + SO4-2 + 2H2O	-4.580905
C4AH13	Ca4Al2(OH)14(H2O)6 + 6H+ = 4Ca+2 + 2AlO2- + 16H2O	58.751897
monocarbonate	Ca4Al2CO9(H2O)11 + 4H+ = CO3-2 + 4Ca+2 + 2AlO2- + 13H2O	24.530285
ettringite	((H2O)2)Ca6Al2(SO4)3(OH)12(H2O)24 + 4H+ = 6Ca+2 + 3SO4-2 + 2AlO2- + 34H2O	11.100288
Fe-ettringite	Ca6Fe2(SO4)3(OH)12(H2O)26 + 4H+ = 2FeO2- + 6Ca+2 + 3SO4-2 + 34H2O	12.000367
AlOHmic	Al(OH)3 = AlO2- + H+ + H2O	-14.670074
Brc	Mg(OH)2 + 2H+ = Mg+2 + 2H2O	16.8401
M4A-OH-LDH	Mg4Al2(OH)14(H2O)3 + 6H+ = 4Mg+2 + 2AlO2- + 13H2O	34.300378
Ferrihydrite	Fe(OH)3 = FeO2- + H2O + H+	-20.40987481
Maghemite	Fe2O3 + H2O = 2FeO2- + 2H+	-39.679752
Mag	FeFe2O4 + 2H2O = 3FeO2- + e- + 4H+	-67.799781
Amor-Sl	Amor-Sl = [SiO2]	-2.714066
Py	FeSS + 10H2O = FeO2- + 2SO4-2 + 15e- + 20H+	-120.499988
hemicarbonat10.5	(CaO)3Al2O3(CaCO3)0.5(CaO2H2)0.5(H2O)10 + 5H+ = 0.5CO3-2 + 4Ca+2 + 2AlO2- + 13H2O	42.602279
5CA	(CaO)1.25(SiO2)1(Al2O3)0.125(H2O)1.625 + 2.25H+ = 1.25Ca+2 + 0.25AlO2- + 2.75H2O + SiO2	15.88995
INFCA	(CaO)1(SiO2)1.1875(Al2O3)0.15625(H2O)1.65625 + 1.6875H+ = Ca+2 + 0.3125AlO2- + 2.5H2O + 1.1875SiO2	8.953727
T2C-CNASHss	(CaO)1.5(SiO2)1(H2O)2.5 + 3H+ = 1.5Ca+2 + 4H2O + SiO2	25.565334
T5C-CNASHss	(CaO)1.25(SiO2)1.25(H2O)2.5 + 2.5H+ = 1.25Ca+2 + 3.75H2O + 1.25SiO2	18.445467
TobH-CNASHss	(CaO)1(SiO2)1.5(H2O)2.5 + 2H+ = Ca+2 + 3.5H2O + 1.5SiO2	12.797208
Aqueous species needed for logK25 conversions	AlO2- + 4H+ = Al+3 + 2H2O	22.879124
	FeO2- + 4H+ = Fe+3 + 2H2O	21.599876
	e- + 4H+ + FeO2- = Fe+2 + 2H2O	34.619927
	{Fe+2 + 2H2O - e- - 4H+} + 4H+ = Fe+3 + 2H2O → Fe+2 - e- = Fe+3	-13.020051
	Fe+3 = Fe+2 - e-	13.020051
	SO4-2 + 8e- + 9H+ = HS- + 4H2O	33.690011
	2H2O = O2 + 4e- + 4H+	-85.986052
	- 4e- - 4H+ = -O2 - 2H2O	-85.986052
	-2e- - 2H+ = -0.5O2 - H2O	-42.993026

Note: yellow highlight = value from ThermoChimie DB; other mineral values from CEMDATA18.1.

Table 2.4-3: Reactions and Equilibrium Constants in the Custom GWB DB.

Mineral	Reaction	logK25
Portlandite	Ca(OH)2 = Ca++ + 2H2O - 2H+	22.79994
Calcite	CaCO3 = CO3-- + Ca++	-8.47997
JenD	Ca1.5Si0.67O5.34H5 = 1.5Ca++ + 2.66H2O + 0.67H4SiO4 - 3H+	28.73036
JenH	Ca1.33Si1.05.5H4.34 = 1.33Ca++ + 1.5H2O + H4SiO4 - 2.66H+	22.17931
TobD	Ca0.83Si0.67O4H3.66 = 0.83Ca++ + 1.32H2O + 0.67H4SiO4 - 1.66H+	13.65531
TobH (revised)	Ca0.67Si1.00O4.17H3 = 0.67Ca++ + 0.17H2O + H4SiO4 - 1.34H+	8.286642
Gypsum	CaSO4:2H2O = 2H2O + SO4-- + Ca++	-4.580905
C4AH13	4CaO.Al2O3.13H2O = 4Ca++ + 2Al+++ + 20H2O - 14H+	104.5101
Monocarboaluminate	3CaO.Al2O3.CaCO3.11H2O = 4Ca++ + 2Al+++ + CO3-- + 17H2O - 12H+	70.28853
Ettringite	Ca6Al2(SO4)3(OH)12.26H2O = 6Ca++ + 2Al+++ + 3SO4-- + 38H2O -12H+	56.85854
Fe-Ettringite	Ca6Fe2(SO4)3(OH)12.26H2O = 6Ca++ + 2Fe+++ + 3SO4-- + 38H2O - 12H+	55.20012
Al(OH)3(mic)	Al(OH)3 = Al+++ + 3H2O - 3H+	8.20905
Brucite	Mg(OH)2 = Mg++ + H2O - 2H+	16.8401
OH-Hydrotalcite	Mg4Al2(OH)14.3H2O = 4Mg++ + 2Al+++ + 17H2O - 14H+	80.05863
Ferrihydrite	Fe(OH)3 = 3H2O + Fe+++ - 3H+	1.19
Maghemite	Fe2O3 = 3H2O + 2Fe+++ - 6H+	3.52
Magnetite	Fe3O4 = -8H+ + Fe++ + 4H2O + 2Fe+++	10.0199
SiO2(a)	SiO2 = -2H2O + H4SiO4	-2.71407
Pyrite	FeS2 = Fe++ - H2O + 2HS- + 0.5O2(aq)	-61.4931
Hemicarboaluminate	3(CaO).(Al2O3).0.5(CaCO3).0.5(CaO2H2).10(H2O) = 4Ca++ + 2Al+++ + 0.5CO3-- + 17H2O - 13H+	88.360527
5CA_CNASHss	(CaO)1.25(SiO2)1(Al2O3)0.125(H2O)1.625 = 1.25Ca++ + 0.25Al+++ + 1.25H2O + H4SiO4 - 3.25H+	21.609731
INFCA_CNASHss	(CaO)1(SiO2)1.1875(Al2O3)0.15625(H2O)1.65625 = Ca++ + 0.3125Al+++ + 0.75H2O + 1.1875H4SiO4 - 2.9375H+	16.10345325
T2C_CNASHss	(CaO)1.5(SiO2)1(H2O)2.5 = 1.5Ca++ + 2H2O + H4SiO4 - 3H+	25.56533
T5C_CNASHss	(CaO)1.25(SiO2)1.25(H2O)2.5 = 1.25Ca++ + 1.25H2O + 1.25H4SiO4 - 2.5H+	18.44547
TobH_CNASHss	(CaO)1(SiO2)1.5(H2O)2.5 = Ca++ + 0.5H2O + 1.5H4SiO4 - 2H+	12.79721

Note: yellow highlight = calculated value; otherwise transcribed from another DB.

3.0 EQUILIBRIUM CHEMISTRY STATES

The equilibrium chemical states of several solutions and cementitious materials are required as initial or boundary conditions for cement chemistry evolution simulations: vadose zone soil moisture for simulations involving tanks above the water table (WT), groundwater for submerged tanks, and grouts and concrete in their initially hydrated (cured) state. Chloride concentrations in soil moisture and groundwater are important for corrosion analysis and considered first. Next, synthetic rainwater representative of SRS conditions is generated as a precursor to soil moisture. SRS soil moisture is then generated from rainwater by considering evapotranspiration and solution equilibration with clay minerals in the facility final cover and/or native sediments. SRS groundwater is developed from representative SRS P-well data. Finally, hydration of dry grout and concrete mixes is simulated to predict the initial states of cured cementitious materials.

3.1 Chloride concentration

Chloride ingress is well known to initiate accelerated reinforcing bar (rebar) corrosion in concrete. Although chloride-induced corrosion is not predicted in this study, chloride concentrations are simulated and may be useful in subsequent corrosion analysis. Therefore, representative chloride concentrations are sought for SRS soil moisture and groundwater, which function as boundary conditions in cement evolution simulations. Chloride (Cl^-) concentrations in WT wells P18D, P20D, P23D, P24D, and P27D range from 1 to 3 parts per million (ppm) (WSRC-TR-2002-00479) and average about 2 ppm. SRNL-L3200-2012-00022 reports 4.13 ppm for well P29D. Based on these references, a chloride concentration of 2 ppm is selected for the level representative of SRS groundwater. Because flow in shallow SRS aquifers is driven by local recharge, the source of this concentration is upstream soil moisture. Therefore, 2 ppm is selected as the target chloride concentration in SRS soil moisture too.

3.2 Rainwater

Rainwater is the starting point for generating synthetic soil moisture in the next section. Following SRNL-STI-2012-00404, a representative SRS rainwater composition is developed herein from data reported in WSRC-RP-92-450 (Strom and Kaback, 1992). Table 3.2-1 presents average rainwater composition data from 15 samples and GWB (SpecE8 module) and PHREEQC (SOLUTION module) simulations. In both simulations, $O_2(aq)$ is equilibrated with $O_2(g)$ at 0.2 atm, ${CO_3}^{--}$ is equilibrated with $CO_2(g)$ at 0.00032 atmospheres (atm) (320 ppm), and electrical charge is balanced on H^+. Redox disequilibrium is assumed for nitrogen species. The GWB and PHREEQC results are nearly identical and very close to the measured data (for dilute solutions concentrations in moles per liter of solution are numerically practically the same as concentrations in moles per kg of solvent). The indicated chloride concentration 9.89E-06 mol/L is equivalent to 0.35 ppm.

Table 3.2-1: Measured and Simulated Rainwater Compositions.

	Average of Strom and Kaback (1992) Rainfall Data	GWB Simulation	Ratio	PHREEQC Simulation	Ratio
pH	4.63	4.620	1.00	4.621	1.00
Species	mol/L	mol/kg		mol/kg	
H+	2.36E-05	2.42E-05	1.03	2.41E-05	1.02
Mg++	1.34E-06	1.34E-06	1.00	1.34E-06	1.00
Ca++	2.06E-06	2.06E-06	1.00	2.05E-06	1.00
Na+	8.69E-06	8.73E-06	1.00	8.69E-06	1.00
K+	1.08E-06	1.09E-06	1.00	1.08E-06	1.00
SO4--	1.35E-05	1.35E-05	1.00	1.34E-05	1.00
Cl-	9.89E-06	9.93E-06	1.00	9.89E-06	1.00
NH4+	7.73E-06	7.76E-06	1.00	7.73E-06	1.00
NO3-	1.15E-05	1.15E-05	1.00	1.15E-05	1.00
O2(aq)		2.22E-04		2.64E-04	
CO2 (H2CO3)		1.09E-05		1.11E-05	
HCO3-	1.86E-07	2.04E-07	1.10	2.07E-07	1.12
CO3--		4.11E-13		4.18E-13	

3.3 Soil Moisture

A representative SRS soil moisture composition is created by simulating evapotranspiration (ET) and solution equilibration with clay minerals, and by adding sufficient $NaCl$ to achieve the target 2 ppm Cl^- concentration. The specific steps are:

1) Equilibrate 1.0 kg SRS rainwater with $CO_2(g)$ at 0.01 atm partial pressure in soil gas (SRNL-L3200-2012-00017) and atmospheric O_2. Equilibration with atmospheric oxygen ensures $O_2(aq)$ saturation, maximizes consumption of cement reducing capacity, and minimizes the time to transition from reducing to oxidizing conditions in reducing grout. Charge balance using H^+ (pH).
2) React 1.0 kg water with:
    a. All minerals suppressed except kaolinite, amorphous silica, and gibbsite.
    b. Fugacities of $CO_2(g)$ and $O_2(g)$ fixed.
    c. 0.67 kg H_2O removed to simulate ET (DPST-85-958, DPST-86-658).
    d. 10 mmol kaolinite and amorphous silica added to simulate contact with clay in the final cover system and native sediments.
    e. 0.009 mmol halite ($NaCl$) added to raise the final chloride concentration from approximately 1 ppm to 2.0 ppm.

These steps are carried out using the React module within GWB and the SOLUTION, EQUILIBRIUM_PHASES, and REACTION components within PHREEQC. Table 3.3-1 summarizes simulation results.

Table 3.3-1: Simulated SRS Soil Moisture Compositions.

Constituent	GWB Simulation	PHREEQC Simulation
pH	4.16	3.98
pe	16.45	16.62
Eh	+0.97	+0.98
	mol/L	mol/L
O2(aq)	2.22E-04	2.64E-04
CO2(aq)	3.42E-04	3.45E-04
Cl-	5.74E-05	5.73E-05
Na+	5.37E-05	5.36E-05
Ca++	6.20E-06	6.19E-06
Mg++	4.05E-06	4.03E-06
Al+++	1.05E-06	3.59E-06
H4SiO4(aq)	1.93E-03	1.93E-03
SO4--	4.03E-05	3.94E-05
Cl- (ppm)	2.03	2.03

The partial pressure of CO_2 in soil gas is much higher than that of atmospheric CO_2 at 0.0004 atm because plant roots respire carbon dioxide and oxidative decay of organic matter also produces $CO_2(g)$. These processes and elevated subsurface CO_2 levels are illustrated in Figure 3.3-1 reproduced from Railsback (2009). Note that both processes consume dissolved oxygen. Thus, P_{CO_2} = 0.01 atm and $O_2(g)$ = 0.2 atm are not likely to occur together in the subsurface, making the assumed conditions pessimistic in relation to cementitious material aging.

Figure 3.3-1: Elevated CO2(g) Levels in the Subsurface.

Reproduced from Railsback (2009)

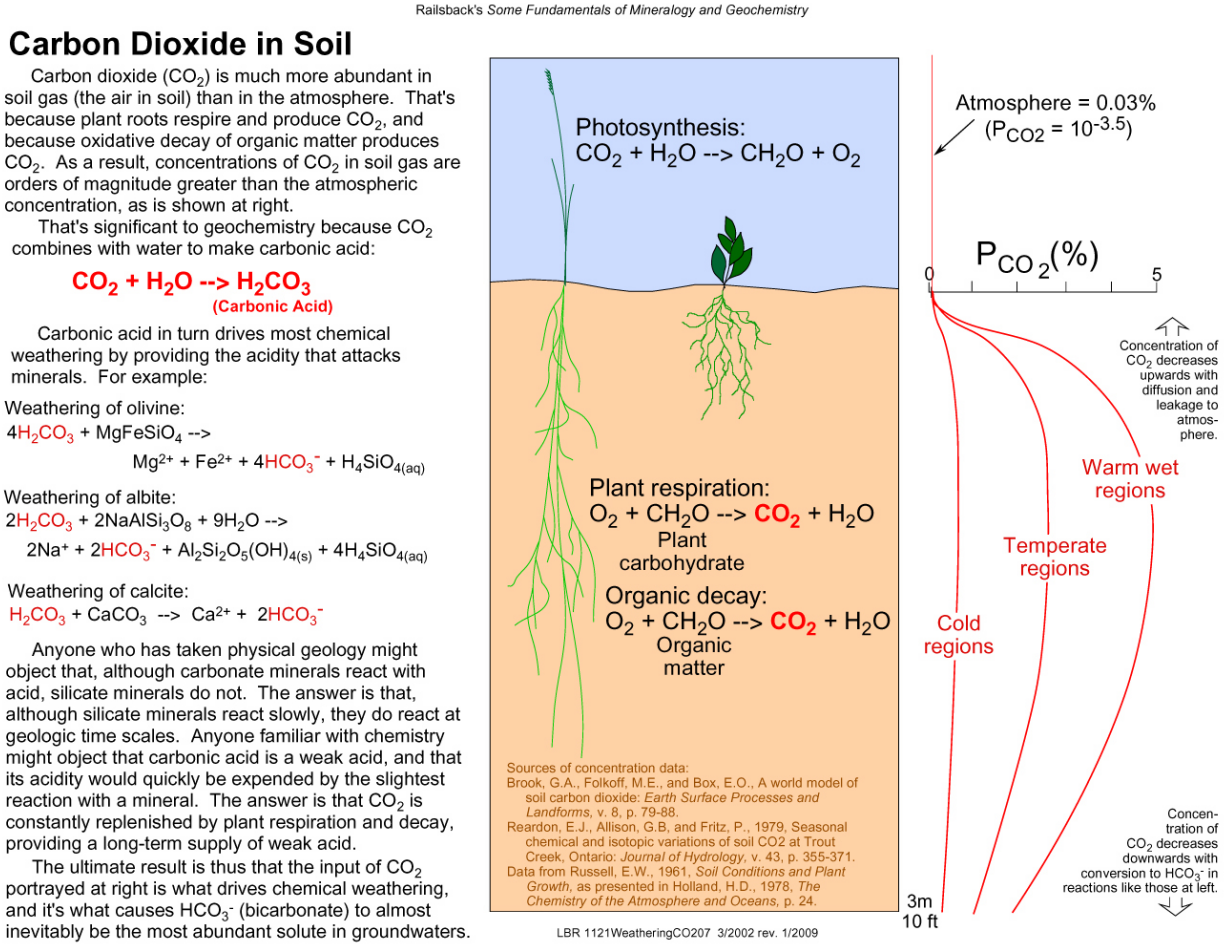

3.4 Groundwater

A representative SRS groundwater composition is derived from P29D water table well data reported in SRNL-L3200-2012-00022 (Table 1) using a process similar to that used to generate the recommended "Case 4" in that reference (Tables 2 and 3):

1) Set pH to the measured value of 5.4
2) Equilibrate $O_2(aq)$ with atmospheric oxygen
3) Charge balance on CO_3^{--}
4) Include 4 ppm NO_3^-
5) Lower the $NaCl$ content to achieve 2 ppm Cl^- concentration.

Water table well P29D was selected for this analysis because the chemistry of the water in this well "reflects the typical geochemistry found in shallow aquifers across the SRS" (SRNL-L3200-2012-00022, pg. 1).

Table 3.4-1 summarizes the simulation results from GWB and PHREEQC. Note that Step 2) produces a simulated Eh of +0.90 volts compared to the measured value of +0.237 volts in P29D. This bias is desirable from the perspective of maximizing consumption of reducing capacity and minimizing the transition time from reducing to oxidizing conditions in reducing grout. Similarly, $log_{10}(P_{CO_2})$ lies at the upper range of measured values (SRNL-L3200-2012-00017) and high dissolved CO_2 maximizes carbonation rates and minimizes the transition times to lower pH. Table 3.4-2 and Table 3.4-3 compare SRNL-L3200-2012-00022 Case 4 to Table 3.4-1 GWB and PHREEQC results, respectively. Note that concentrations in moles per liter of solution are numerically practically the same as concentrations in moles per kg of solvent for dilute solutions.

Table 3.4-1: Simulated SRS Groundwater Compositions.

	GWB	PHREEQC	GWB	PHREEQC
pH	5.4	5.4	5.4	5.4
Eh (volts)	+0.90	+0.90	+0.90	+0.90
log10(PCO2)	-1.73	-1.74	-1.73	-1.74
Constituent	**mol/kg**	**mol/kg**	**mg/kg**	**mg/kg**
CO2(aq)	6.31E-04	6.27E-04	27.8	27.6
O2(aq)	2.22E-04	2.64E-04	7.11	8.43
Cl-	5.66E-05	5.64E-05	2.01	2.00
H4SiO4	7.67E-05	7.64E-05	7.37	7.34
Na+	4.59E-05	4.57E-05	1.05	1.05
Ca++	7.47E-05	7.45E-05	2.99	2.99
NO3-	6.48E-05	6.45E-05	4.02	4.00
HCO3-	7.18E-05	7.15E-05	4.38	4.36
SO4--	2.35E-05	2.36E-05	2.26	2.26
Mg++	1.56E-05	1.56E-05	0.379	0.378
K+	8.73E-06	8.70E-06	0.341	0.340
H+	4.07E-06	4.07E-06	0.0041	0.0041
CaSO4	4.08E-07	2.95E-07		
Fe(OH)2+	3.02E-07	2.94E-07		
Al(OH)2+	9.54E-08	9.34E-08		
AlOH++	1.76E-07	1.72E-07		
CaHCO3+	6.31E-08	6.24E-08		
Al+++	7.02E-08	6.88E-08		
MgSO4	7.26E-08	7.24E-08		
Al(OH)3	3.41E-08	3.33E-08		
Other	<1.E-08	<1.E-08		

Table 3.4-2: GWB GW Simulation Compared to SRNL-L3200-2012-00022 Case 4.

Case 4 Constituent	Case 4 (mg/L)	GWB Element	GWB (mg/kg)	as Species	GWB (mg/kg)
Al+++	0.0104	Al	0.0106	as Al+++	0.0106
Ca++	2.95	Ca	3.01	as Ca++	3.01
Fe++	0.0172	Fe	0.0176	as Fe++	0.0176
K+	0.335	K	0.341	as K+	0.341
Mg++	0.374	Mg	0.382	as Mg++	0.382
Na+	2.26	Na	1.05	as Na+	1.05
Cl-	4.31	Cl	2.01	as Cl-	2.01
HCO3-	38.3	C	8.441	as HCO3-	42.9
NO3-	3.94	N	0.907	as NO3-	4.02
SO4--	2.26	S	0.77	as SO4--	2.31
O2(aq)	7.19	O	7.11	as O2(aq)	7.11
H4SiO4	7.23	Si	2.15	as H4SiO4	7.38
log10(PCO2)	-1.86	-1.73			
pH	5.4	5.4			

Table 3.4-3: PHREEQC GW Simulation Compared to SRNL-L3200-2012-00022 Case 4.

Case 4 Constituent	Case 4 (mg/L)	PHREEQC Element	PHREEQC (mg/kg)	as Species	PHREEQC (mg/kg)
Al+++	0.0104	Al	0.0104	as Al+++	0.0104
Ca++	2.95	Ca	3.00	as Ca++	3.00
Fe++	0.0172	Fe	0.0172	as Fe++	0.0172
K+	0.335	K	0.340	as K+	0.340
Mg++	0.374	Mg	0.380	as Mg++	0.380
Na+	2.26	Na	1.05	as Na+	1.05
Cl-	4.31	Cl	2.00	as Cl-	2.00
HCO3-	38.3	C	8.387	as HCO3-	42.6
NO3-	3.94	N	0.904	as NO3-	4.00
SO4--	2.26	S	0.768	as SO4--	2.30
O2(aq)	7.19	O	8.432	as O2(aq)	8.43
H4SiO4	7.23	Si	2.145	as H4SiO4	7.35
log10(PCO2)	-1.86	-1.74			
pH	5.4	5.4			

3.5 Hydrated Cementitious Materials

Several cementitious materials are analyzed in this study (Table 3.5-1):

1) "LP#8-16" (C-SPP-F-00055) is the grout used in recent years for operational closure of SRS liquid waste tanks (SRR-CWDA-2020-00045 Table 2). It has regulatory approval for, and is a candidate for, future SRS tank closures. SREL exposed LP#8-16 to representative aging/leaching conditions, monitored the evolution of aqueous and solid phase chemistry, and refer to this material as "Tank Fill Grout" (TFG) in R-21-0001.
2) "Vault 4 Clean Cap" grout (C-SPP-Z-00012) originating from the Saltstone Disposal Facility has been used to fill the last remaining void space in a tank, as the grout level approaches the underside of the roof liner, due to its lack of aggregate and free-flowing consistency. Abbreviated "Clean Cap" going forward, this grout also has regulatory approval for future SRS tank closures.
3) "ZB-FF-8-D" (C-SPS-G-00096, C-DCF-G-00397, C-DCF-G-00400), also referred to as "Zero-Bleed CLSM" (Controlled Low Strength Material), is a strong candidate for future SRS tank closures (SRR-CWDA-2020-00045).

The two other grouts tested by SREL are of interest from an experimental insights perspective:

4) "Tank Fill Grout w/No Blast Furnace Slag" (TFG-NBFS), and
5) "Controlled Low Strength Material", a common CLSM identified in C-SPS-G-00096/C-DCF-G-00397 as mix "EXE-X-P-0-X".

Finally,

6) "B3000-6-0-2-A" (C-SPS-G-00096, C-DCF-G-00397) is a contemporary concrete mix selected as a surrogate for all tank concretes, for which precise compositions are generally unavailable.

The initial hydrated/cured state of each material is needed to initiate simulations of chemical aging. In addition to the ingredients and proportions listed in Table 3.5-1, the chemical compositions of the dry ingredients are needed to estimate initial mineralogy. The best available cement oxide data are summarized by SRR-CWDA-2020-00066, Table 2. The averages of this data are used in this study and presented in Table 3.5-2, except that the composition of slag was adjusted slightly for Clean Cap grout to have enough Fe to represent its measured reduction capacity with pyrite. Only the reducing capacity of the slag is credited, even though the other binders have reducing capacity (SRNL-STI-2009-00637). This assumption is conservative and carried over from SRNL-STI-2012-00404.

Table 3.5-1: Grout and Concrete Mixes.

Ingredient	LP#8-16 Grout (TFG)	TFG-NBFS	ZB-FF-8-D Grout	Common CLSM	Clean Cap Grout	B3000-6-0-2-A Concrete
Cement (lbs/yd^3)	125	125	150	50	193	520
Slag (lbs/yd^3)	210	–	–	–	867	–
Fly Ash (lbs/yd^3)	363	573	500	600	867	–
Sand (lbs/yd^3)	1790	1790	1850	2515	–	1165
Gravel (lbs/yd^3)	800	800	800	–	–	1850
Water (gal)	48.5	48.5	50.0	66	116	36
water/cement mass ratio	0.58	0.58	0.64	0.85	0.50	0.58

Table 3.5-2: Major Oxides Assumed in Dry Cements and Pozzolans.

Oxide (g/100g)	Cement	Slag	Slag (Clean Cap)	Fly Ash
CaO	64.6	39.0	38.0	4.2
SiO2	20.4	36.5	35.5	50.9
Al2O3	5.0	10.5	10.2	27.9
Fe2O3	3.5	0.4	3	8.7
SO3	2.8	2.3	2.2	0.3
MgO	1.2	10.1	9.9	0.9
Other	2.6	1.2	1.2	7.0

Another consideration affecting initial mineralogy is the degree of hydration (chemical reaction) that occurs after the dry binders contact mix water. Table 4 of SRR-CWDA-2020-00066 summarizes degree of hydration inferences over experimental timeframes of a few months to two years, and the following degrees of hydration were proposed for the "long-term": cement 100%, slag 70%, and fly ash 40%. The upper bound is obviously 100% hydration of each binder, and this condition might be realized given enough curing time prior to aging (hundreds to thousands of years or more). A lower bound on hydration for the grouts of interest, characteristic of curing through no more than a few months, can be roughly estimated from SREL testing on LP#8-16/TFG, TFG-NBFS, and EXE-X-P-0-X/CLSM. SREL Doc. R-21-0001 presents X-Ray Diffraction (XRD) Rietveld Refinement data describing the kind and mass of crystalline solids detected in these mixes.

In a parametric study summarized in Appendix A, the best match to general mineralogy based on Rietveld Refinement and pH data was achieved with these hydrations: cement 100%, slag 70%, and fly ash 20%. The unreacted dry binders are considered inert. Assuming complete hydration of all binders lowers the Ca/Si ratio and initial pH and maximizes the times to transition to lower pH and higher Eh values. Assuming partial hydration increases the initial pH due to a higher Ca/Si ratio and minimizes pH and Eh transition times. That is, partial hydration accelerates chemical evolution/aging. On this basis, partial hydration at 100/70/20% is assumed for baseline chemical evolution simulations. 100% hydration of all binders is considered in a sensitivity case.

The initially cured and saturated cementitious materials of interest are created using these steps:

1) Assuming 100% cement, 70% slag, and 20% fly ash hydration, compute the molar amounts of reactive cement oxides (CaO, SiO_2, Al_2O_3, FeO/Fe^{II}, Fe_2O_3/Fe^{III}, SO_3, and MgO) for a 1.0 m^3 volume of cured material.
2) Using the GWB React module, react the active cement oxides with the prescribed mass of mix water.
3) Extract the molar quantities of hydrated minerals from GWB output and calculate porosity, water content, and water saturation using mineral molar volume data.
4) Calculate the amount of additional water required to achieve 100% saturation (replace air with additional water) and increase the mix water by that amount.
5) Re-simulate the hydration process with GWB React and confirm 100% water saturation.

As an example, Table 3.5-3 presents the calculation of reactive oxide content for grout LP#8-16, Table 3.5-4 shows the initially cured state of LP#8-16 as simulated by GWB, and Table 3.5-5 shows the initially cured and saturated state of LP#8-16. The predicted porosity is 24.3% compared to a measured value of 21% (SRR-CWDA-2020-00045 Table 10). As-cured saturation is simulated to be 76%. Appendix B provides these sets of results for the LP#8-16, ZB-FF-8-D, Vault 4 Clean Cap, and B3000-6-0-2-A mixes further analyzed in Section 4.0.

Table 3.5-3: Example Calculation of Reactive Cement Oxide Content.

Tanks 5, 6, 12, 16, 18, 19 Grout (Mix LP#8-16)														
Parameter	Cement	Slag	Fly Ash	Silica Fume	Metakaolin	Inert B	Dry mix	Water	w/c (weight) ratio	w/dry mix		Notes:		
Mix (lbs/yd3)	125	210	363			2590	3288	404.0	0.579	0.123		-- C-SPP-F-00055 Rev. 6		
(kg/m3)	74	125	215	0	0	1537	1951	239.7				2190		
All ingredients fraction	0.034	0.057	0.098	0.000	0.000	0.702	0.891	0.109						
Dry ingredients fraction	0.038	0.064	0.110	0.000	0.000	0.788	1							
Binders fraction	0.18	0.30	0.52	0.00	0.00		1							
Parameter	Cement	Slag	Fly Ash	Silica Fume	Metakaolin	Inert B		Binders	Dry Mix		MW	mol/	GWB /	PHREEQC
Proportions	g/100g	g/100g	g/100g	g/100g	g/100g			g/100g	g/100g	g/kg	g/mol	kg dry mix		mol/m3
Reactive ingredients	97.4	98.8	93.0	96.3	98.5									
C (CaO)	64.6	39.0	4.2	0.6	0.2			20.2	4.29	42.9	56	0.766	C (CaO)	1494
S (SiO2)	20.4	36.5	50.9	95.0	53.1			16.6	3.53	35.3	60	0.589	S (SiO2)	1148
A (Al2O3)	5.0	10.5	27.9	0.2	43.6			6.0	1.27	12.7	102	0.125	A (Al2O3)	243.7
F (Fe2O3)	3.5	0.4	8.7	0.1	1.6			1.6	0.35	3.5	160	0.022	F (Fe2O3)	42.11
Sbar (SO3)	2.8	2.3	0.3	0.2	0.0			1.0	0.21	2.1	80	0.027	Sbar (SO3)	51.87
M (MgO)	1.2	10.1	0.9	0.2	0.1			2.4	0.52	5.2	40	0.130	M (MgO)	252.9
Inert A	2.6	1.2	7.0	3.8	1.5	100.0		52.1	11.06	110.6				
Inert B									78.77	787.7				
Water									12.29	122.9	18	6.826	H (H2O)	13316
checks	100	100	100	100	100	100		100	100	1000				
Degree of rxn/hydration	100%	70%	20%	20%	20%				0.579	0.579				
Parameter	Cement	Slag	Fly Ash	Silica Fume	Metakaolin	Total							Fe	84.2
Reducing capacity (µeq/g)		819											FeO (FeII)	71.43
Reducing capacity (eq/m3)	0.0	71.4	0.0	0.0	0.0	71.43							Fe2O3 (FeIII)	6.40
Unreacted dry mix (kg/m3)	0	37.376	172.29	0	0	209.66								

Table 3.5-4: Example Simulation of Initially Cured Grout.

LP#8-16													
GWB hydration -- initial				**Mass (g)**	**Volume (mL)**	**Density (g/mL)**	**Volume Fraction**	**Porosity**	**Water Content**	**Saturation**	**Water Addition (g)**	**Water Addition (mol)**	**Comments**
pH	11.414		Inert:	1.747E+06	6.641E+05	2.63	66.4%						Inert B + unreacted binders
pe	-8.347		Minerals:	2.528E+05	9.251E+04	2.73	9.3%						Hydrated minerals
Eh (V)	-0.49	Water (unreacted):		1.851E+05	1.851E+05	1.00	18.5%	**24.3%**	**18.5%**	**76.0%**	5.83E+04	**3239**	Compared to measured n=21%
Water mass	185.07	kg	Air:		5.830E+04		5.8%						
			Total:	2.185E+06	1.000E+06	**2.18**	100.0%						
Phase	**MW (g/mol)**	**MV (mL/mol)**	**Moles**	**Mass (g)**	**Volume (mL)**	**Density (g/mL)**							
5CA	172.205675	57.3	1.067E+03	1.837E+05	6.114E+04	3.01							
AlOHmic	78.0055	31.956	4.217E+01	3.289E+03	1.348E+03	2.44							
Brc	58.328	24.63		0	0	0							
C4AH13	560.491	274.47001		0	0	0							
Cal	100.0911	36.934	2.312E-03	2.314E-01	8.539E-02	2.71							
Fe-ettringite	1312.878	717.55997		0	0	0							
Ferrihydrite	106.8677	106.8677		0	0	0							
Gp	172.176	74.69		0	0	0							
INFCA	173.200825	59.31	6.855E+01	1.187E+04	4.066E+03	2.92							
M4A-OH-LDH	443.371	219.1	6.322E+01	2.803E+04	1.385E+04	2.02							
Mag	231.5386	44.524	2.710E+01	6.275E+03	1.207E+03	5.20							
Maghemite	159.691	29.087		0	0	0							
Portlandite	74.096	33.06		0	0	0							
Py	119.975	23.94	2.941E+00	3.528E+02	7.041E+01	5.01							
Qtz	60.0843	22.688		0	0	0							
T2C-CNASHss	189.2443	80.6		0	0	0							
T5C-CNASHss	190.245375	79.3		0	0	0							
TobH-CNASHss	191.24645	85		0	0	0							
ettringite	1255.147	707.03003	1.531E+01	1.922E+04	1.082E+04	1.78							
hemicarbonat10.5	537.45655	261.264		0	0	0							
monocarbonate	568.4701	261.95801		0	0	0							

Table 3.5-5: Example Simulation of Initially Cured and Saturated Grout.

LP#8-16													
GWB hydration -- water add to achieve 100% sat.				**Mass (g)**	**Volume (mL)**	**Density (g/mL)**	**Volume Fraction**	**Porosity**	**Water Content**	**Saturation**	**Water Addition (g)**	**Water Addition (mol)**	**Comments**
pH	11.414		Inert:	1.747E+06	6.641E+05	2.63	66.4%						Inert B + unreacted binders
pe	-8.347		Minerals:	2.526E+05	9.245E+04	2.73	9.2%						Hydrated minerals
Eh (V)	-0.49	Water (unreacted):		2.434E+05	2.434E+05	1.00	24.3%	**24.3%**	**24.3%**	**100.0%**	1.24E+00	**0**	Compared to measured n=21%
Water mass	243.42	kg	Air:		1.244E+00		0.0%						
3x	**730.3**	kg	Total:	2.243E+06	1.000E+06	**2.24**	100.0%						
-2x	**-486.8**	kg											
halite	**6.5723**	mmol	9.000E-03	mmol									
Phase	**MW (g/mol)**	**MV (mL/mol)**	**Moles**	**Mass (g)**	**Volume (mL)**	**Density (g/mL)**							
5CA	172.205675	57.3	1.066E+03	1.836E+05	6.108E+04	3.01							
AlOHmic	78.0055	31.956	4.215E+01	3.288E+03	1.347E+03	2.44							
Brc	58.328	24.63		0	0	0							
C4AH13	560.491	274.47001		0	0	0							
Cal	100.0911	36.934	1.794E-03	1.796E-01	6.626E-02	2.71							
Fe-ettringite	1312.878	717.55997		0	0	0							
Ferrihydrite	106.8677	106.8677		0	0	0							
Gp	172.176	74.69		0	0	0							
INFCA	173.200825	59.31	6.870E+01	1.190E+04	4.075E+03	2.92							
M4A-OH-LDH	443.371	219.1	6.322E+01	2.803E+04	1.385E+04	2.02							
Mag	231.5386	44.524	2.710E+01	6.275E+03	1.207E+03	5.20							
Maghemite	159.691	29.087		0	0	0							
Portlandite	74.096	33.06		0	0	0							
Py	119.975	23.94	2.941E+00	3.528E+02	7.041E+01	5.01							
Qtz	60.0843	22.688		0	0	0							
T2C-CNASHss	189.2443	80.6		0	0	0							
T5C-CNASHss	190.245375	79.3		0	0	0							
TobH-CNASHss	191.24645	85		0	0	0							
ettringite	1255.147	707.03003	1.530E+01	1.920E+04	1.082E+04	1.78							
hemicarbonat10.5	537.45655	261.264		0	0	0							
monocarbonate	568.4701	261.95801		0	0	0							

4.0 CHEMICAL EVOLUTION OF GROUT AND CONCRETE

After initial curing and saturation, the chemical composition of each cementitious material is expected to slowly evolve due to advective and/or diffusive exchange of pore solution with the surrounding environment. Advection-based chemical evolution is simulated by removing the pore solution, replacing it with soil moisture (vadose zone) or groundwater (saturated zone), re-equilibrating with solid phases, and repeating the process many times. Each iteration is referred to a "pore volume" (PV) exchange and functions as pseudo-time. The actual timing of the evolving grout chemistry depends on the scale of the porous medium and Darcy velocity through time. This process is also referred to as reaction path modeling. Diffusion-based chemical evolution is simulated with a diffusion-only reactive transport model.

4.1 Advection-Based Chemical Evolution

Reaction path modeling with GWB React is performed on grouts and concrete through 10,000 pore volume exchanges. Because the porosities of these materials vary, 10,000 pore volume exchanges correspond to different infiltrate volumes. Table 4.1-1 summarizes the porosities, water contents, and saturations simulated for the initially cured cementitious materials (Section 3.5 and Appendix B). These materials are assumed to fully saturate upon contact with the surrounding environment and remain saturated during the reaction path. Porosity is assumed to be invariant.

Table 4.1-1: Simulated Porosity, Water Content, and Saturation in Initially Cured Materials.

Material	Porosity	Water Content	Saturation
LP#8-16 grout	24.3%	18.5%	76.0%
ZB-FF-8-D grout	24.0%	20.8%	86.9%
Clean Cap grout	50.6%	41.5%	82.1%
B3000-6-0-2-A concrete	11.9%	5.6%	46.7%

Mineral composition, pH, and Eh are plotted for each baseline and sensitivity case considered:

1) LP#8-16 grout: Figure 4.1-1 through Figure 4.1-3
2) ZB-FF-8-D grout: Figure 4.1-4 through Figure 4.1-6
3) Clean Cap grout: Figure 4.1-7 through Figure 4.1-9
4) B3000-6-0-2-A concrete: Figure 4.1-10 through Figure 4.1-12
5) LP#8-16 grout with 100% hydration of binders: Figure 4.1-13 through Figure 4.1-15
6) LP#8-16 grout with CSHQ solid solution model: Figure 4.1-16 through Figure 4.1-18
7) LP#8-16 grout with soil moisture equilibrated with atmospheric CO_2 at 0.000410 atm: Figure 4.1-19 through Figure 4.1-21
8) LP#8-16 grout with a 90% groundwater / 10% soil moisture infiltrate: Figure 4.1-22 through Figure 4.1-24

Figure 4.1-1: Mineral Evolution of LP#8-16 Through 10,000 Pore Volumes.

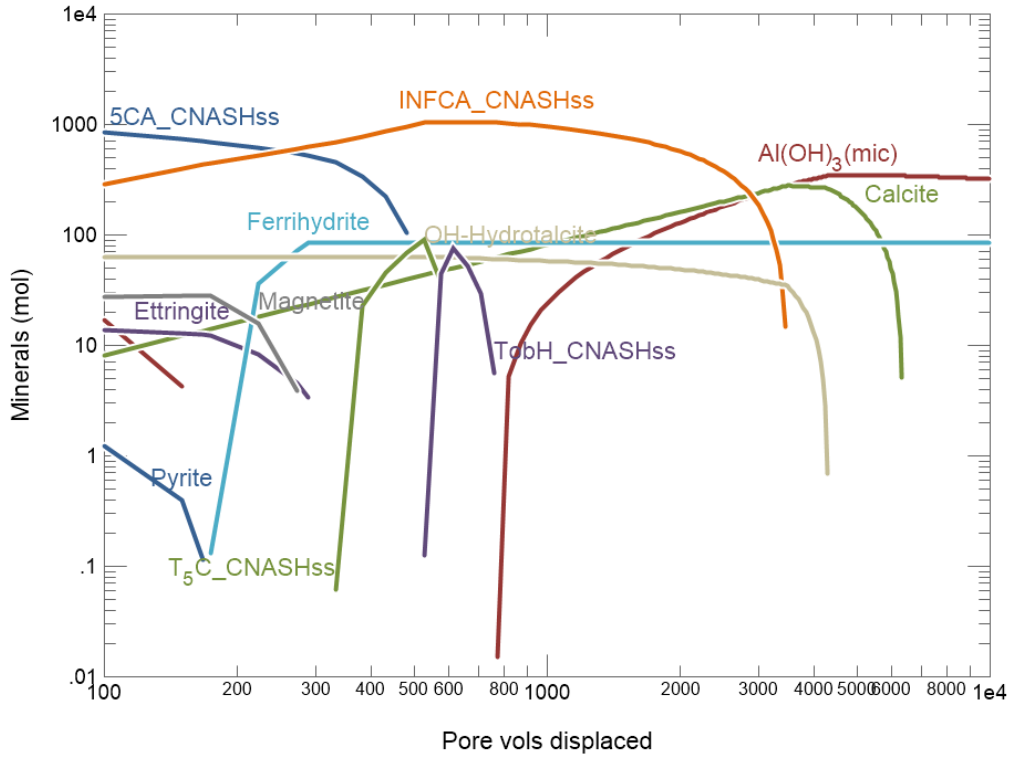

Figure 4.1-2: pH Evolution of LP#8-16 Through 10,000 Pore Volumes.

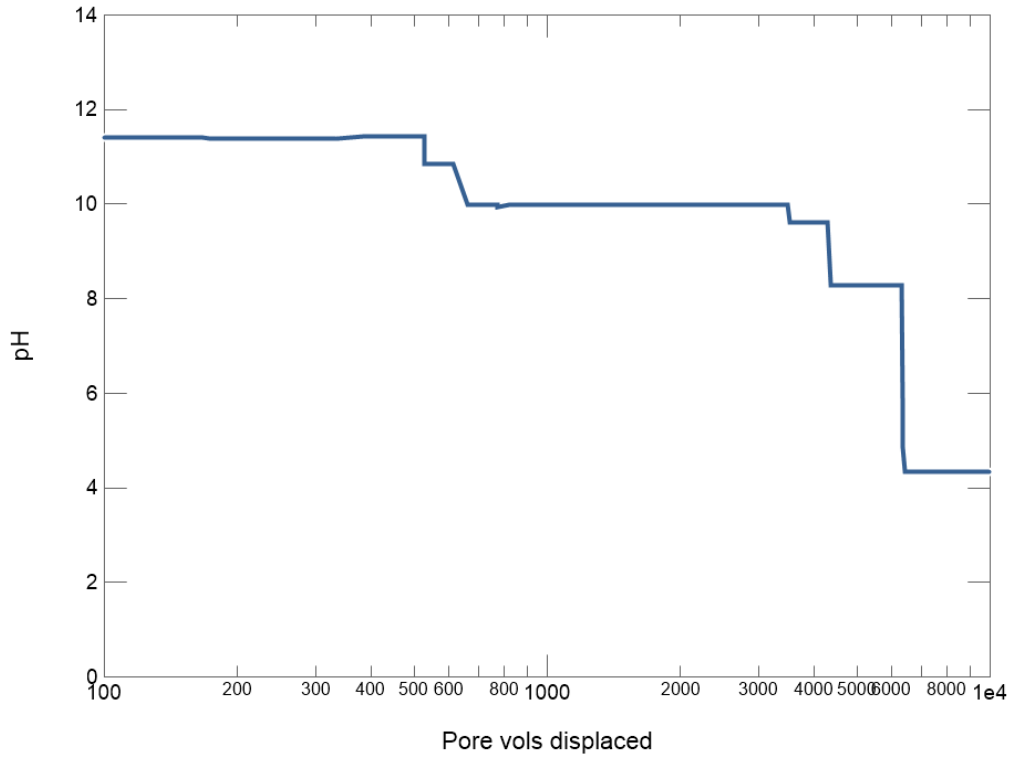

Figure 4.1-3: Eh Evolution of LP#8-16 Through 10,000 Pore Volumes.

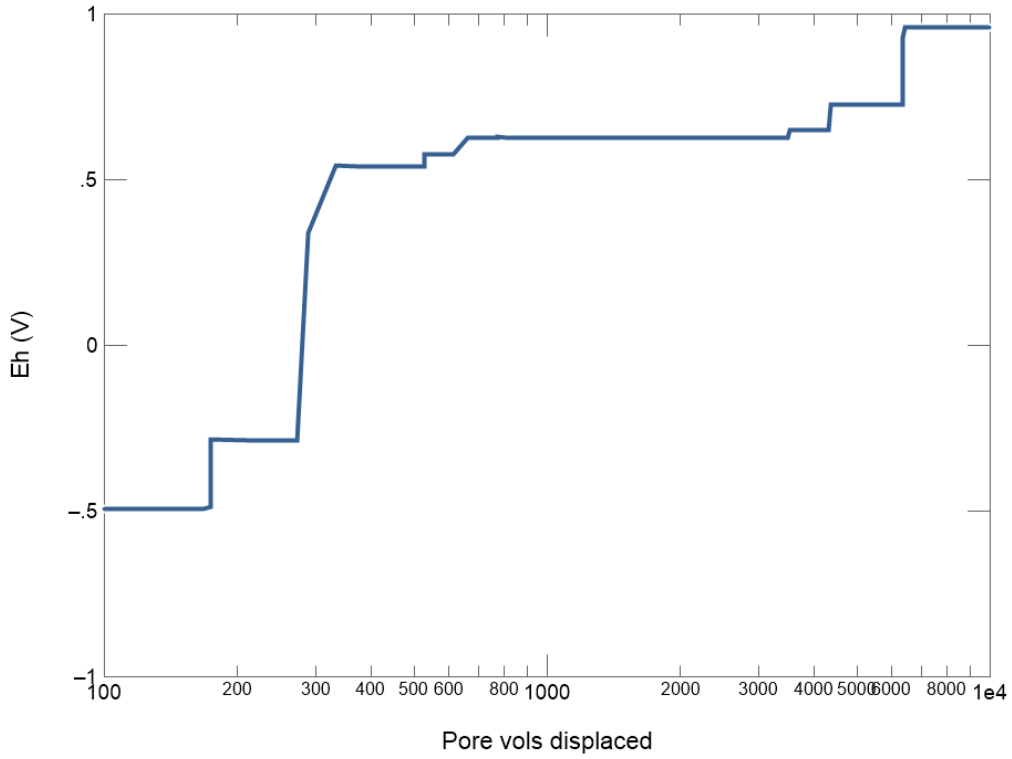

Figure 4.1-4: Mineral Evolution of ZB-FF-8-D Through 10,000 Pore Volumes.

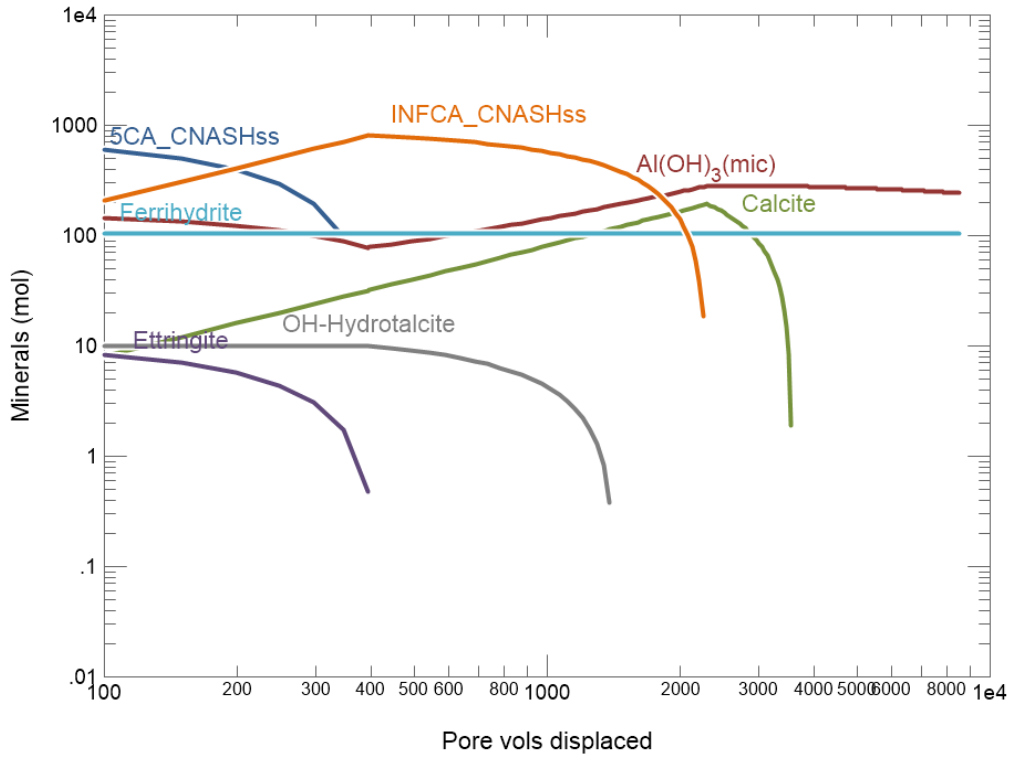

Figure 4.1-5: pH Evolution of ZB-FF-8-D Through 10,000 Pore Volumes.

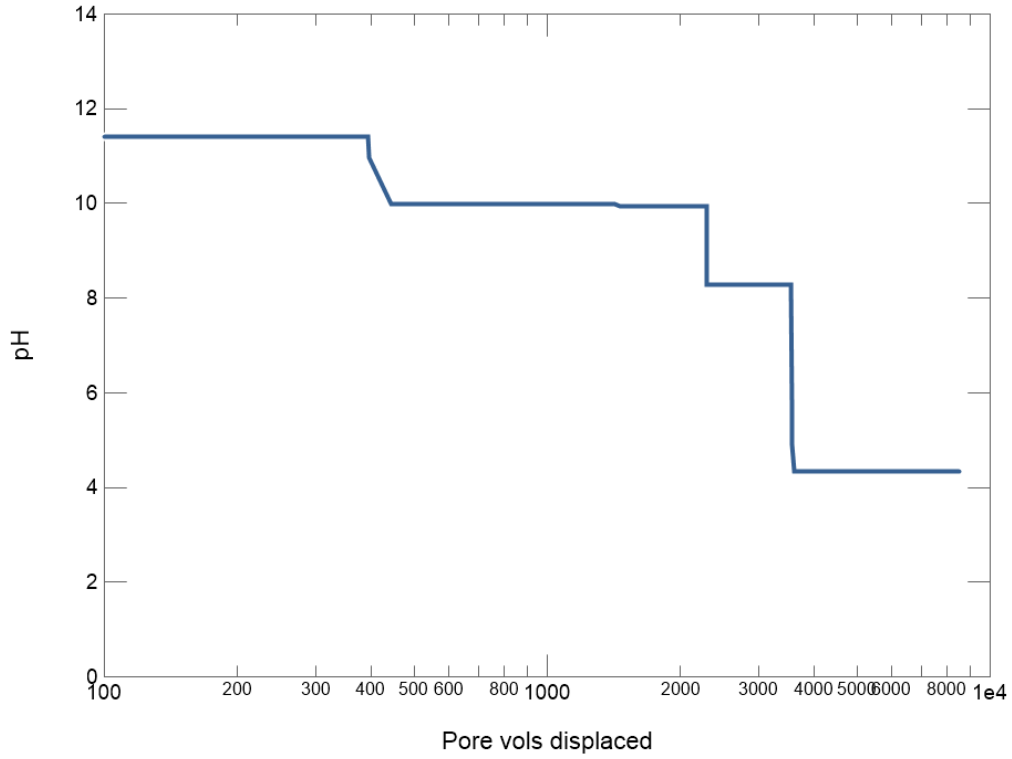

Figure 4.1-6: Eh Evolution of ZB-FF-8-D Through 10,000 Pore Volumes.

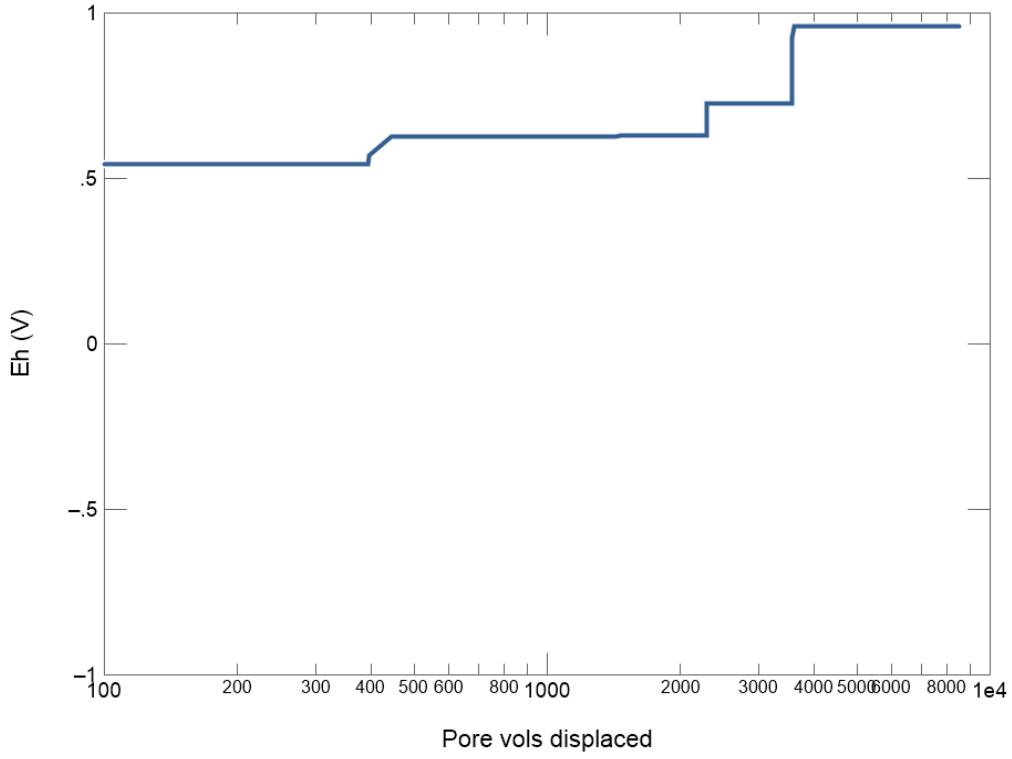

Figure 4.1-7: Mineral Evolution of Clean Cap Through 10,000 Pore Volumes.

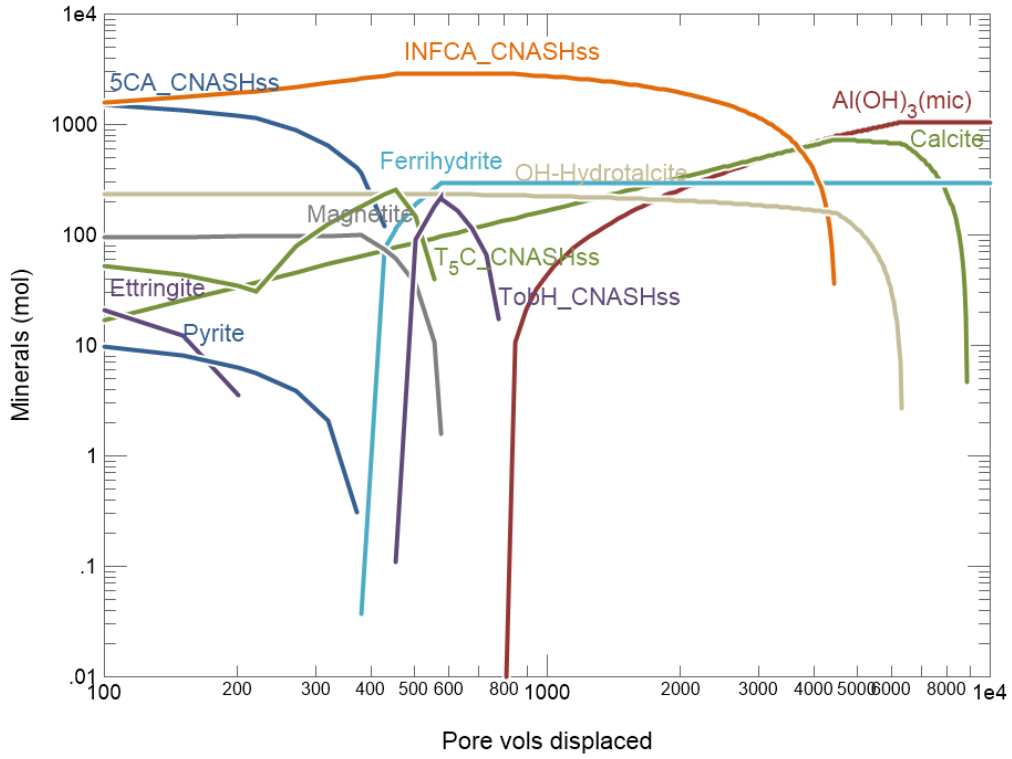

Figure 4.1-8: pH Evolution of Clean Cap Through 10,000 Pore Volumes.

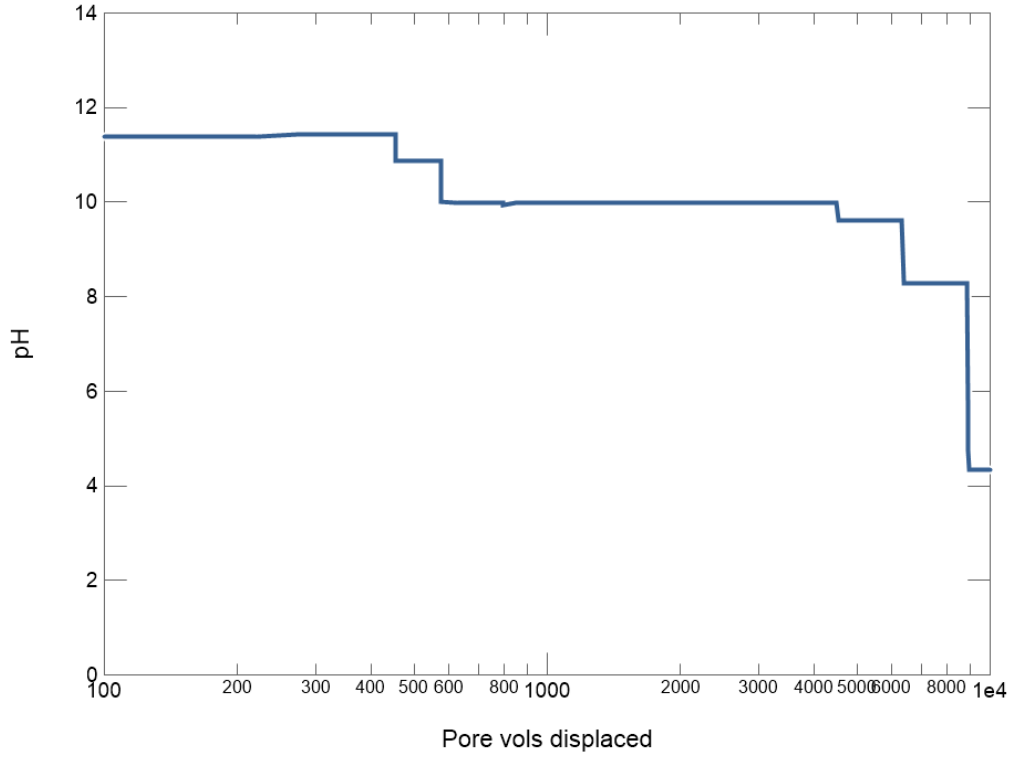

Figure 4.1-9: Eh Evolution of Clean Cap Through 10,000 Pore Volumes.

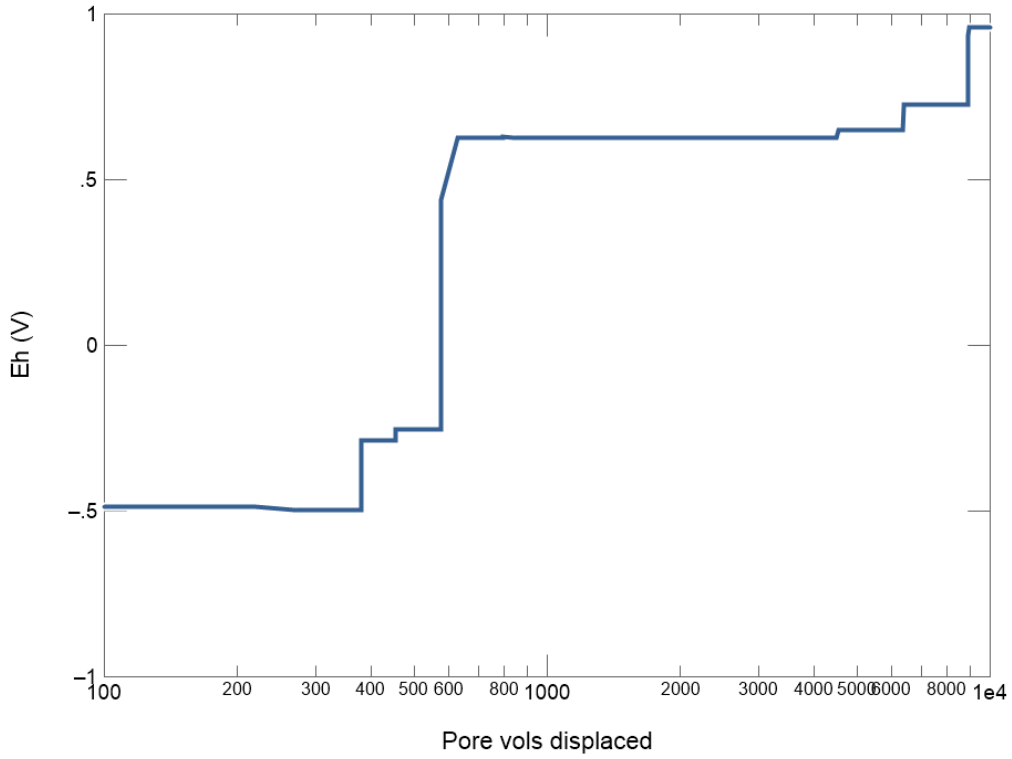

Figure 4.1-10: Mineral Evolution of Concrete Through 10,000 Pore Volumes.

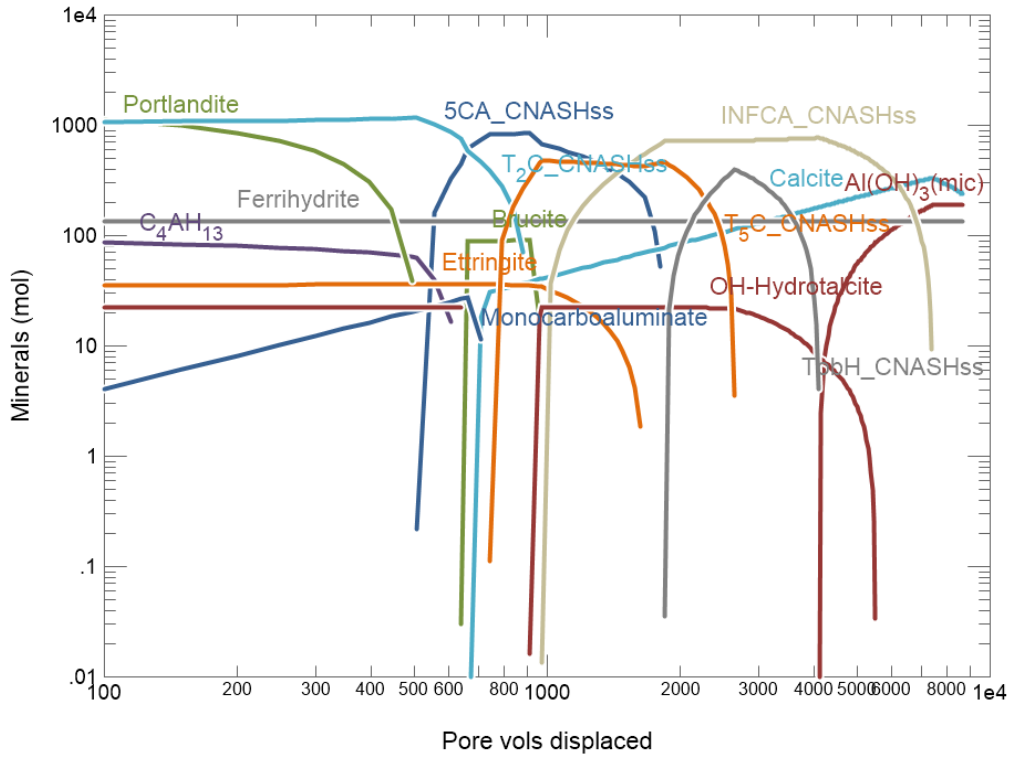

Figure 4.1-11: pH Evolution of Concrete Through 10,000 Pore Volumes.

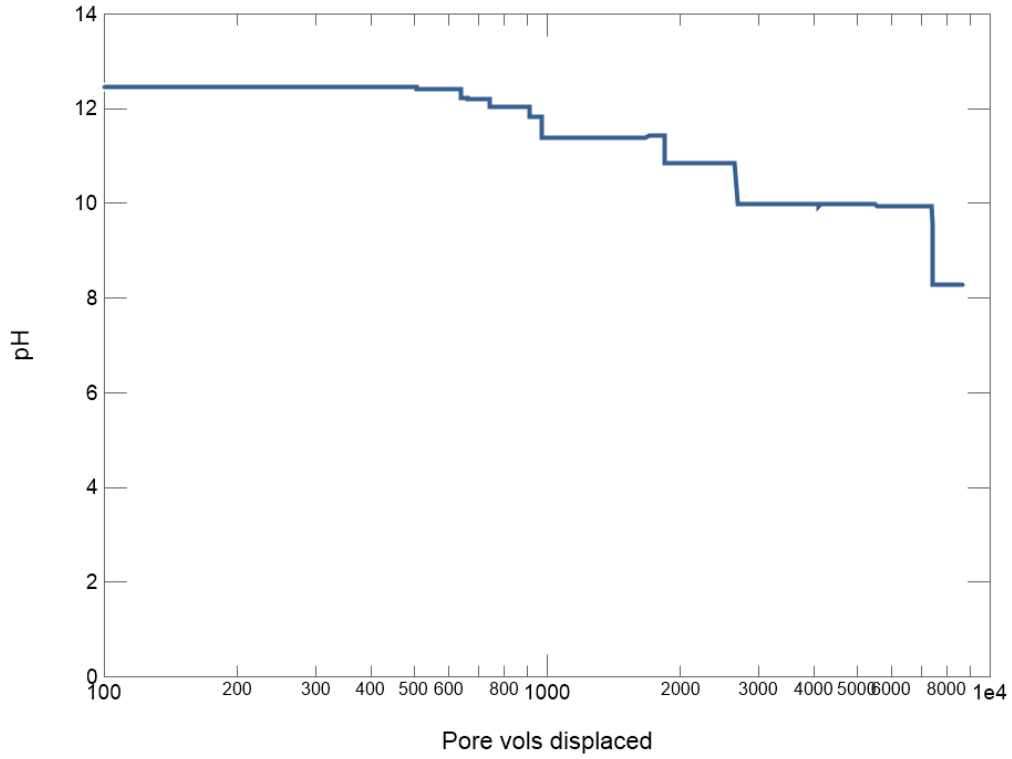

Figure 4.1-12: Eh Evolution of Concrete Through 10,000 Pore Volumes.

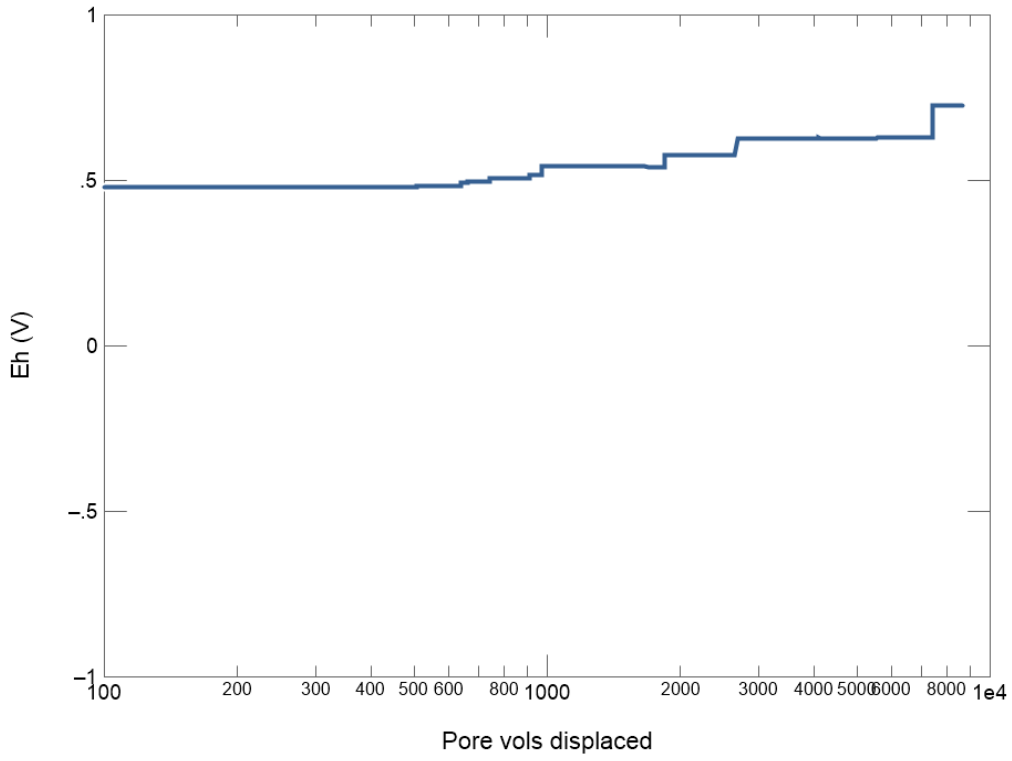

Figure 4.1-13: Mineral Evolution of LP#8-16 Assuming 100% Hydration.

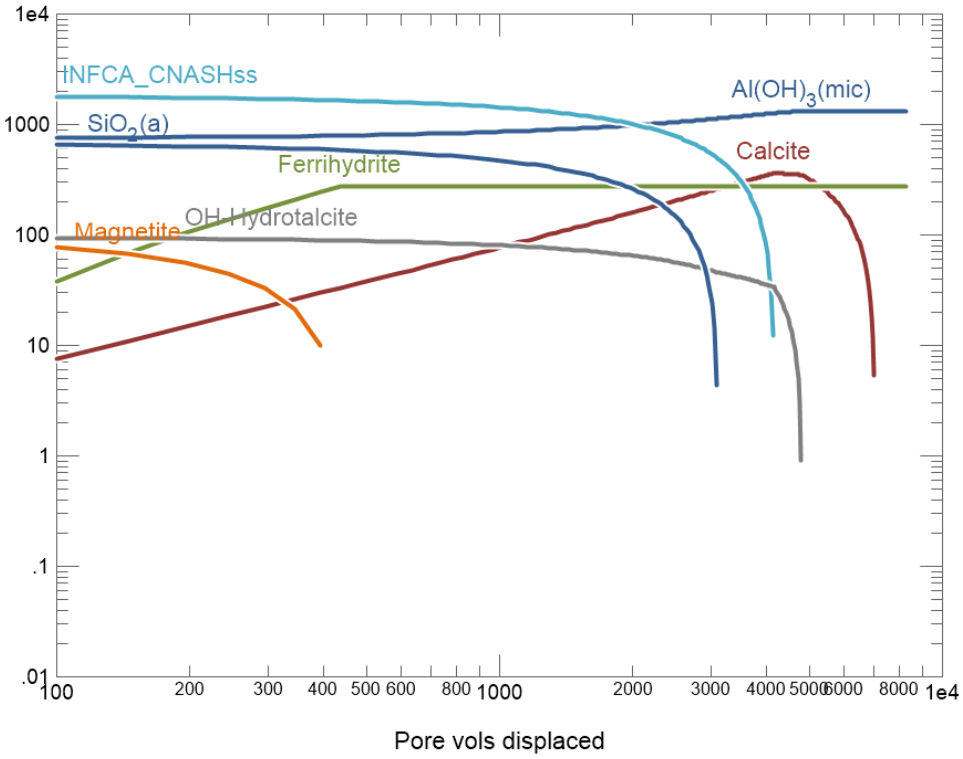

Figure 4.1-14: pH Evolution of LP#8-16 Assuming 100% Hydration.

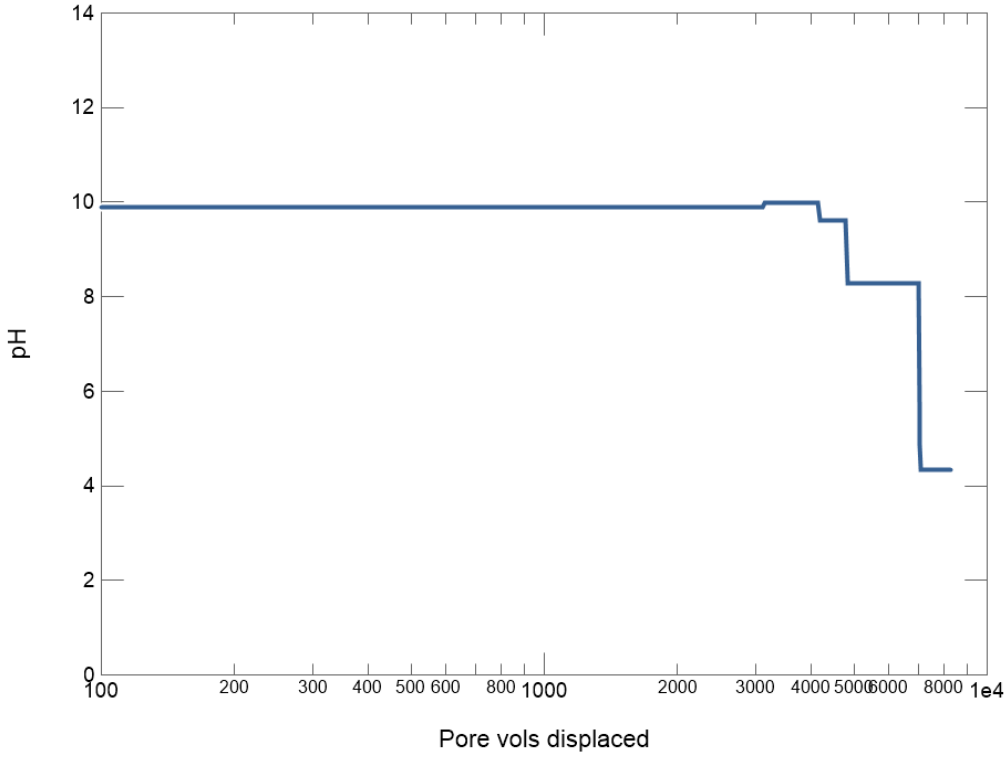

Figure 4.1-15: Eh Evolution of LP#8-16 Assuming 100% Hydration.

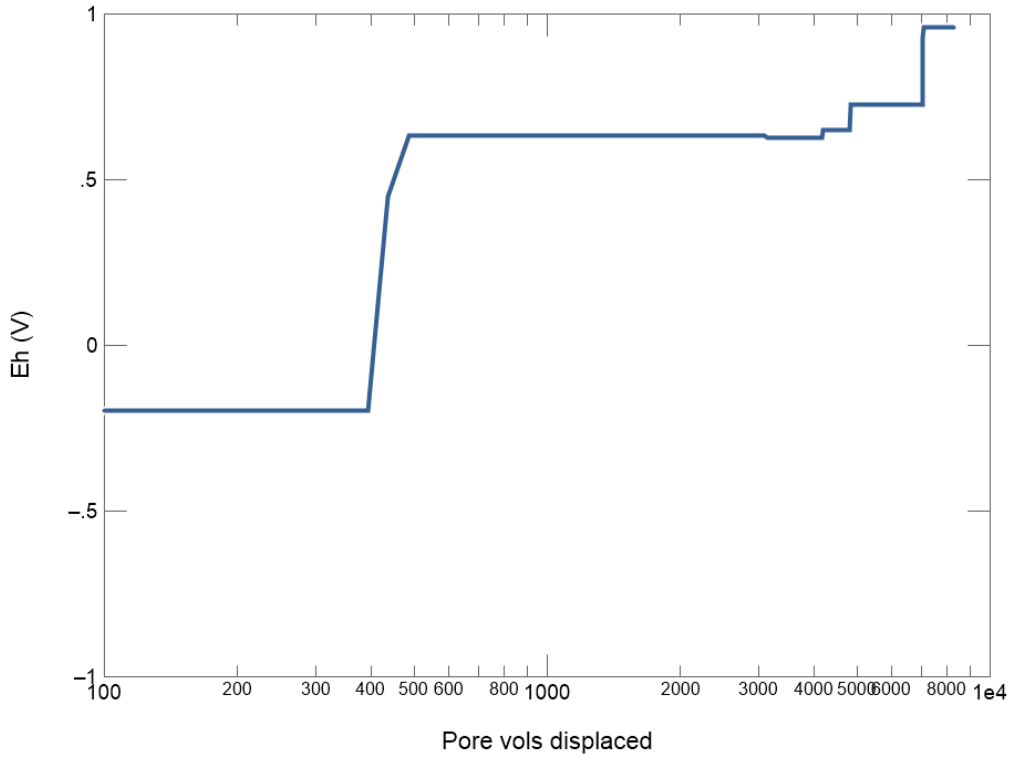

Figure 4.1-16: Mineral Evolution of LP#8-16 Assuming CSHQ Solid Solution Model.

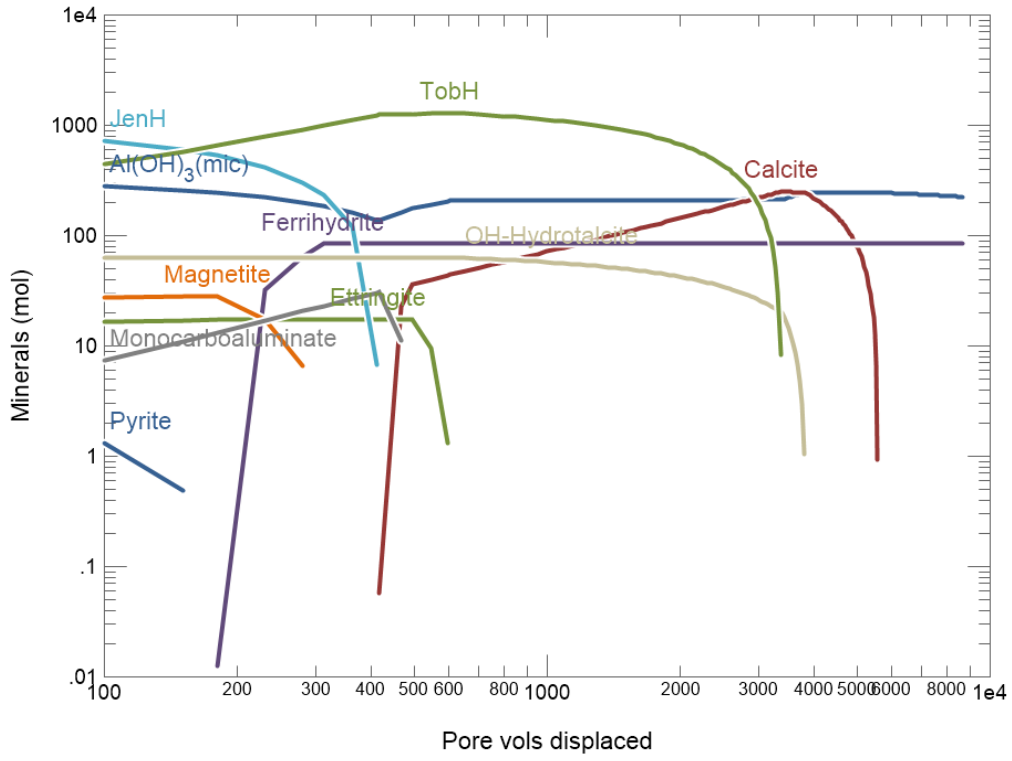

Figure 4.1-17: pH Evolution of LP#8-16 Assuming CSHQ Solid Solution Model.

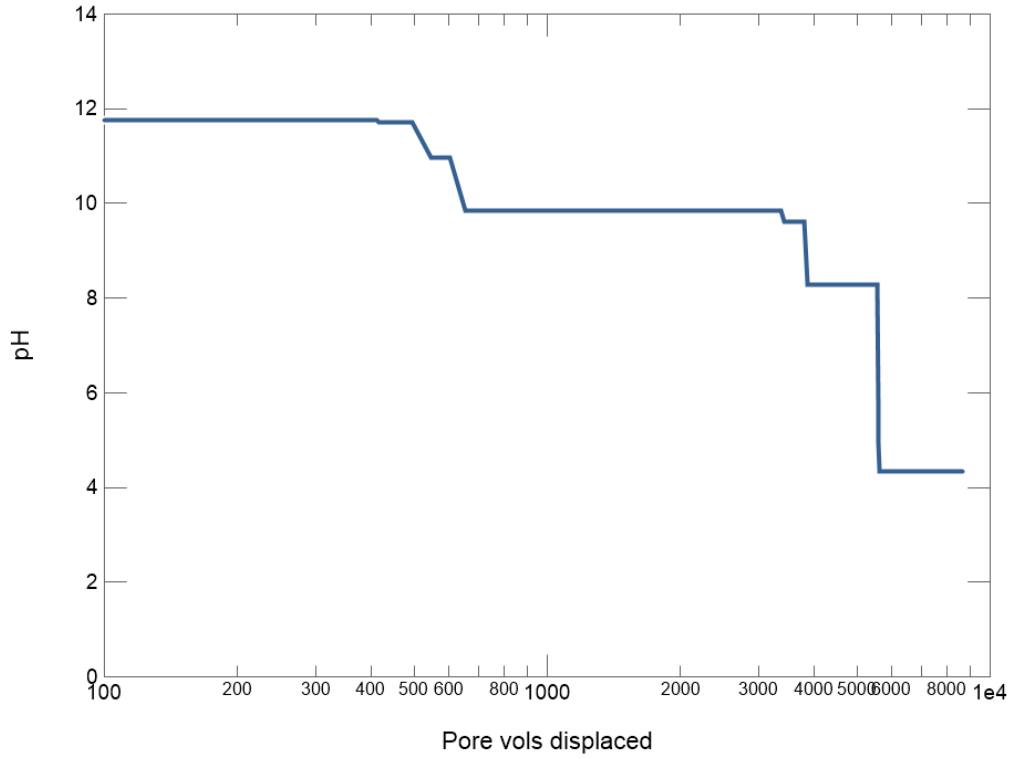

Figure 4.1-18: Eh Evolution of LP#8-16 Assuming CSHQ Solid Solution Model.

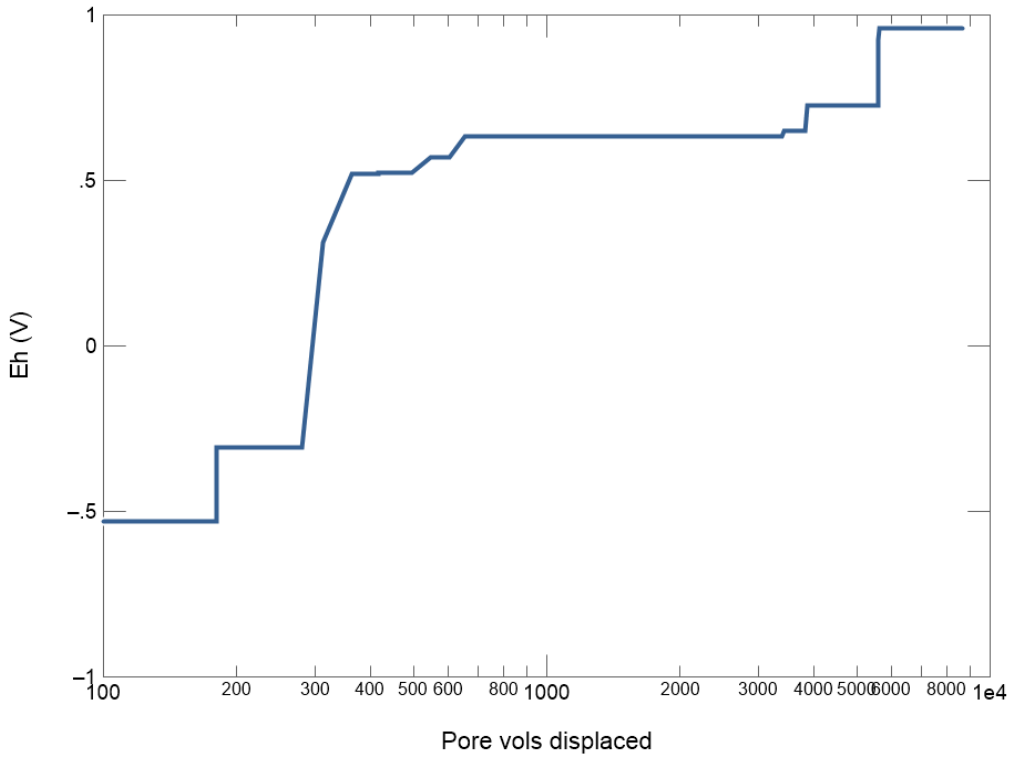

Figure 4.1-19: Mineral Evolution of LP#8-16 Assuming PCO2 = 0.000410 atm.

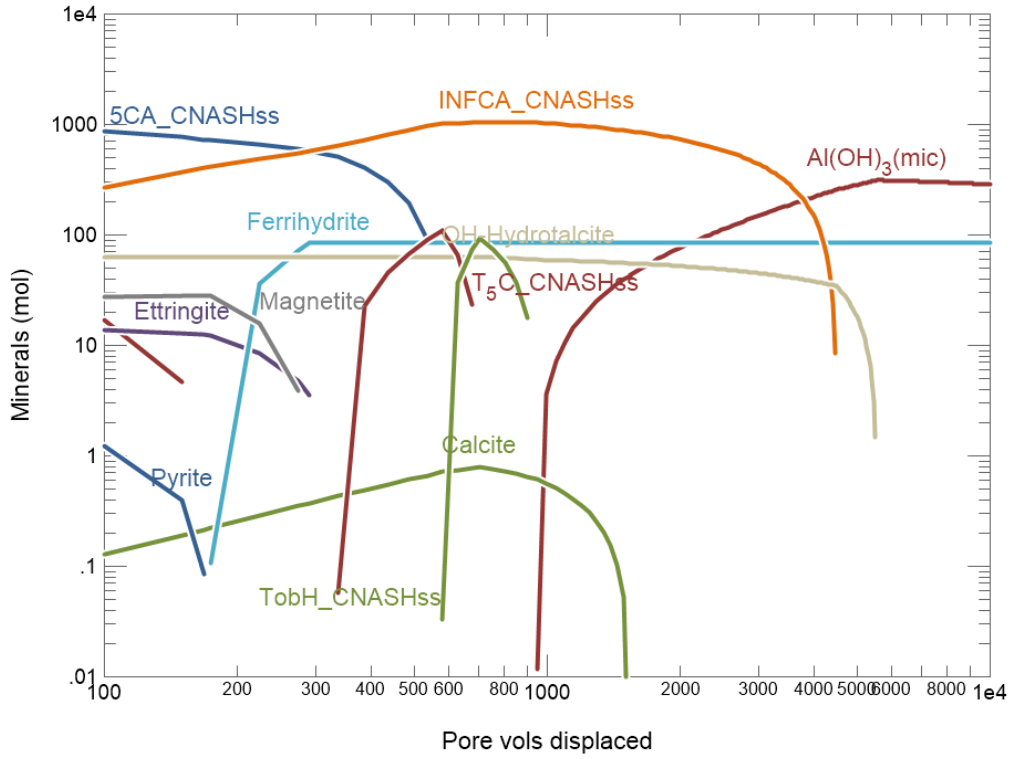

Figure 4.1-20: pH Evolution of LP#8-16 Assuming PCO2 = 0.000410 atm.

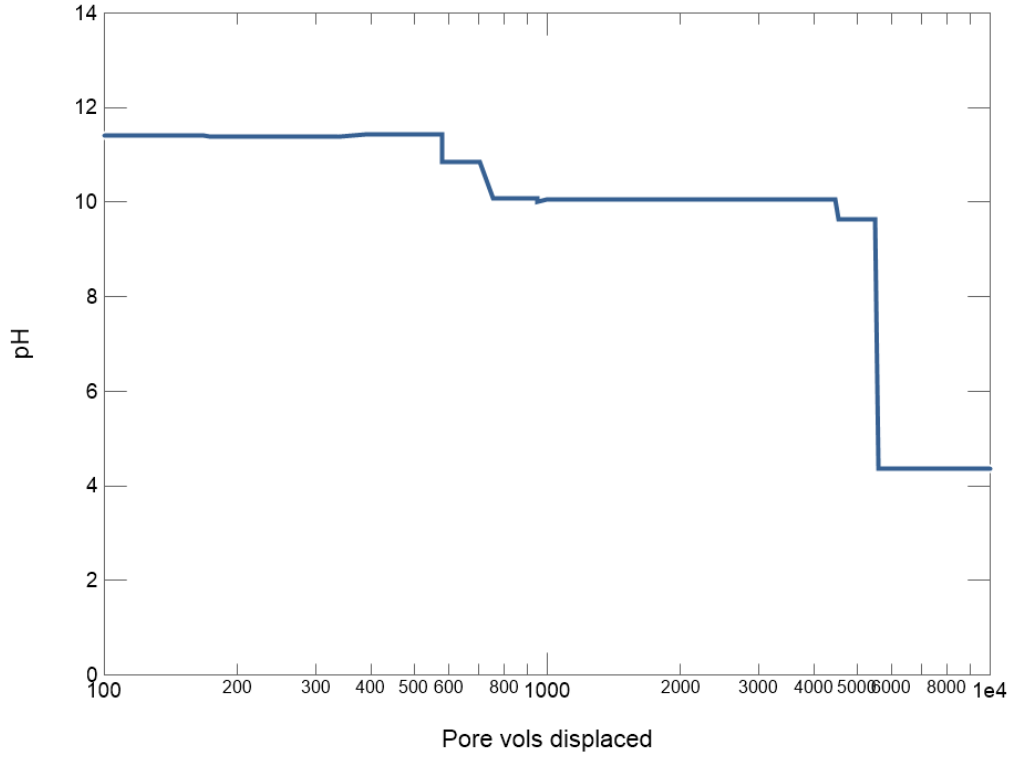

Figure 4.1-21: Eh Evolution of LP#8-16 Assuming PCO2 = 0.000410 atm.

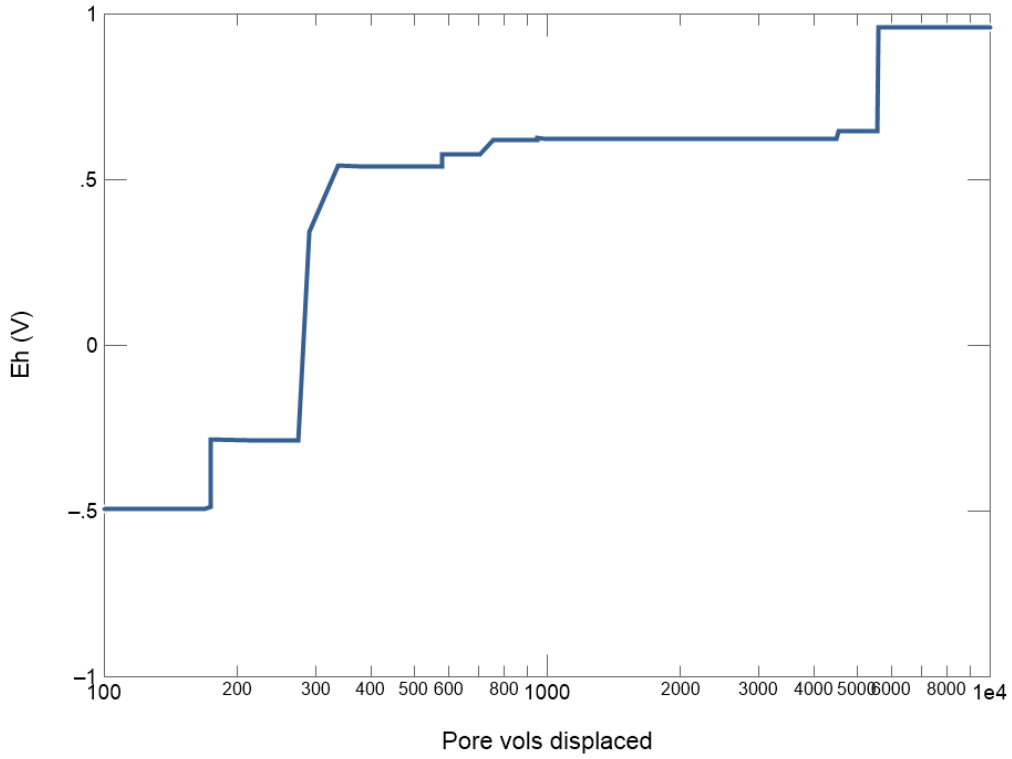

Figure 4.1-22: Mineral Evolution of LP#8-16 Assuming Submerged Tank.

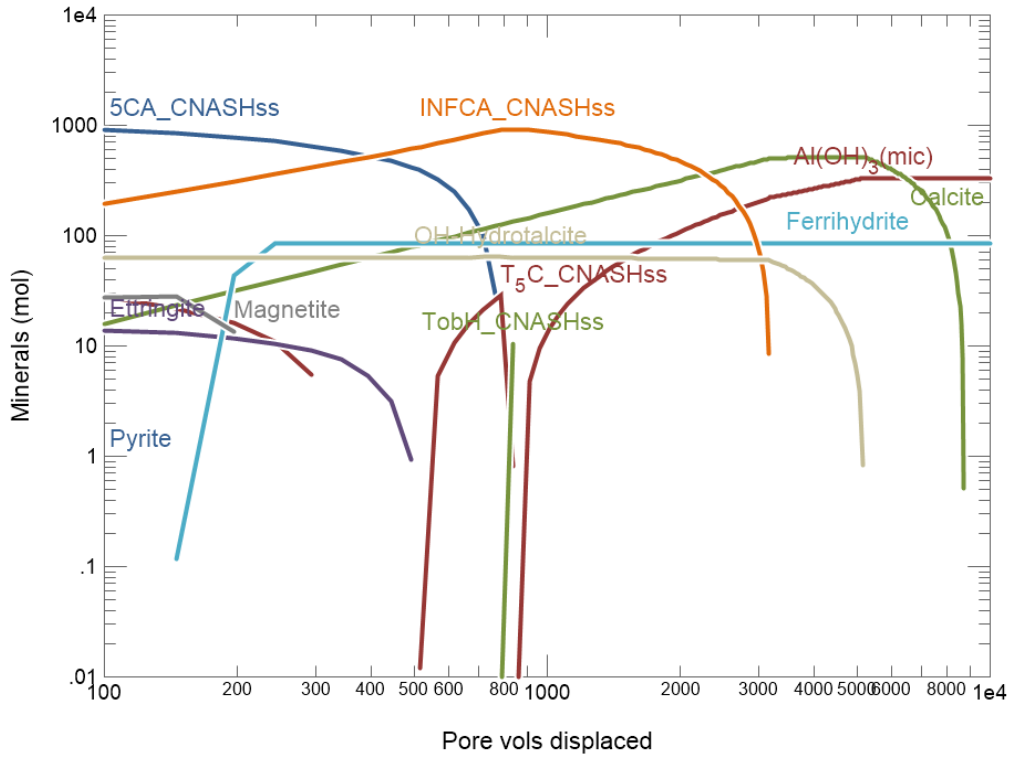

Figure 4.1-23: pH Evolution of LP#8-16 Assuming Submerged Tank.

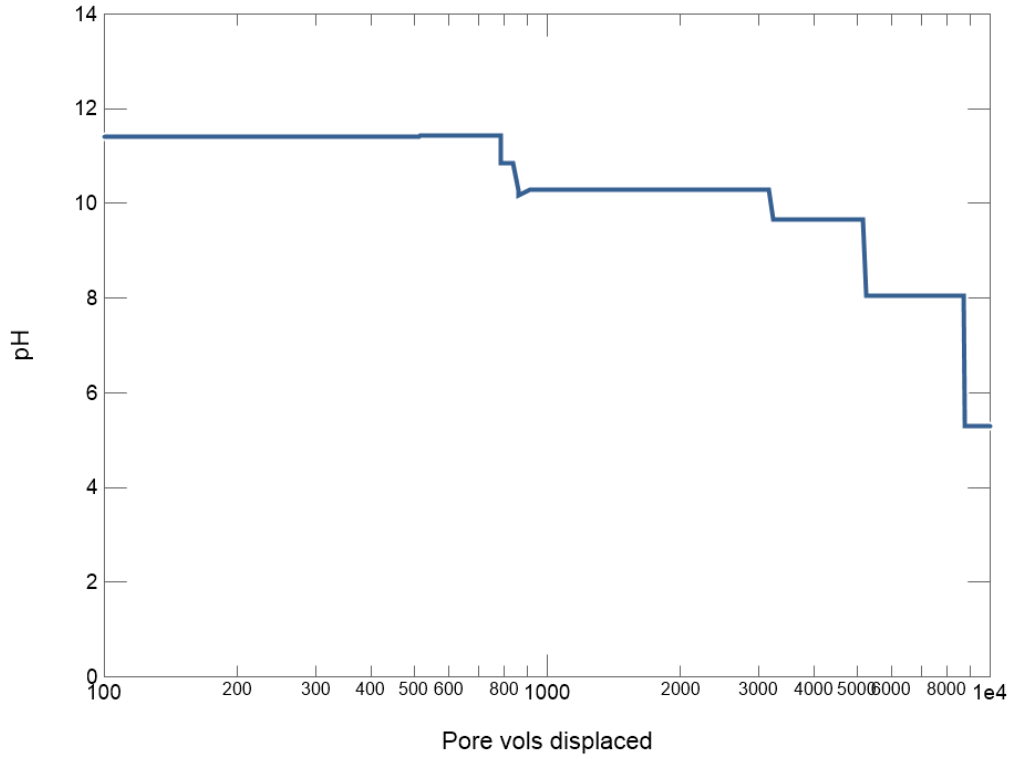

Figure 4.1-24: Eh Evolution of LP#8-16 Assuming Submerged Tank.

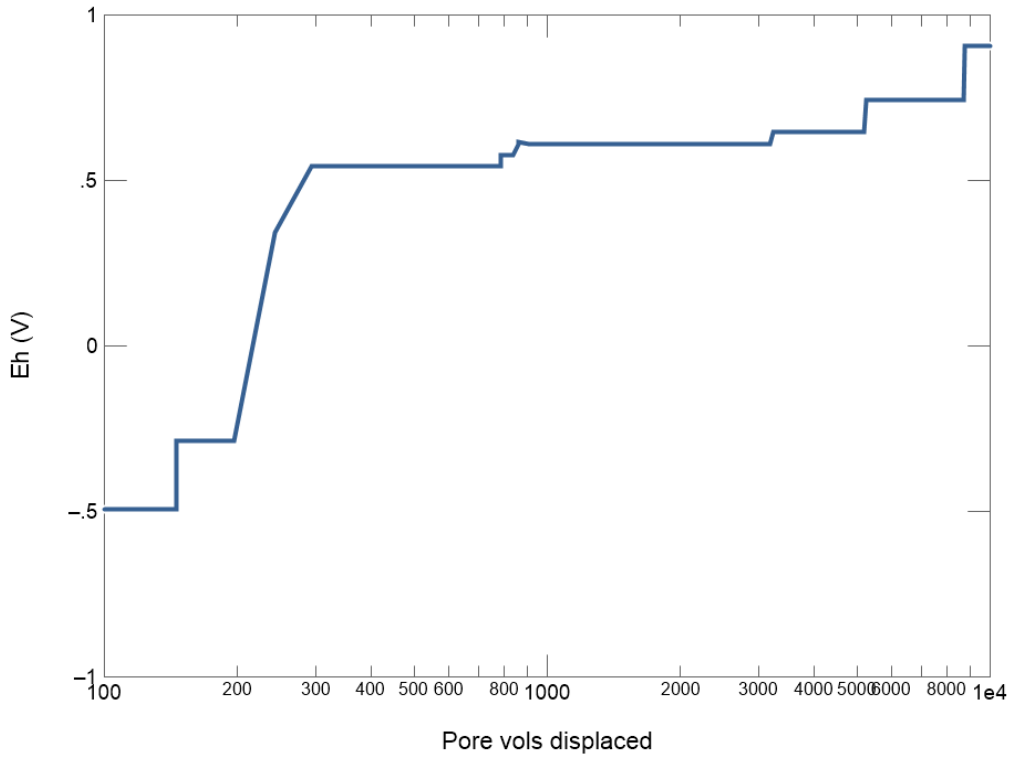

Cases 1) through 4) are baseline simulations assuming 100% cement / 70% slag / 20% fly ash hydration based on the parametric study described in Appendix A, which demonstrated that the best match to general mineralogy and pH data was achieved with these hydrations. These first four cases also assume the CNASH solid solution model for $C\text{-}S\text{-}H$ gel, an above-ground tank (soil moisture infiltrate), and soil moisture equilibrated with gaseous CO_2 at a partial pressure of 0.01 atm. The sensitivity cases use LP#8-18 as the reference material and examine the effects of altering the degree of hydration, solid solution model, P_{CO_2}, and infiltrate composition. Figure 4.1-1 through Figure 4.1-24 use a logarithmic scale starting at 100 pore volumes. Figure 4.1-25 through Figure 4.1-27 for the reference LP#8-16 grout show that minimal pH and Eh variation occurs prior to 100 pore volumes. Thus, the former figures do not obscure important phenomena with respect to this study.

Figure 4.1-25: Mineral Evolution of LP#8-16 using Linear Pore Volume Scale.

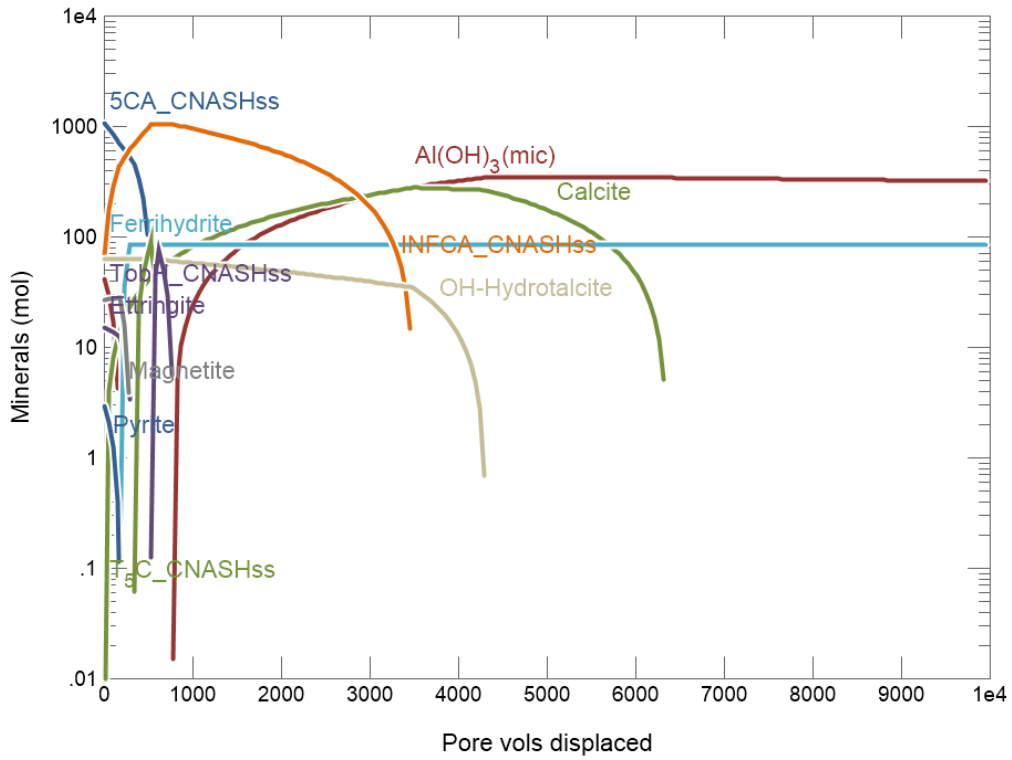

Figure 4.1-26: pH Evolution of LP#8-16 using Linear Pore Volume Scale.

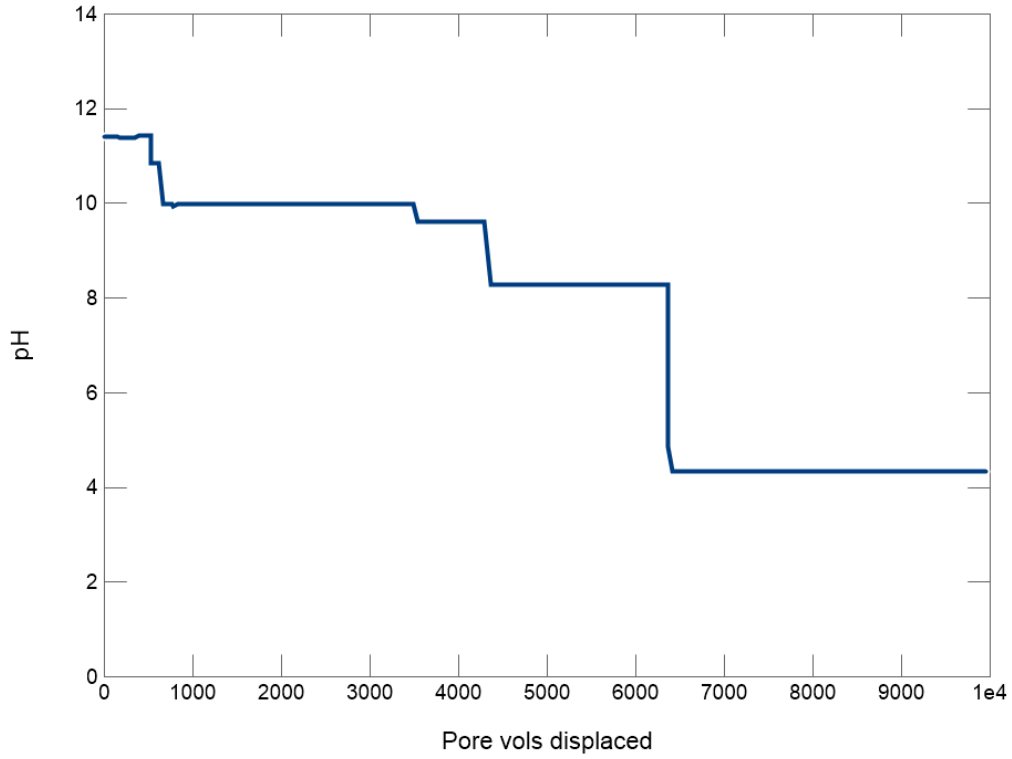

Figure 4.1-27: Eh Evolution of LP#8-16 using Linear Pore Volume Scale.

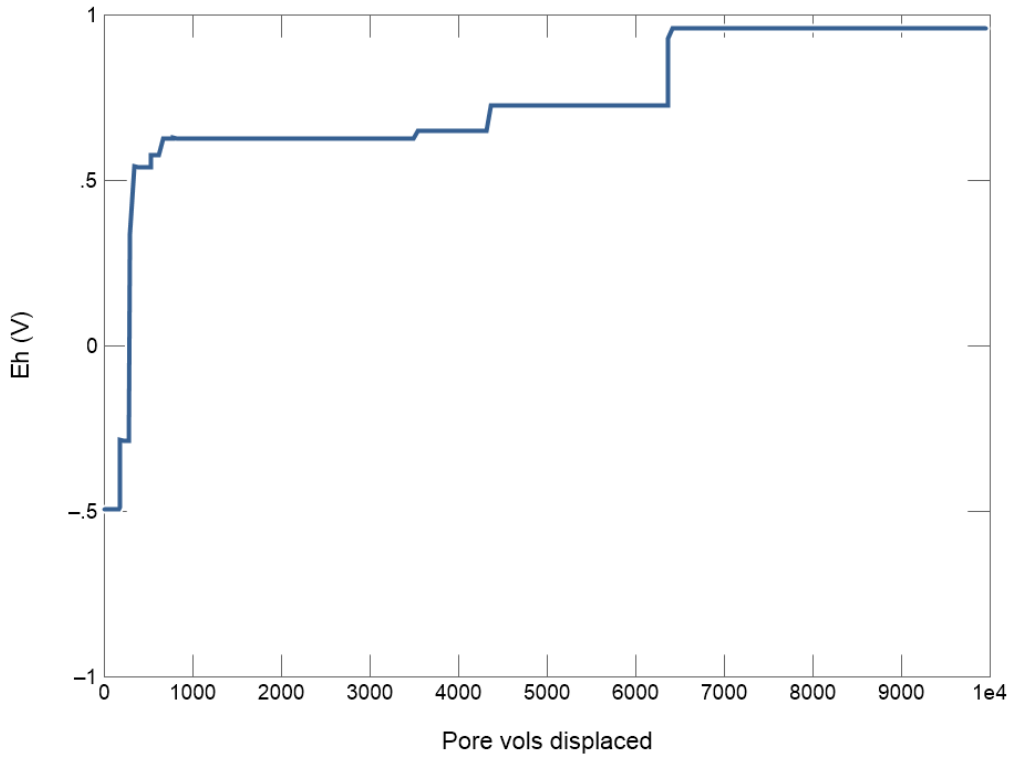

General trends observed in the chemical evolution plots include:

1) The composition of $C\text{-}S\text{-}H$ gel transitioning from higher to lower Ca/Si minerals, consistent with leaching of the more soluble calcium.
2) Carbonation, that is, calcite formation due to reaction with dissolved CO_2.
3) Distinct pH levels due to different buffers as the mineral composition evolves. The major plateaus are generally
    a. 12.5 = Portlandite, if initially present (concrete)
    b. 11.4 = 5CA, if initially present
    c. 10.0 = INFCA
    d. 8.3 = Calcite
    e. 4.3 = infiltrate

    with shorter-lived plateaus interspersed. The simulated pH stairsteps are an artifact of approximating the $C\text{-}S\text{-}H$ / $C\text{-}A\text{-}S\text{-}H$ solid solution with a set of five distinct minerals. The actual pH transient is expected to be smoother.
4) For reducing grouts, transition to positive Eh within a few hundred pore volumes. The simulated transitions for reducing grouts occur about 15% sooner than calculated based on the initial reduction capacity and dissolved oxygen concentration of the infiltrate. This effect is presumably due to magnetite dissolution and leaching, a non-oxidative loss of reduction capacity. The bias is accepted as a modest conservatism relative to SRNL-STI-2012-00404.

The sensitivity cases provide the following insights:

1) 100% hydration eliminates the pH = 11.4 plateau due to the lower initial Ca/Si ratio and absence of 5CA. The transition to Calcite buffered pH at 8.3 is delayed and less conservative than the baseline assumption of partial hydration.
2) Replacing the $C\text{-}S\text{-}H$ / $C\text{-}A\text{-}S\text{-}H$ solid solution model with the CSHQ model has a minor effect on pH levels and pore volume transitions.
3) Lowering P_{CO_2} from 0.01 atm (soil gas) to 0.00041 atm (0.000410 atm, atmospheric CO_2) eliminates calcite buffering at pH = 8.3, with other effects being more minor.
4) Replacing soil moisture infiltrate with a 90% groundwater / 10% soil moisture blend delays pH transitions and accelerates the Eh transition.

Thus, the baseline configuration is generally like or more conservative than these alternative configurations, the Eh transition being an exception.

4.2 Diffusion-Based Chemical Evolution

Diffusion may be the dominant transport mechanism for thinner and/or lower permeability cementitious materials. For example, the concrete barriers surrounding annulus grout, steel liners, and fill grout are likely to evolve primarily via diffusive leaching to the surrounding environment, at least initially, whereas chemical evolutions of the much thicker fill grouts in whole are more likely to occur through advection. Nonetheless, both concrete and grouts are analyzed in this section. During preliminary software testing on a simple Portlandite dissolution and carbonation simulation, GWB exhibited problems with mineral phase disappearance and numerical results did not align with expectations. These issues were not encountered with PHREEQC so it is used to simulate diffusion-based chemical evolution. Because a code-to-code comparison is not feasible, Appendix C provides an alternative independent calculation of carbonation, dissolution, and diffusive transport for a simplified mineral system. The analytic solution and PHREEQC results are in close agreement, which provides confidence in the results for more complex mineral systems analyzed with PHREEQC.

The specific baseline and sensitivity cases considered are:

1) B3000-6-0-2-A concrete exposed to soil moisture through 20k years (Figure 4.2-1 through Figure 4.2-8)
2) LP#8-16 grout exposed to soil moisture through 10k years (Figure 4.2-9 through Figure 4.2-14)
3) ZB-FF-8-D grout exposed to soil moisture through 10k years (Figure 4.2-15 through Figure 4.2-20)
4) Clean Cap grout exposed to soil moisture through 10k years (Figure 4.2-21 through Figure 4.2-26)
5) B3000-6-0-2-A concrete exposed to a 90% groundwater / 10% soil moisture blend through 1000 years (Figure 4.2-27 through Figure 4.2-30)

Cases 1) through 4) are baseline simulations representing tanks above the water table. Concrete was simulated past 10,000 years to assess long-term carbonation depth relative to analytic model predictions discussed in Section 7.0. Case 5) tests the sensitivity of concrete evolution to an alternative boundary solution composed primarily of SRS groundwater and representing submerged tank conditions. The material thickness in each case is 30 cm = 0.30 m, or approximately 1 ft. The horizontal axis in Figure 4.2-1 through Figure 4.2-30 indicates distance from the exposure boundary (x) in meters.

Like the advection-based simulations, exposure to soil moisture leads to a gradual conversion of Portlandite (concrete) to high Ca/Si C-S-H to low Ca/Si C-S-H to calcite and finally amorphous silica and aluminum hydroxide. With these mineral changes comes pH lowering, initially from 12.5 (concrete) or 11.4 (grout) to the boundary solution pH (4). Passivation of rebar and corrosion protection typically occurs for $pH \geq 10$. Figure 4.2-8 indicates the $pH = 10$ front in concrete at approximately 2.5 cm (1 in), which is less than the typical thickness of rebar cover and suggests low corrosion rates through 20,000 years. Concrete rebar corrosion is further discussed in Section 7.0. Penetration of the $pH = 10$ front is faster in grouts than concrete due to higher porosities, lower bulk density, and lower Ca/Si ratio.

Figure 4.2-1: Mineral Evolution of B3000-6-0-2-A Concrete at 100 years.

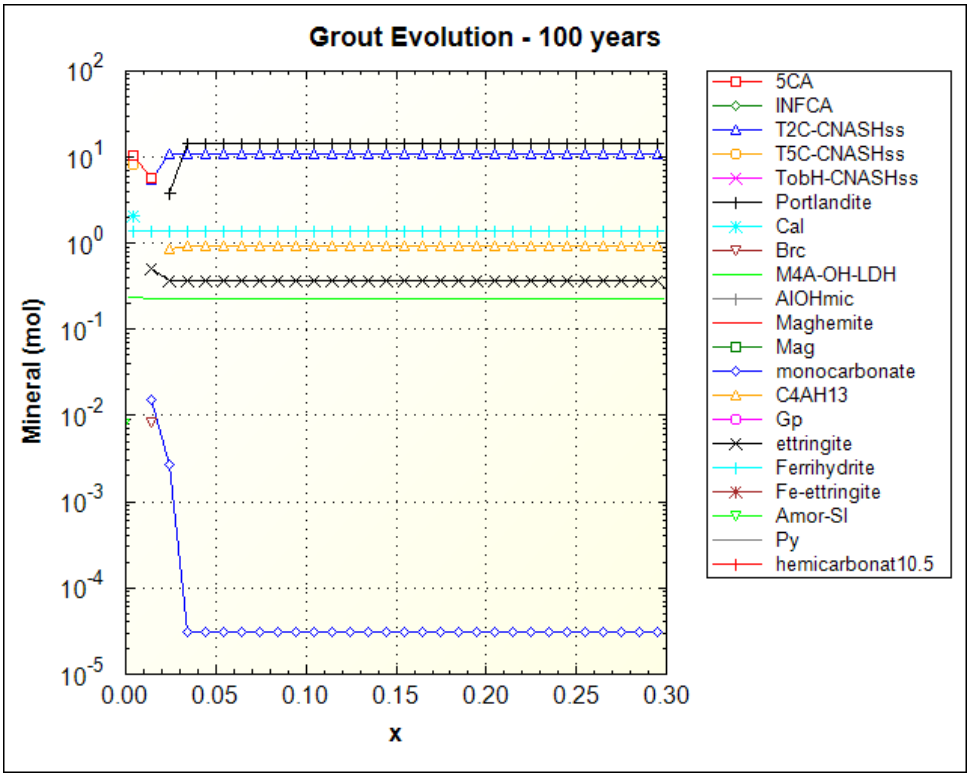

Figure 4.2-2: Mineral Evolution of B3000-6-0-2-A Concrete at 1000 years.

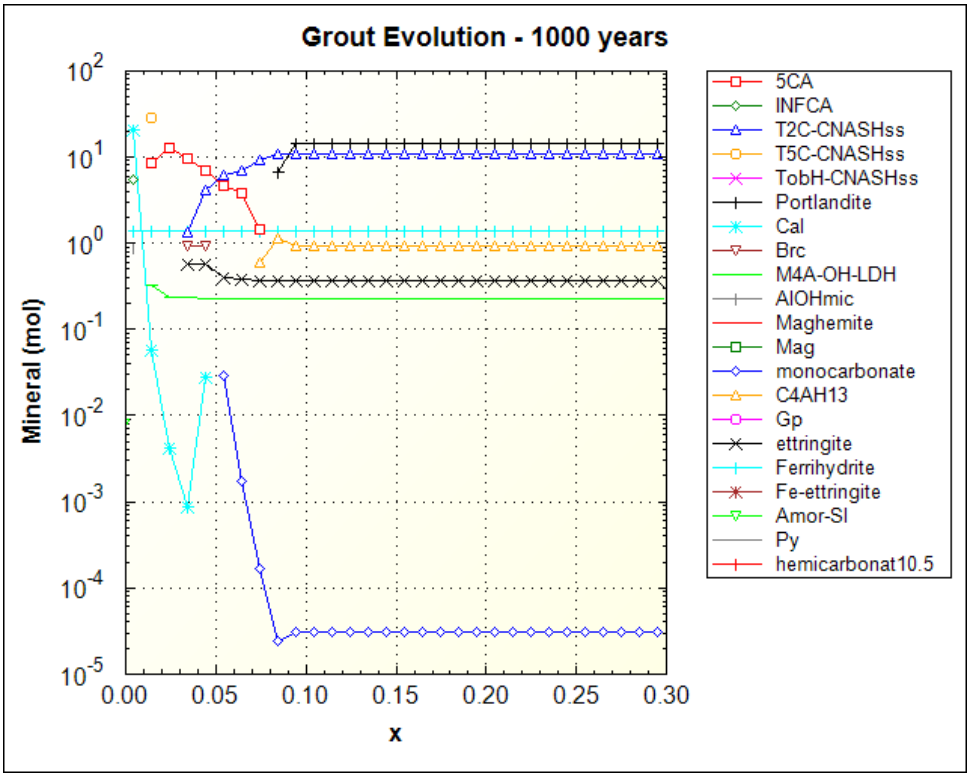

Figure 4.2-3: Mineral Evolution of B3000-6-0-2-A Concrete at 10,000 years.

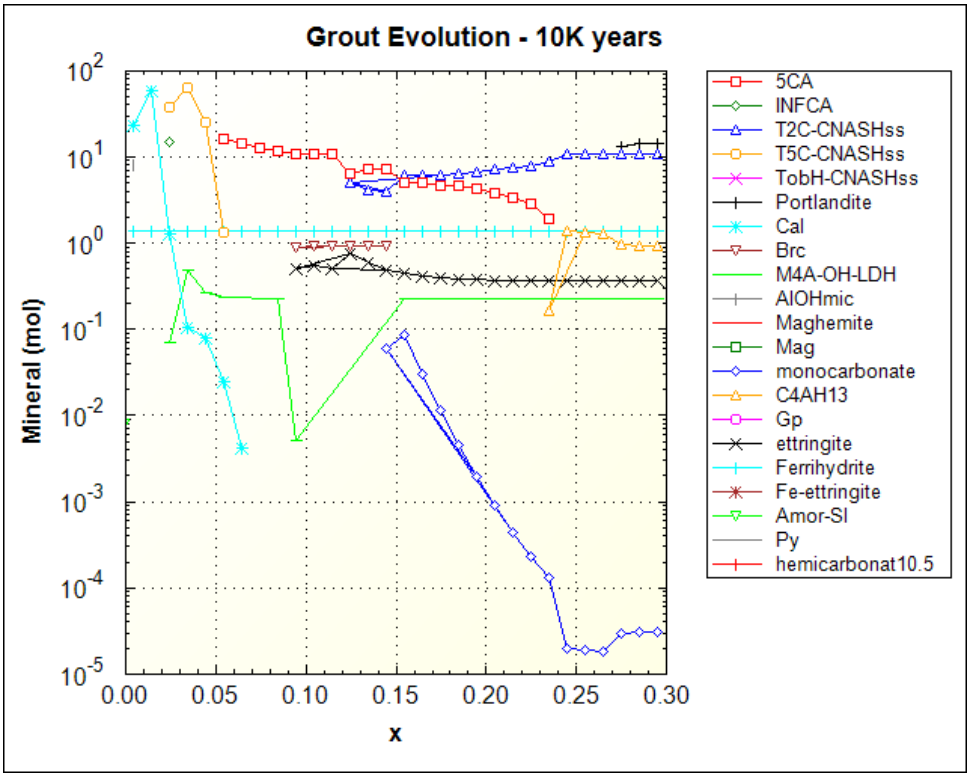

Figure 4.2-4: Mineral Evolution of B3000-6-0-2-A Concrete at 20,000 years.

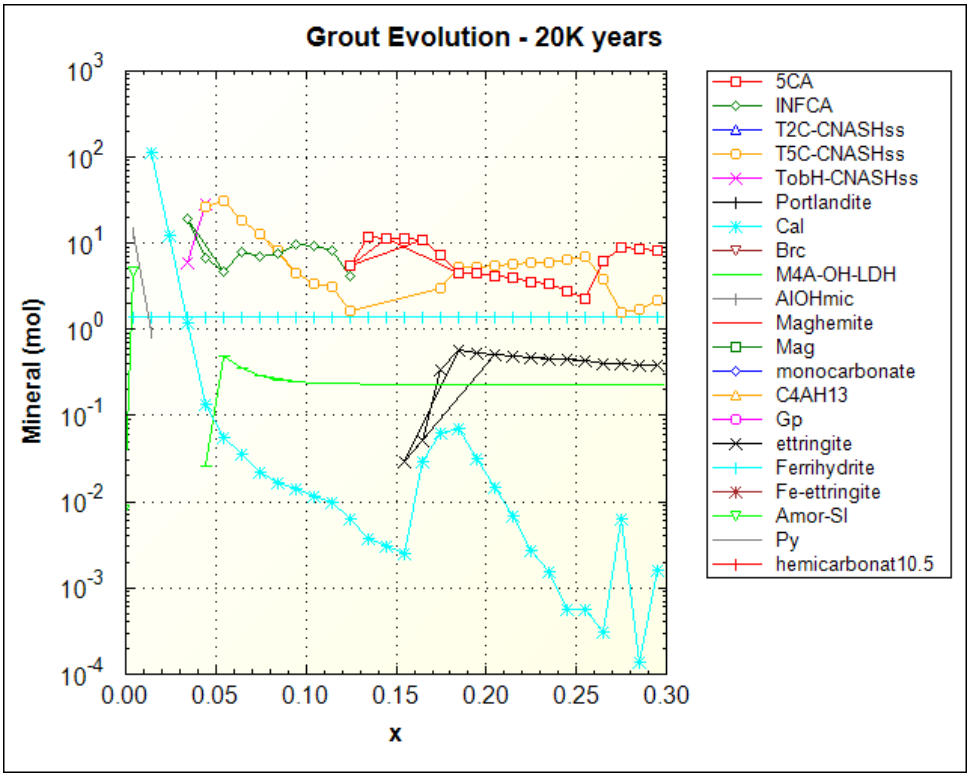

Figure 4.2-5: pH Evolution of B3000-6-0-2-A Concrete at 100 years.

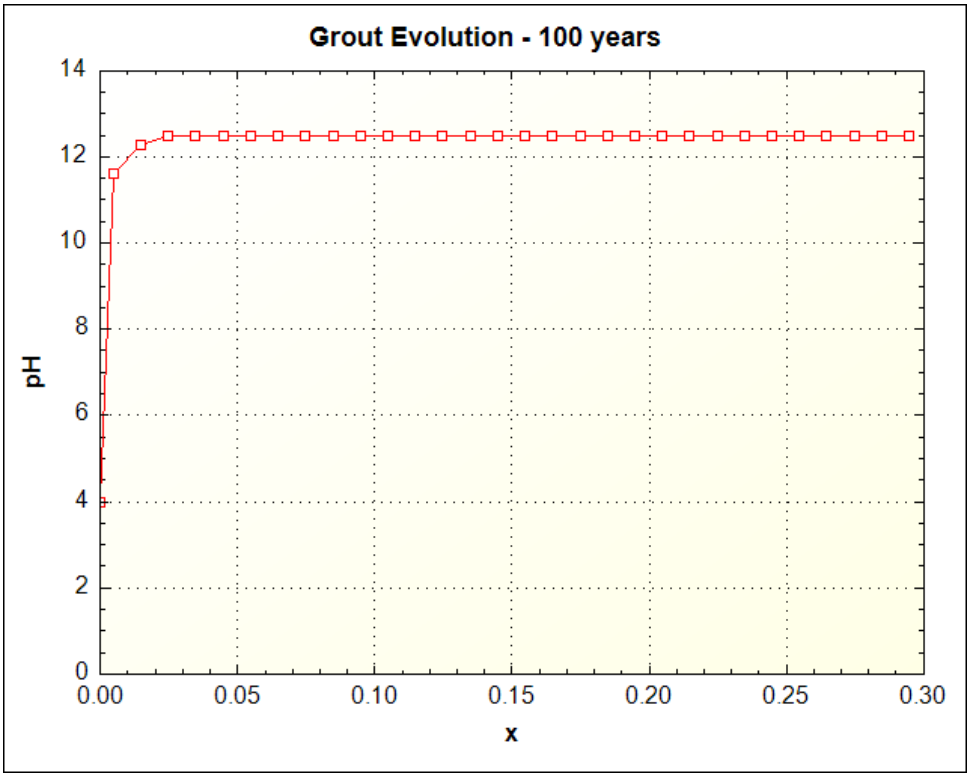

Figure 4.2-6: pH Evolution of B3000-6-0-2-A Concrete at 1000 years.

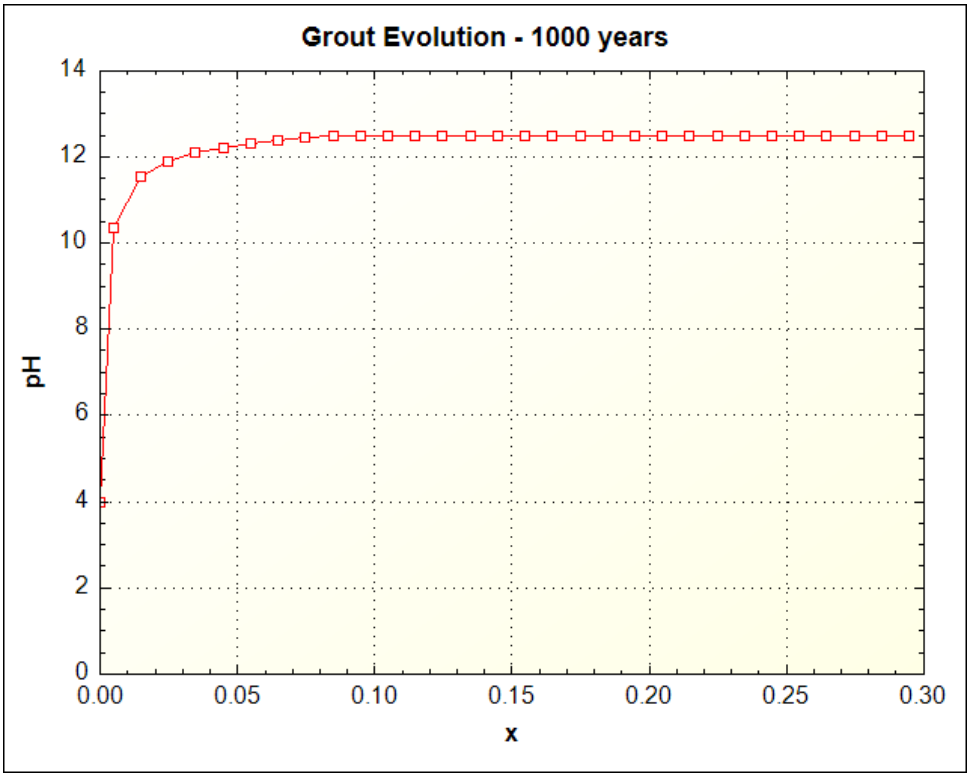

Figure 4.2-7: pH Evolution of B3000-6-0-2-A Concrete at 10,000 years.

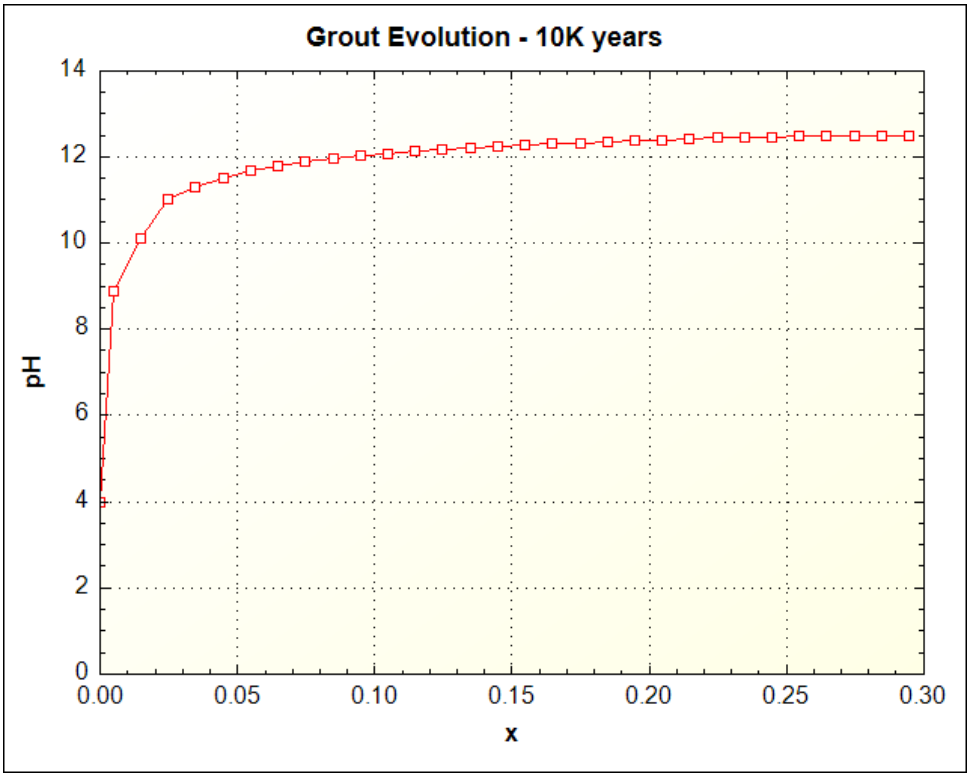

Figure 4.2-8: pH Evolution of B3000-6-0-2-A Concrete at 20,000 years.

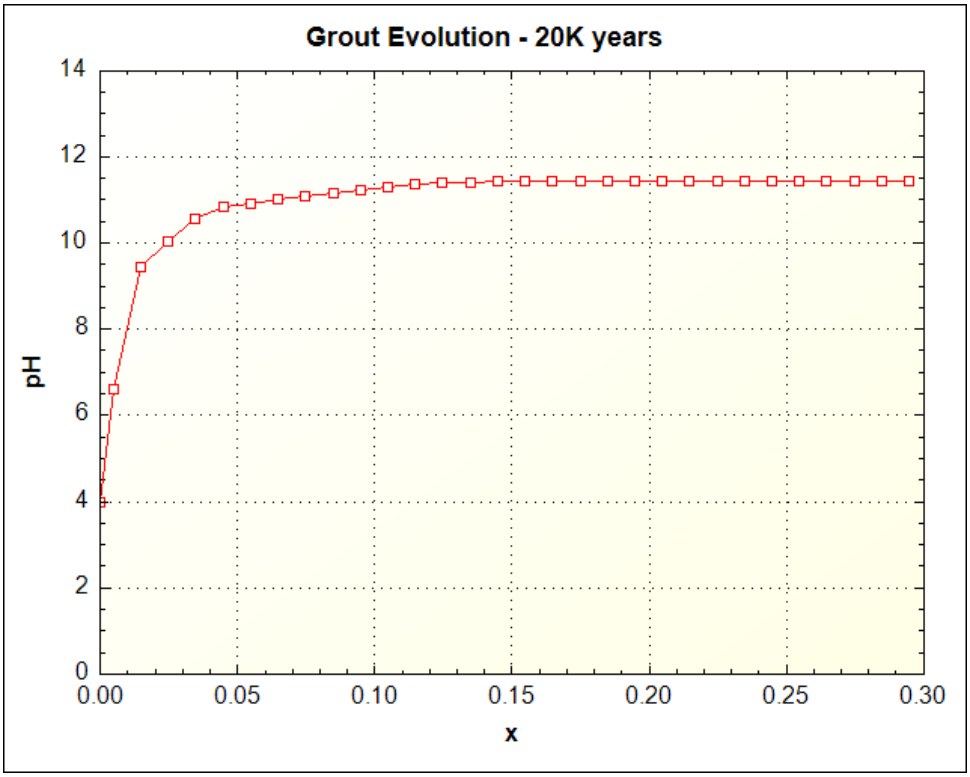

Figure 4.2-9: Mineral Evolution of LP#8-16 Grout at 100 years.

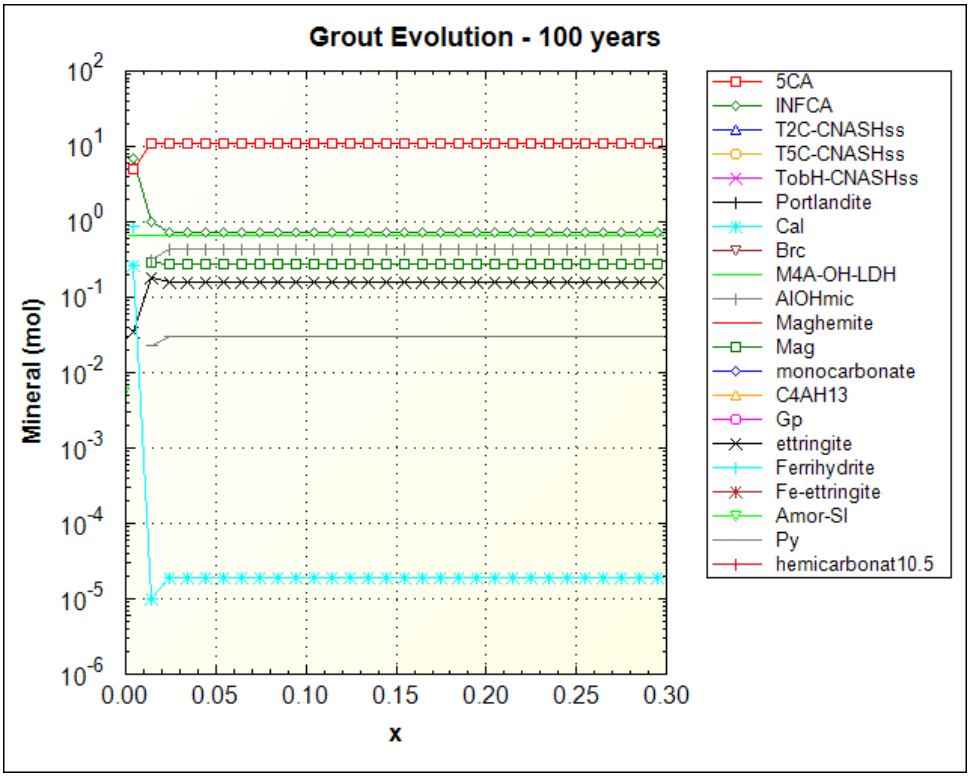

Figure 4.2-10: Mineral Evolution of LP#8-16 Grout at 1000 years.

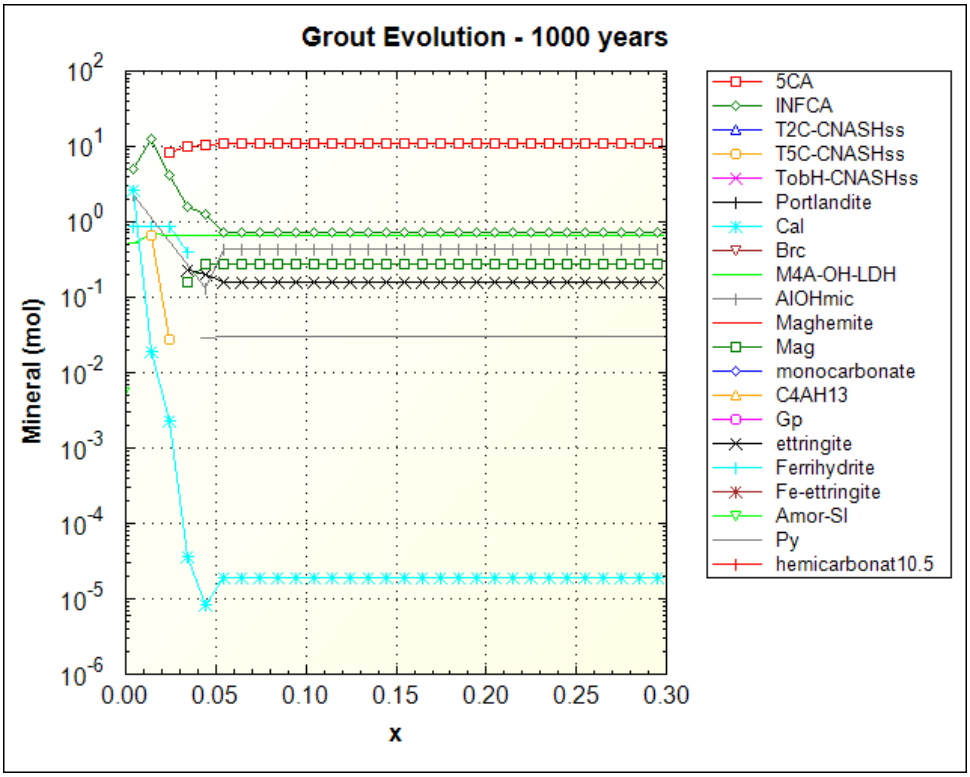

Figure 4.2-11: Mineral Evolution of LP#8-16 Grout at 10,000 years.

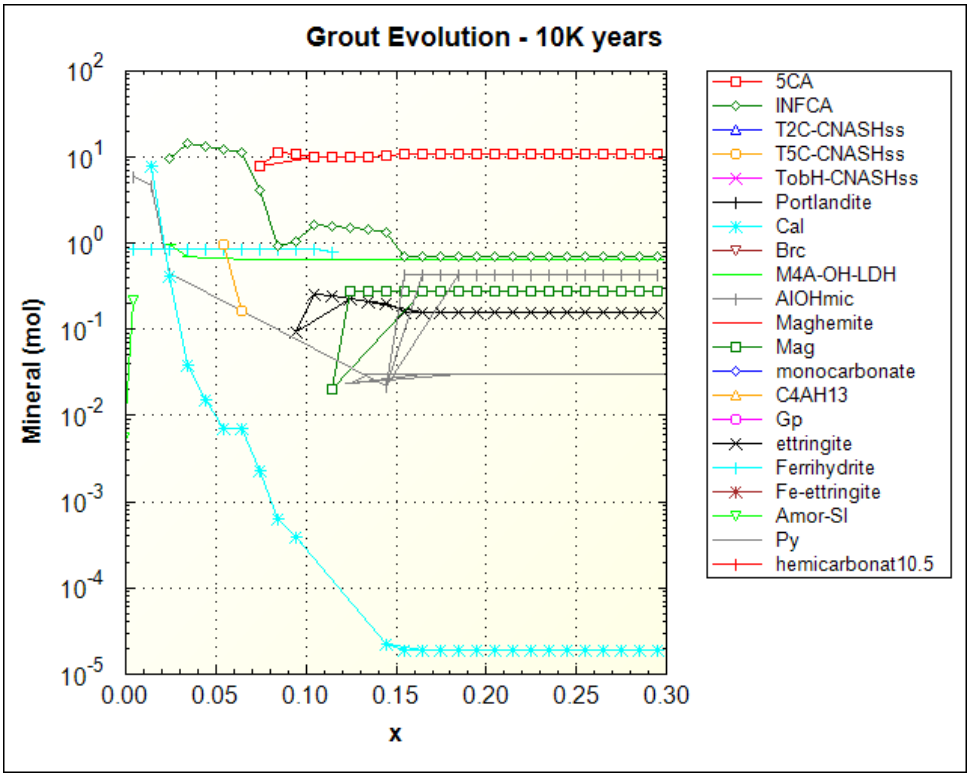

Figure 4.2-12: pH Evolution of LP#8-16 Grout at 100 years.

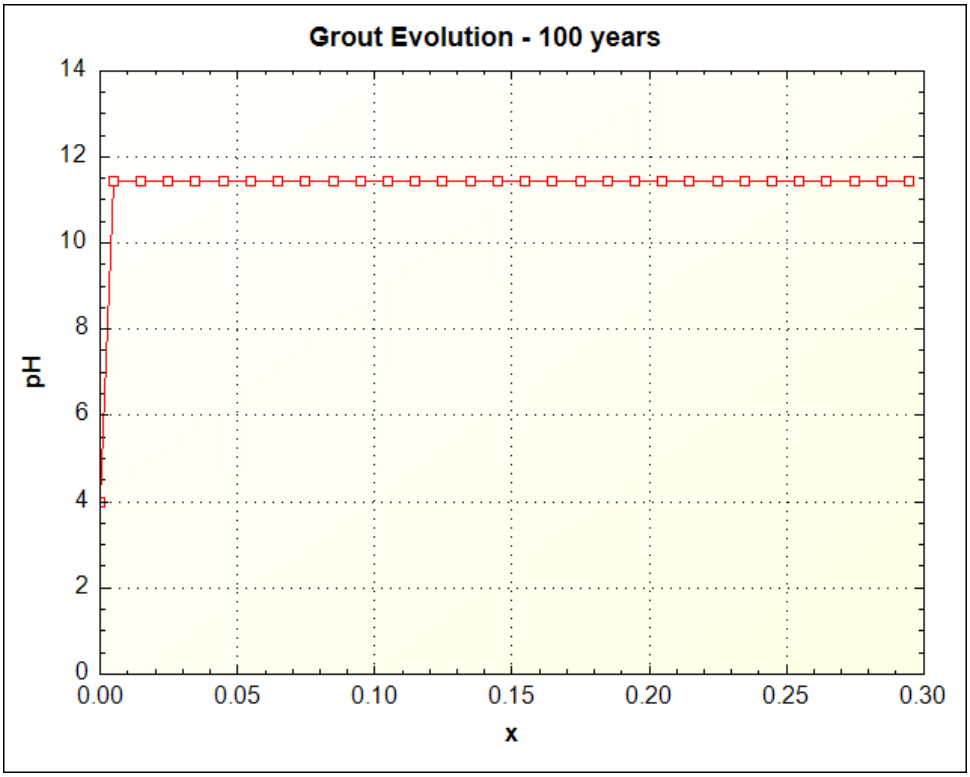

Figure 4.2-13: pH Evolution of LP#8-16 Grout at 1000 years.

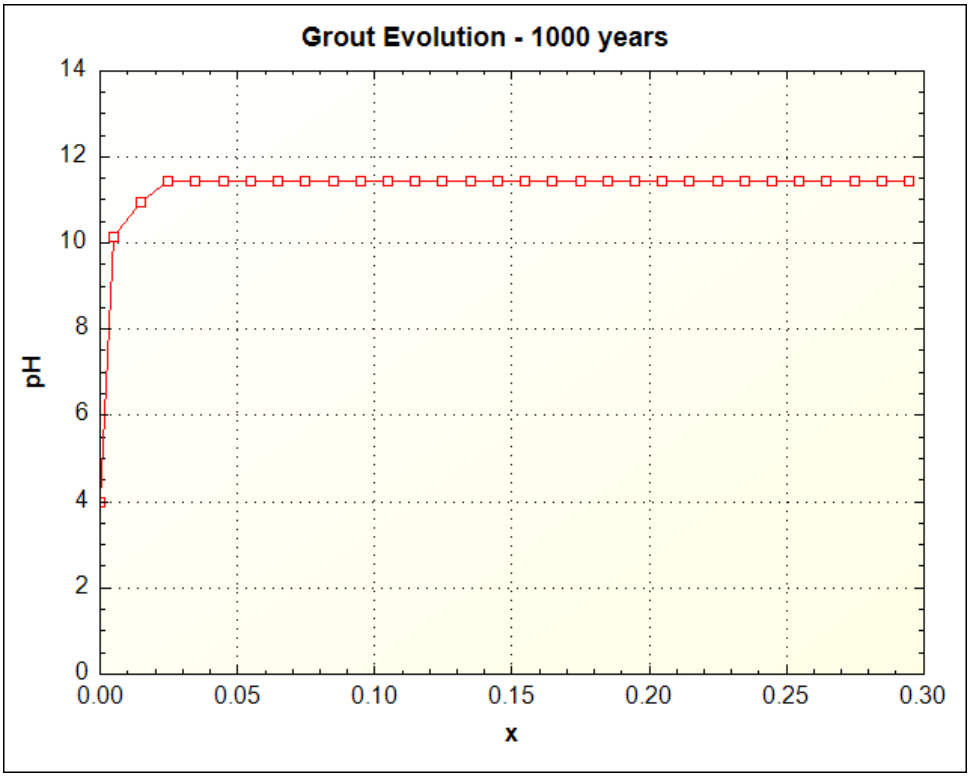

Figure 4.2-14: pH Evolution of LP#8-16 Grout at 10,000 years.

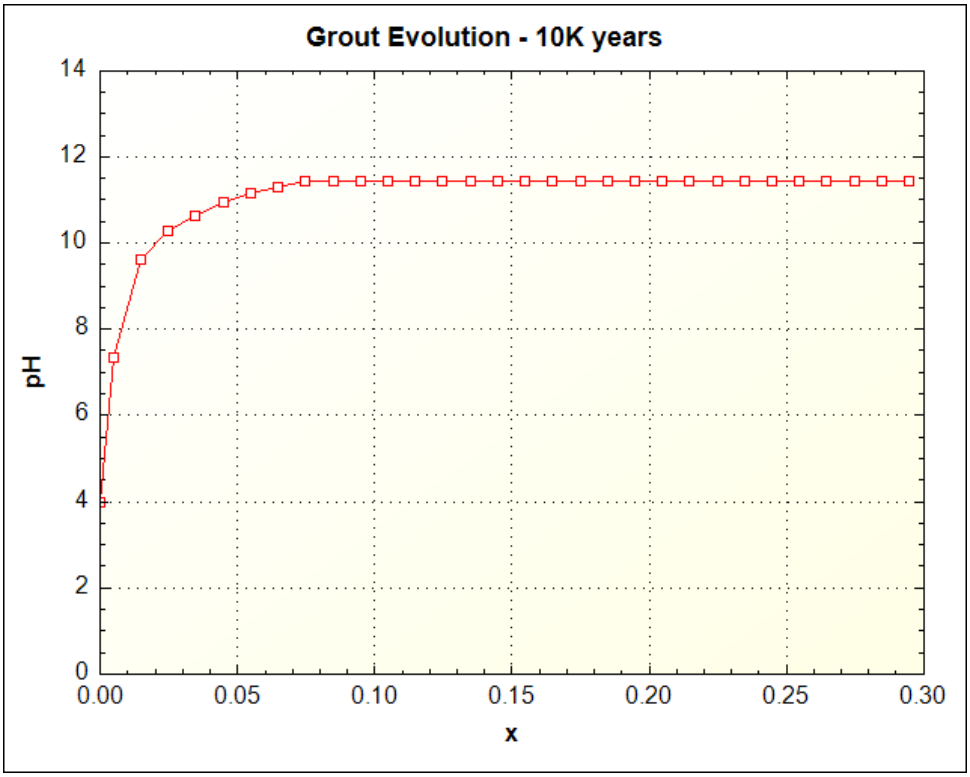

Figure 4.2-15: Mineral Evolution of ZB-FF-8-D Grout at 100 years.

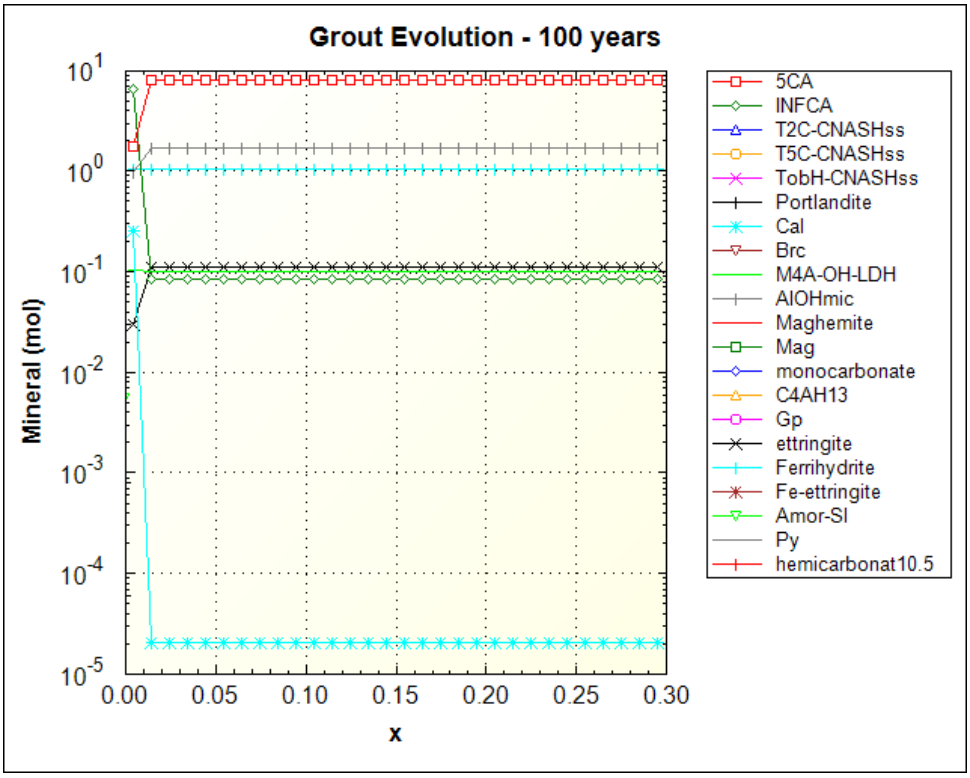

Figure 4.2-16: Mineral Evolution of ZB-FF-8-D Grout at 1000 years.

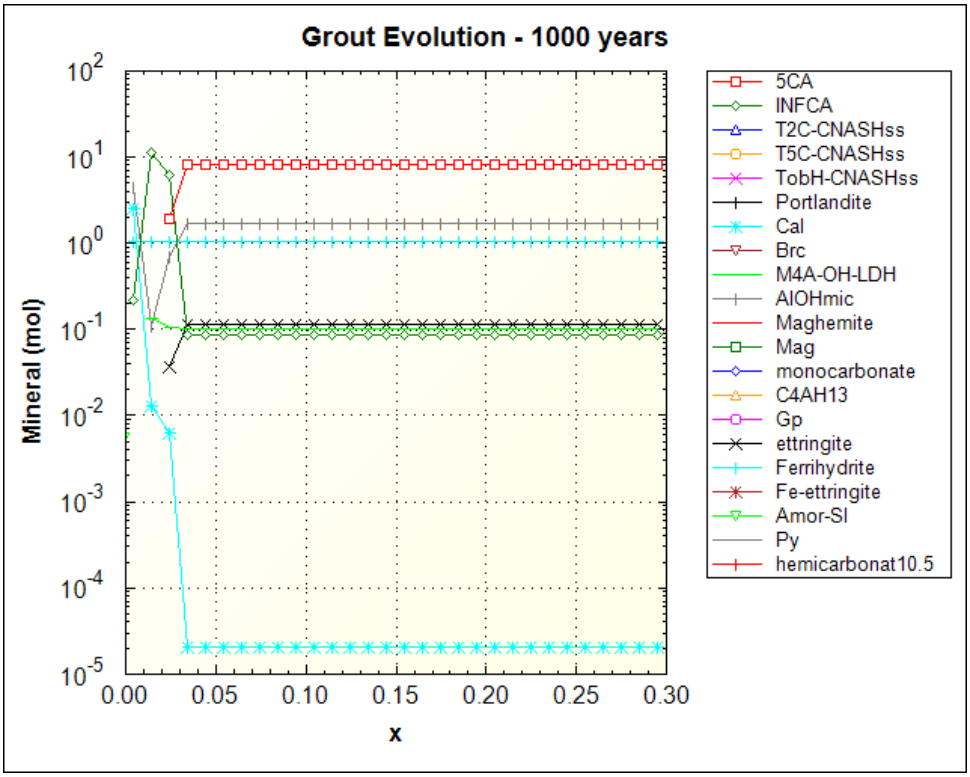

Figure 4.2-17: Mineral Evolution of ZB-FF-8-D Grout at 10,000 years.

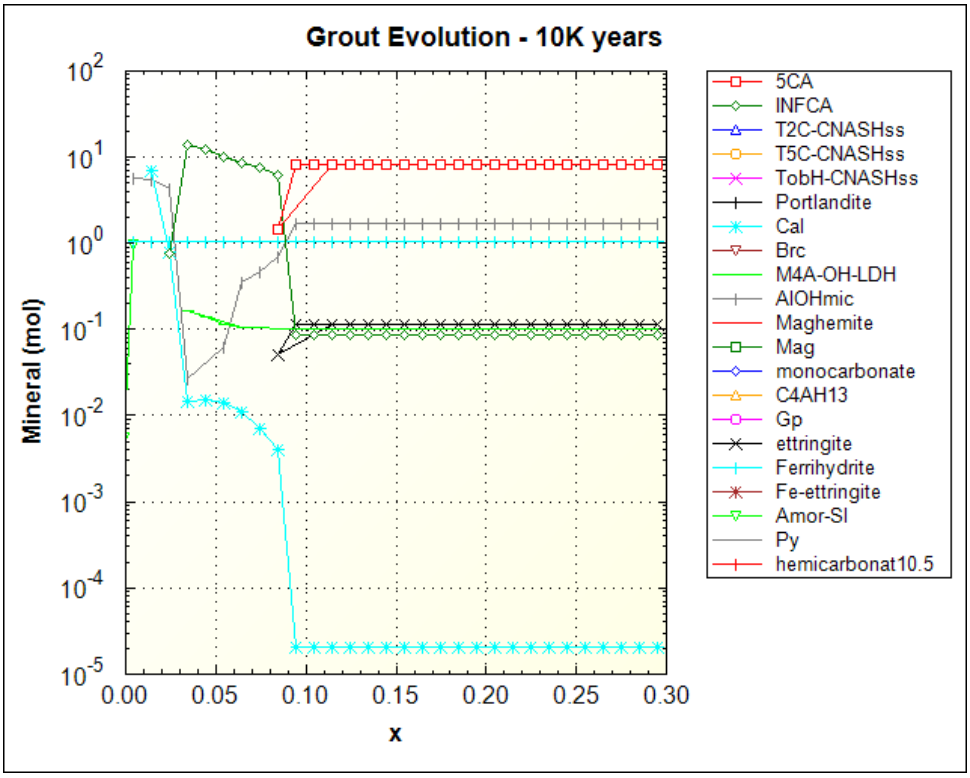

Figure 4.2-18: pH Evolution of ZB-FF-8-D Grout at 100 years.

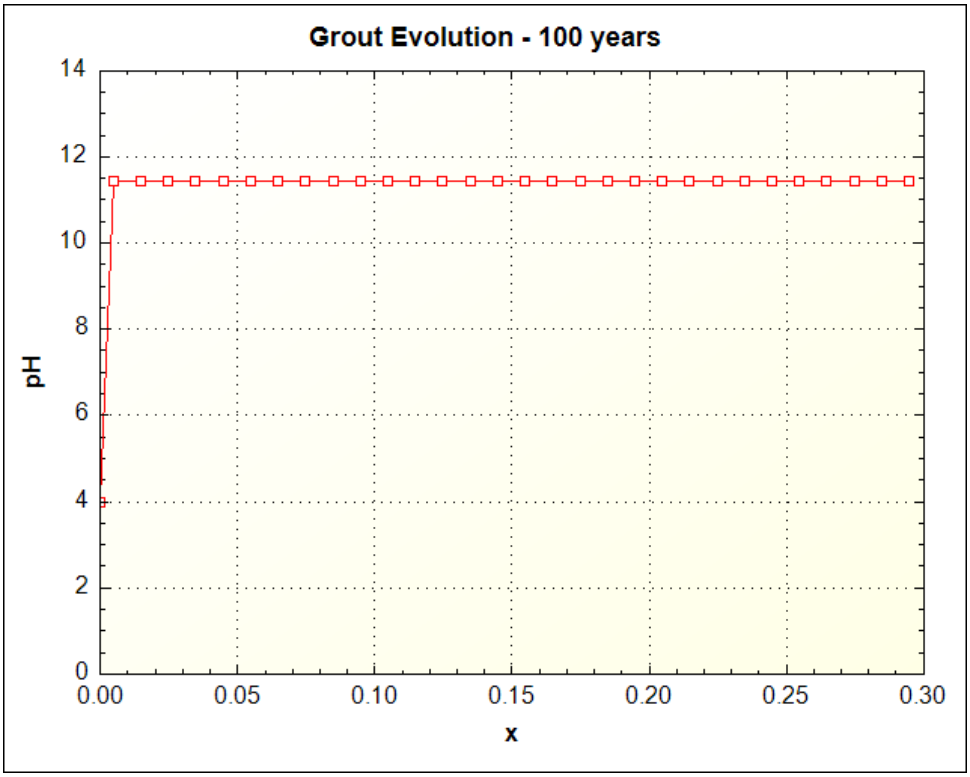

Figure 4.2-19: pH Evolution of ZB-FF-8-D Grout at 1000 years.

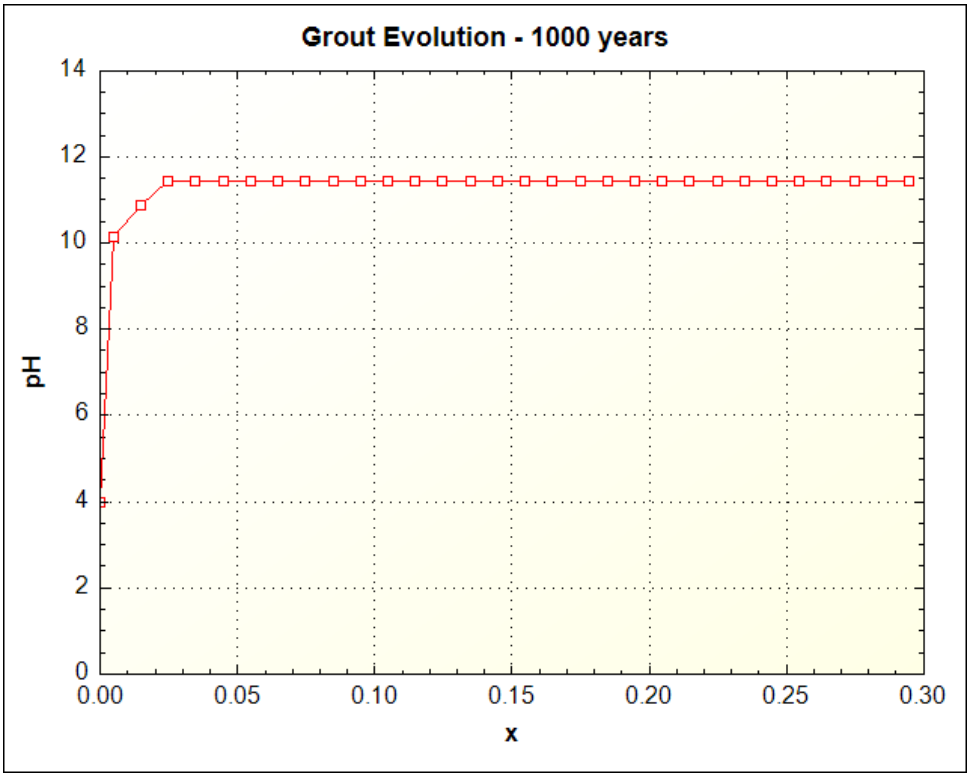

Figure 4.2-20: pH Evolution of ZB-FF-8-D Grout at 10,000 years.

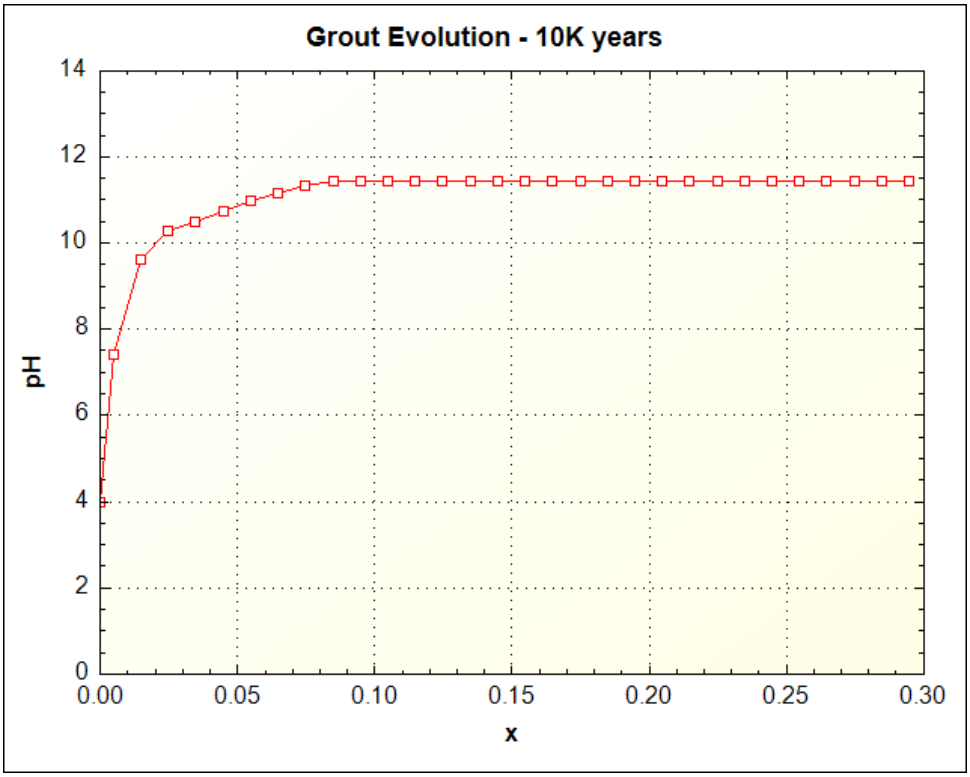

Figure 4.2-21: Mineral Evolution of Clean Cap Grout at 100 years.

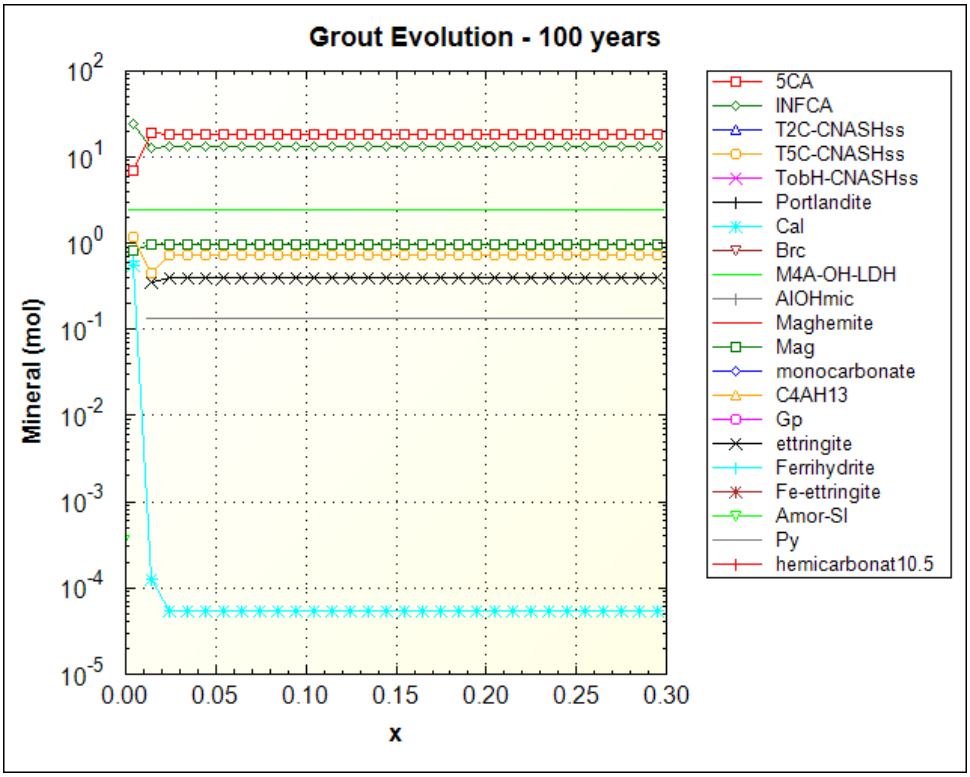

Figure 4.2-22: Mineral Evolution of Clean Cap Grout at 1000 years.

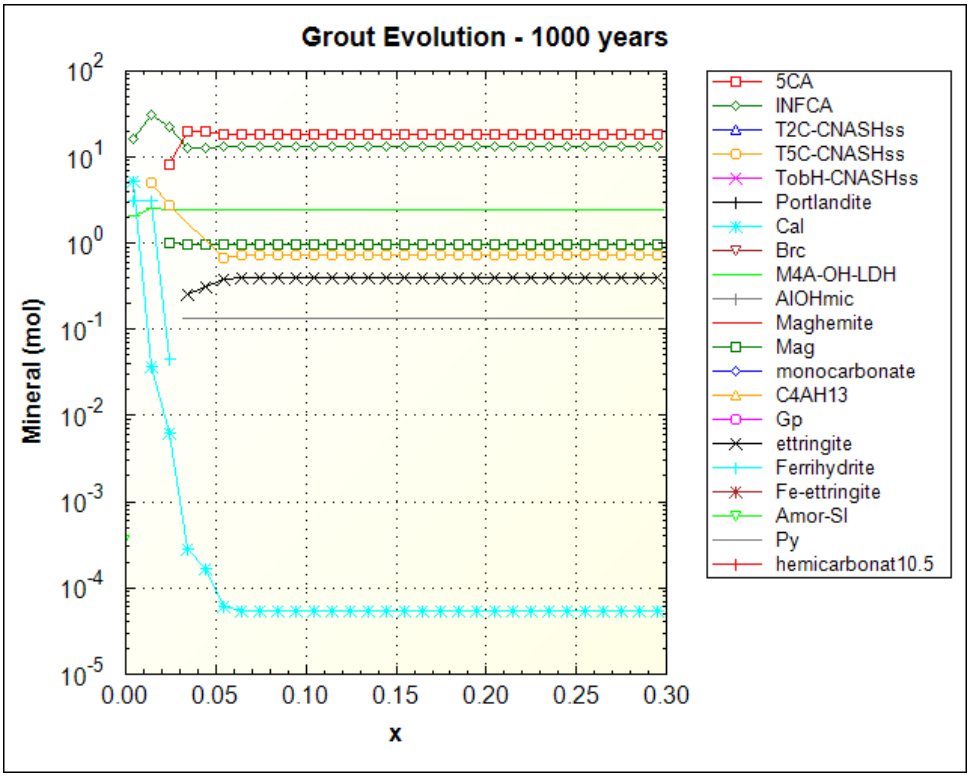

Figure 4.2-23: Mineral Evolution of Clean Cap Grout at 10,000 years.

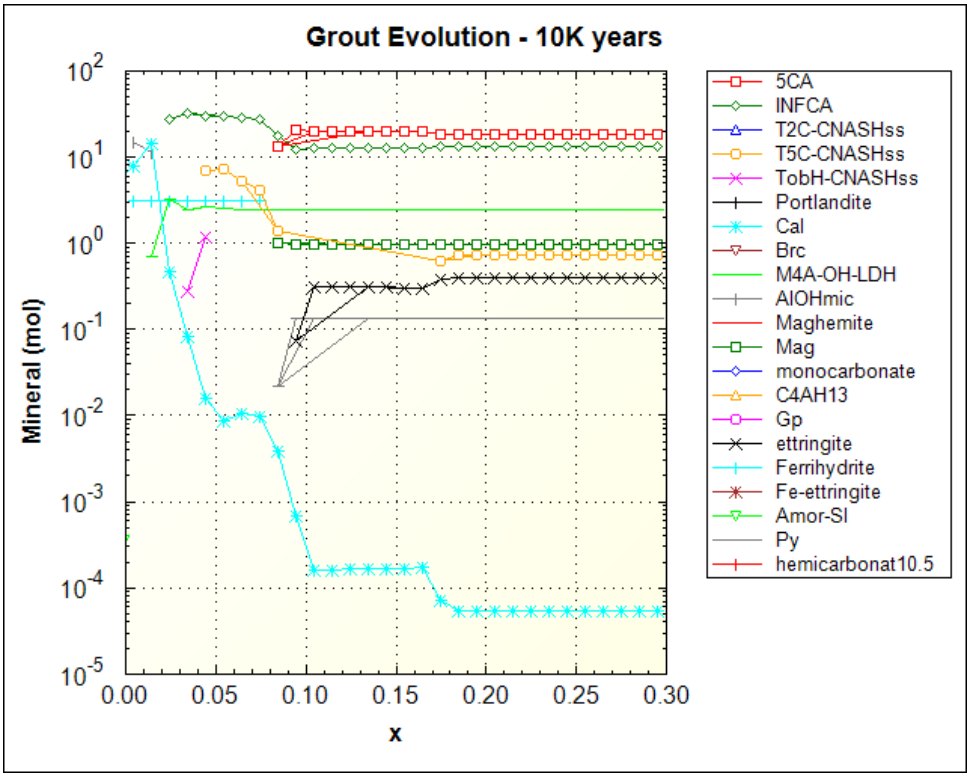

Figure 4.2-24: pH Evolution of Clean Cap Grout at 100 years.

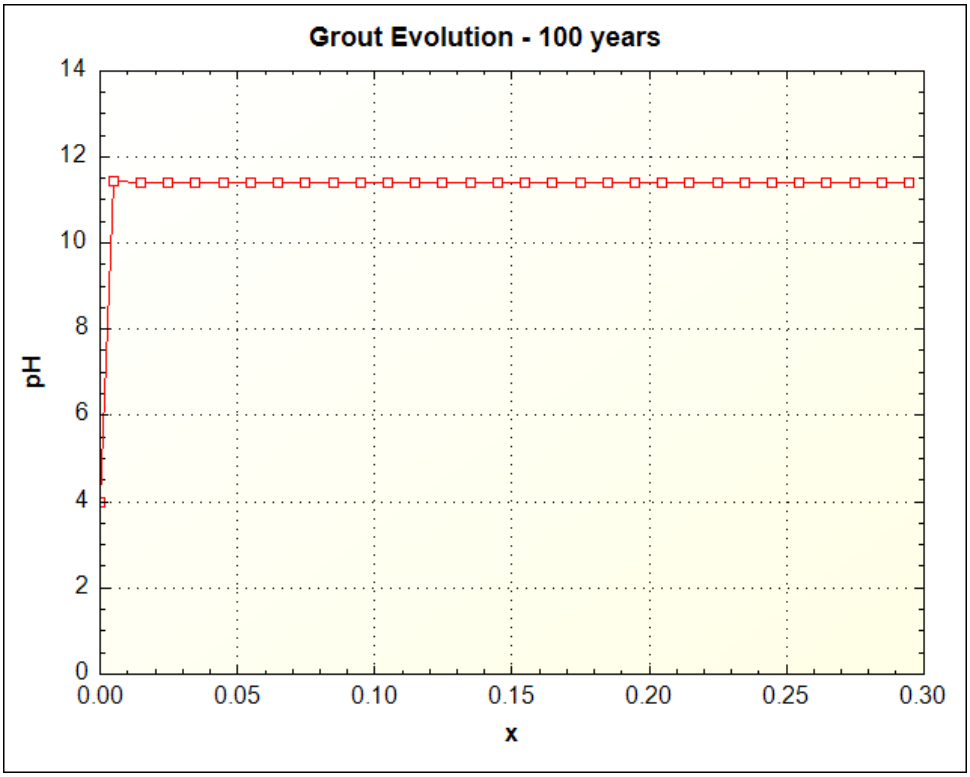

Figure 4.2-25: pH Evolution of Clean Cap Grout at 1000 years.

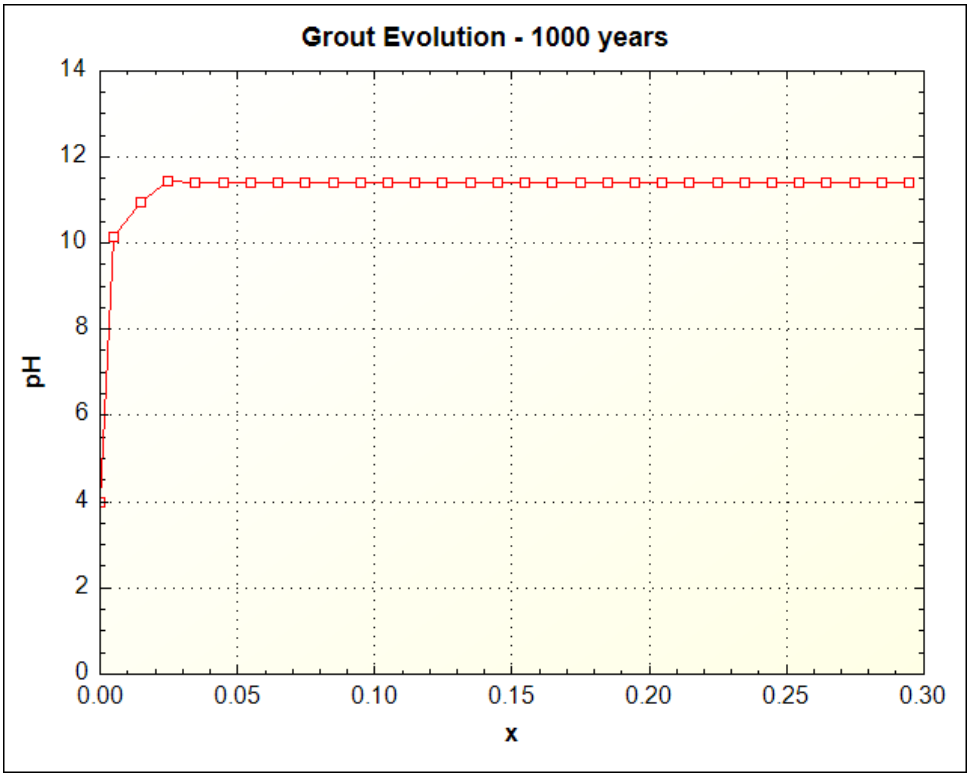

Figure 4.2-26: pH Evolution of Clean Cap Grout at 10,000 years.

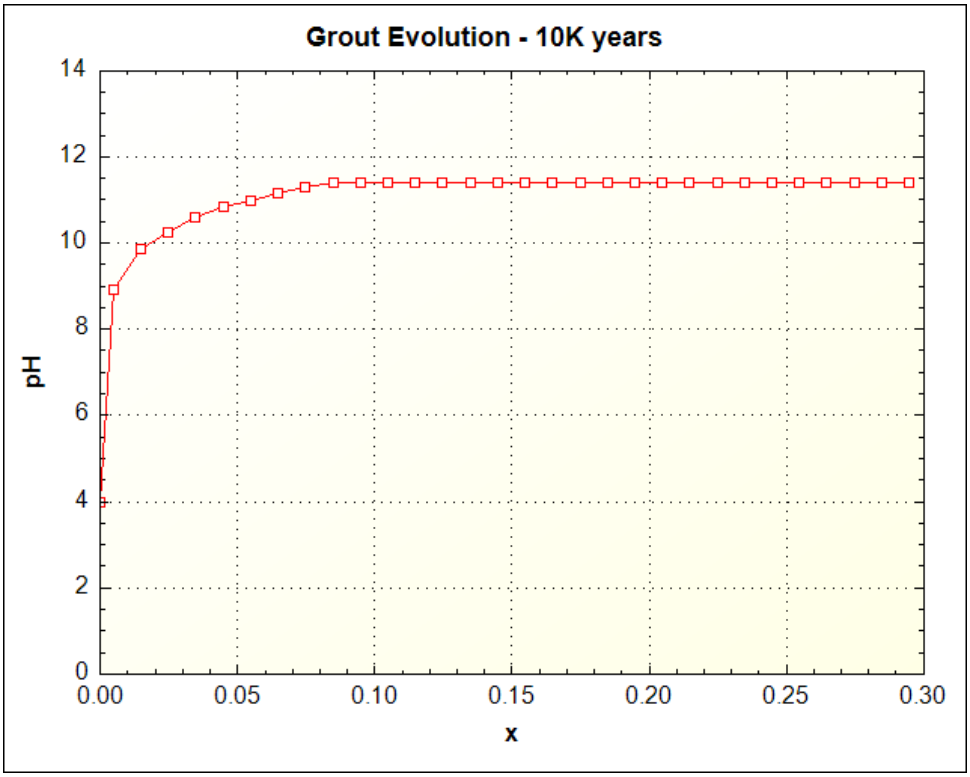

Figure 4.2-27: Mineral Evolution of Submerged Concrete at 100 years.

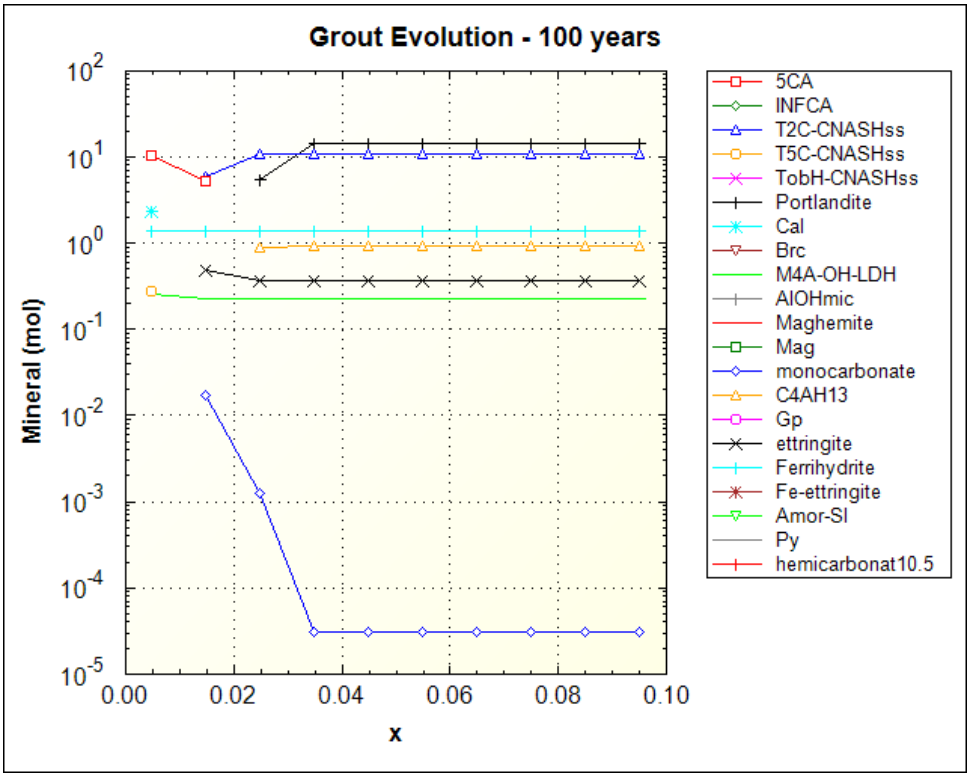

Figure 4.2-28: Mineral Evolution of Submerged Concrete at 1000 years.

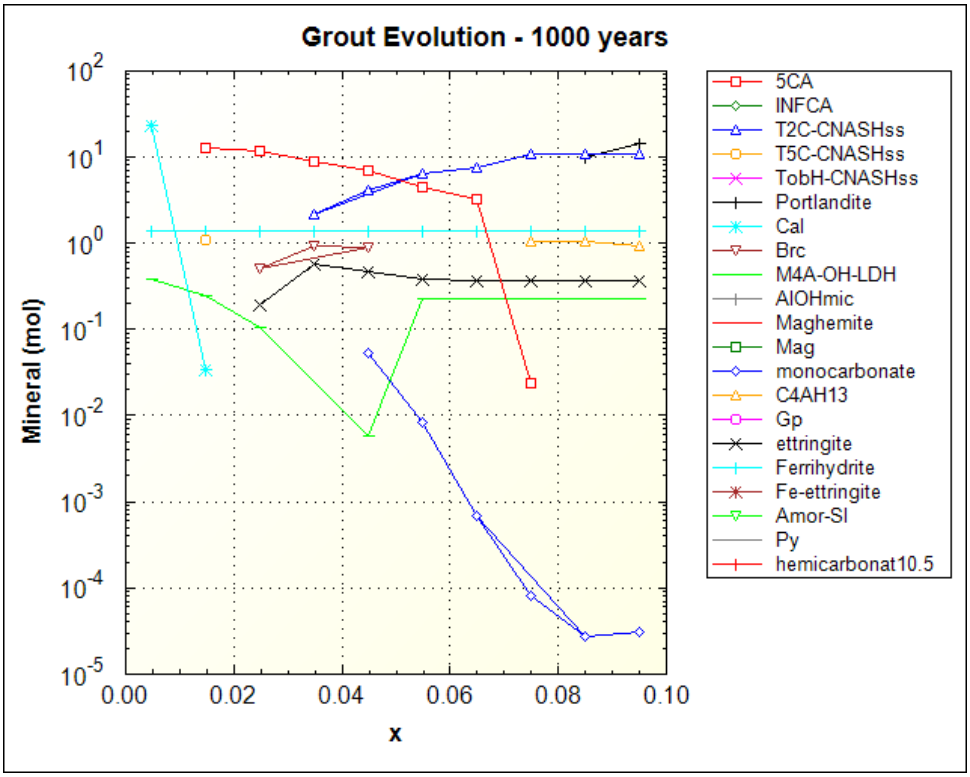

Figure 4.2-29: pH Evolution of Submerged Concrete at 100 years.

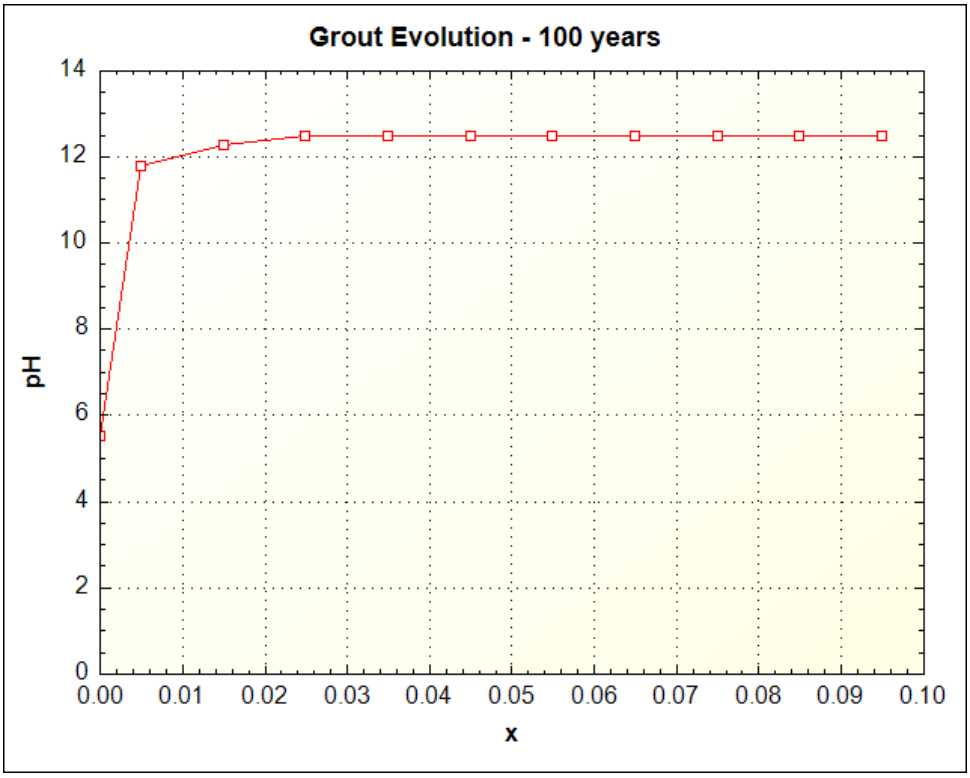

Figure 4.2-30: pH Evolution of Submerged Concrete at 1000 years.

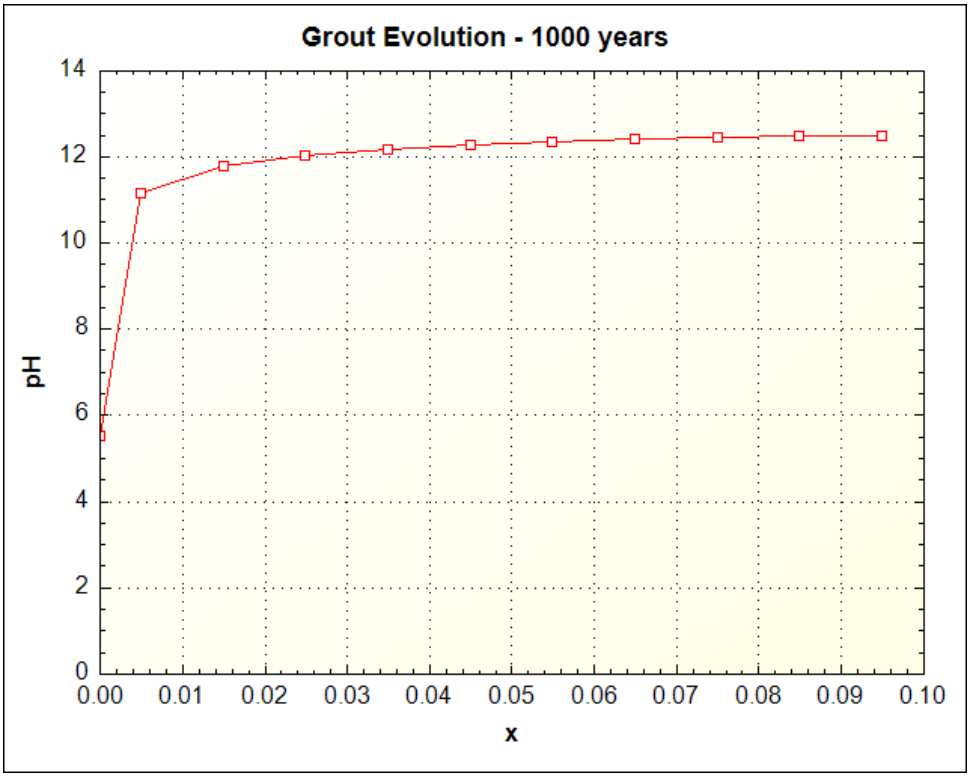

5.0 CHEMISTRY REGIMES CONTROLLING SOLUBILITY

The solubilities of radioactive and chemical elements in a thin waste layer on the bottom of a tank and in contact with grout will be controlled by the chemistry of the grout pore solution for tanks in the vadose zone where flow is predominantly downward. For submerged tanks exposed to groundwater the controlling solution is less certain, and four potential conditions were considered in SRNL-STI-2012-00404. This section summarizes the grout pore solution compositions typical of vadose zone simulations, proposes alternative solutions for analysis of submerged tanks, and develops modified solutions reflecting Eh levels observed in the field for both vadose zone and submerged tank settings. The various solutions are intended to support subsequent solubility studies involving redox sensitive elements in vadose zone and submerged tank environments.

5.1 Vadose Zone Tanks

As discussed in Section 4.1, five major pH levels are generally observed in advection-based chemical evolution simulations; these are labeled

1) pH =12.5 → Region a
2) pH =11.4 → Region b
3) pH =10.0 → Region c
4) pH =8.3 → Region d
5) pH =4.3 → Region e

Table 5.1-1 summarizes the pore solution chemistries observed in LP#8-16 grout simulations with soil moisture as the infiltrate. Also indicated for reference is an approximate alignment with the pH regions defined in SRNL-STI-2012-00404 and SRNL-STI-2021-00017. Compared to SRNL-STI-2012-00404, Table 10, "Tanks Above the Water Table", Regions II and III, the corresponding Regions b and c in Table 5.1-1 exhibit somewhat higher dissolved inorganic carbon (DIC) levels, due to a higher assumed P_{CO_2} in soil gas (0.01 atm versus atmospheric).

Oxalic acid has been used to clean some closed SRS waste tanks and SRNL-STI-2012-00404 assumed that calcium oxalate ($CaC_2O_4 \cdot (H_2O)_x$ where x varies from 0 to 3) will be present in the residual waste layer. Pore solution leaving grout and entering the residual waste layer is assumed to equilibrate with calcium oxalate monohydrate with solubility product K_{sp} = 2.32e-9 (*Physical Constants of Organic Compounds* in CRC Handbook, Rumble 2020). Table 5.1-2 shows the resulting oxalate concentration and minor perturbations to other species. The Nuclear Energy Agency (2020) thermodynamic database indicates K_{sp} = 1.86e-9 for calcium oxalate monohydrate (`CaOx:H2O(cr), log_K = -8.730`), which would slightly lower oxalate concentrations if adopted.

As discussed in SRNL-STI-2012-00404 and Denham (2020), simulated Eh values in grout pore fluids overstate the range of values expected based on laboratory and field observations. Table 5.1-3 shows grout pore solutions that have been equilibrated with calcium oxalate monohydrate and adjusted to align with an expected Eh value chosen for each pH level. The lower positive Eh values are drawn from Figure 17 of SRNL-STI-2012-00404, reproduced here as Figure 5.1-1. The higher negative value of -0.20 volts approximates measurements reported by Walter and

Dinwiddie (2019, 2020) for reducing grouts and represents a middle-ground between model results (Table 5.1-2) and measurements from short-term, small-scale, experiments reported in R-21-0001.

Table 5.1-1: Pore Solution Evolution Typical of LP#8-16 Grout Exposed to Soil Moisture.

Attribute	Region a	Reducing b	Oxidizing b	Region c	Region d	Region e
Mineral buffer	Portlandite	5CA	5CA	INFCA	Calcite	Infiltrate
pH	12.5	11.4	11.4	10.0	8.3	4.3
Eh (volts)	–	-0.49	+0.54	+0.63	+0.73	+0.96
log(PCO2)	–	-10.3	-10.3	-7.27	-3.56	-2.00
Ca++ (molar)	–	2.3E-03	2.0E-03	1.3E-03	5.4E-04	6.2E-06
Dissolved Inorganic Carbon (molar)	–	9.0E-06	9.3E-06	1.9E-05	8.8E-04	3.4E-04
SO4-- (molar)	–	3.8E-04	4.1E-05	4.1E-05	4.1E-05	4.1E-05
Na+ (molar)	–	5.3E-05	5.3E-05	5.3E-05	5.3E-05	5.3E-05
Cl- (molar)	–	5.7E-05	5.7E-05	5.7E-05	5.7E-05	5.7E-05
H4SiO4 (molar)	–	2.9E-04	5.2E-04	3.8E-03	1.9E-03	1.9E-03
SRNL-STI-2012-00404 Region	–	II	II	II/III	B-D	A
SRNL-STI-2021-00017 Region	II	III	III	III	III	IV

Table 5.1-2: Pore Solutions from LP#8-16 Grout Equilibrated with Calcium Oxalate.

Attribute	Reducing b	Oxidizing b	Region c	Region d
pH	11.414	11.391	9.995	8.294
Eh (volts)	-0.49	+0.54	+0.63	+0.73
log(PCO2)	-10.33	-10.18	-7.27	-3.56
Ca++ (molar)	2.3E-03	1.8E-03	1.3E-03	5.5E-04
Dissolved Inorganic Carbon (molar)	8.9E-06	9.6E-06	1.9E-05	8.8E-04
SO4-- (molar)	3.8E-04	4.1E-05	4.1E-05	4.1E-05
Na+ (molar)	5.3E-05	5.3E-05	5.3E-05	5.3E-05
Cl- (molar)	5.7E-05	5.7E-05	5.7E-05	5.7E-05
H4SiO4 (molar)	2.8E-04	5.2E-04	3.8E-03	1.9E-03
Oxalate (molar)	2.2E-06	2.7E-06	3.4E-06	6.3E-06

Table 5.1-3: Pore Solutions from LP#8-16 Grout Equilibrated with Calcium Oxalate and Eh Adjusted to Field Expectations.

Attribute	Reducing b	Oxidizing b	Region c	Region d
pH	11.414	11.4	10.011	8.533
Eh (volts)	-0.20	+0.21	+0.28	+0.32
log(PCO2)	-10.33	-10.20	-7.30	-3.80
Ca++ (molar)	2.3E-03	1.8E-03	1.3E-03	5.5E-04
Dissolved Inorganic Carbon (molar)	8.9E-06	9.6E-06	1.9E-05	8.8E-04
SO4-- (molar)	3.8E-04	4.1E-05	4.1E-05	4.1E-05
Na+ (molar)	5.3E-05	5.3E-05	5.3E-05	5.3E-05
Cl- (molar)	5.7E-05	5.7E-05	7.5E-05	5.7E-05
H4SiO4 (molar)	2.8E-04	5.2E-04	3.8E-03	1.9E-03
Oxalate (molar)	2.2E-06	2.7E-06	3.4E-06	6.3E-06

Figure 5.1-1: Eh-pH diagram showing Eh of SRS background water table wells in relation to iron speciation.

Reproduced from SRNL-STI-2012-00404

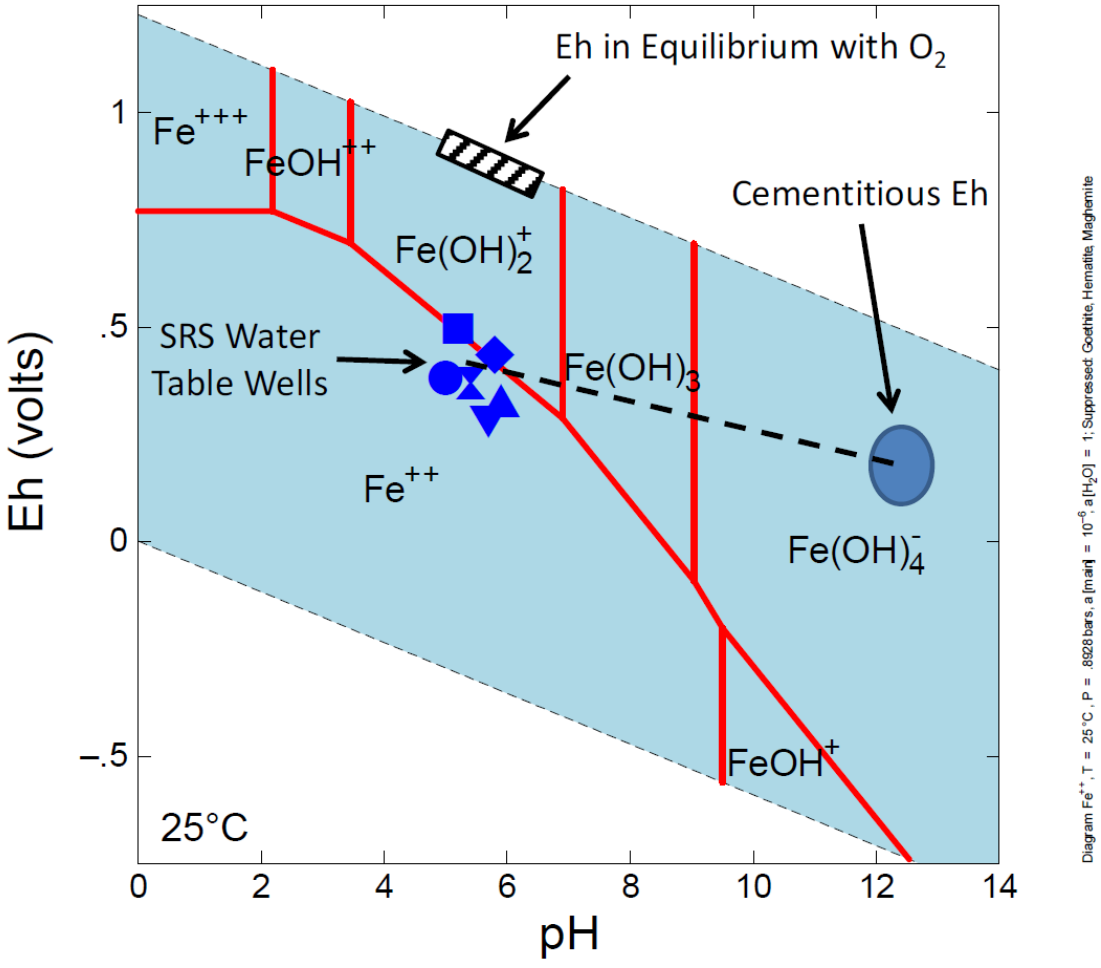

5.2 Submerged Tanks

SRNL-STI-2012-00404 considered four conditions for tanks below the water table:

1) Condition A: "Groundwater flows laterally directly into the residual waste layer with no effect of outer concrete"
2) Condition B: "Groundwater equilibrates with outer concrete, assumed to be fully carbonated, before passing through the residual waste layer where it mixes with a small amount of Oxidized Region II grout pore fluid"
3) Condition C: "Groundwater flows laterally directly into the residual waste layer with no effect of outer concrete and mixes with a small amount of Reducing Region II grout pore fluid"
4) Condition D: "Groundwater flows laterally directly into the residual waste layer with no effect of outer concrete and mixes with a small amount of Oxidizing Region II grout pore fluid"

The mixing proportion was 90% groundwater and 10% grout pore solution, based on groundwater flow simulations where the downward velocity component was approximately 10% of the magnitude. The solutions resulting from Conditions B, C, and D are very similar.

In this study four alternative solutions are proposed for solubility analysis involving submerged tanks (Table 5.2-1):

1) Groundwater equilibrated with atmospheric oxygen
2) Groundwater at Eh = +0.37 volts
3) Solution 1) equilibrated with calcite and calcium oxalate monohydrate
4) Solution 2) equilibrated with calcite and calcium oxalate monohydrate with Eh fixed at +0.37

These alternative solutions do not credit any influence of grout on residual waste layer chemistry. Solution 1) is based on Section 3.4 with charge balancing on chloride instead of carbonate and carbonate concentration fixed by P_{CO_2} = 0.01 atm. For Solution 2) Eh is set to +0.37 volts representative of field expectations following SRNL-STI-2012-00404, again with charge balancing on chloride and P_{CO_2} = 0.01 atm. Solutions 1) and 2) correspond to Condition A in SRNL-STI-2012-00404, where groundwater directly contacts waste. The conceptual models for Solutions 3) and 4) resemble SRNL-STI-2012-00404 Condition B where infiltrating groundwater equilibrates with aged concrete and then calcium oxalate monohydrate in the residual waste layer. Aged concrete is approximated by equilibration with calcite. The paired solutions provide a range of possible redox conditions that may be considered in solubility analysis.

Table 5.2-1: Solutions Proposed for Submerged Tank Solubility Analysis.

Solution: Species	1) O2 saturation	2) Eh = +0.37	3) O2 saturation + Calcite + Oxalate	4) Eh = +0.37 + Calcite + Oxalate	Units
pH	5.4	5.4	8.442	8.441	
Eh	+0.90	+0.37	+0.72	+0.37	volt
Ca++	7.5E-05	7.5E-05	4.5E-04	4.5E-04	mol/kg
DIC	3.8E-04	3.8E-04	7.5E-04	7.5E-04	mol/kg
SO4--	2.4E-05	2.4E-05	2.4E-05	2.4E-05	mol/kg
Na+	4.6E-05	4.6E-05	4.6E-05	4.6E-05	mol/kg
Cl-	9.0E-05	1.6E-04	9.0E-05	1.6E-04	mol/kg
H4SiO4	7.7E-05	7.7E-05	7.7E-05	7.7E-05	mol/kg
Oxalate	–	–	7.5E-06	7.5E-06	mol/kg
log10(PCO2)	-1.99	-1.99	-3.78	-3.78	

6.0 PHYSICAL EVOLUTION OF GROUT

The preceding analyses consider chemical evolution/aging of cementitious materials. This section considers the timing of physical evolution/degradation of grout due to gradual dissolution and leaching of cement binders (decalcification), using methods developed for saltstone grout in SRNL-STI-2018-00077. Also considered is potential alteration of grout physical properties from corrosion of coiling coils. Degradation times are estimated for Realistic, Compliance, and Pessimistic Cases in order of increasing conservatism. The Realistic Case is an as-designed performance case incorporating best-estimate values where feasible. The Compliance Case is a moderately conservative case intended to assess compliance with facility performance objectives. The Pessimistic Case is a strongly conservative case for assessing performance approaching worst-case.

6.1 Analytic Model for Decalcification

The conceptual model for grout physical degradation is that calcium is leached at its solubility limit via advective flow, slowing dissolving cement binders and leaving a more porous and permeable residual material. The process is assumed to begin immediately after any upstream concrete has chemically and/or physically degraded. Assuming one-dimensional downward flow, a quasi-steady state advective mass balance for decalcification is

$$U \cdot c_{Ca^{2+}} \cdot t = c_{Ca} \cdot h \tag{6-1}$$

where U = Darcy velocity (volumetric water flux) [cm/yr], t = elapsed time [yr], h = monolith height [cm], $c_{Ca^{2+}}$ = dissolved Ca^{2+} concentration [mol / cm^3 liquid], and c_{Ca} = calcium concentration in solid phase [mol / cm^3 total]. Equation (6-1) assumes that advection occurs uniformly through the entire vertical thickness, the dissolution front advances uniformly, and the exit concentration coincides with Ca^{2+} solubility. Solving for time yields

$$t = \frac{c_{Ca}}{c_{Ca^{2+}}} \cdot \frac{h}{U} \equiv \left(\frac{1}{A_U}\right) \cdot h \tag{6-2}$$

where A_U [cm/yr] is the rate coefficient for this advection-based degradation:

$$A_U = \frac{c_{Ca^{2+}}}{c_{Ca}} U \tag{6-3}$$

The hydraulic head gradient in vadose zone soil tends to be one or less (e.g., Wilson 1980 Figure 15, Nimmo et al. 2002 Figure 2), such that the flowrate is equal to or less than the saturated hydraulic conductivity (K_{sat}), per Darcy's law:

$$U \leq -K_{sat} \frac{dH}{dz} \tag{6-4}$$

For a cementitious monolith placed in the vadose zone, the head gradient can be higher as infiltration flows around the lower permeability obstacle. An upper bound on the gradient can be computed by assuming that water is hydrostatically ponded on the waste tank roof up to the ground surface, and the underside of the floor is at gravity equilibrium with the water table. Table 6.1-1 shows this calculation using bounding values for all inputs. The result is a bounding gradient of roughly 5 ft/ft. The assumptions for the Realistic, Compliance, and Pessimistic Cases are dH/dz = 1, 3, and 5 ft/ft, respectively.

Table 6.1-1: Calculation of Bounding Hydraulic Gradient.

Parameter	Value	Units	Comments
Distance from roof to ground, Type I	75	ft	SRR-CWDA-2019-00080, attached drawings
Distance from roof to ground, Type II	35	ft	SRR-CWDA-2019-00080, attached drawings
Distance from roof to ground, Type III/IIIA	25	ft	SRR-CWDA-2019-00080, attached drawings
Distance from roof to ground, Type IV	30	ft	SRR-CWDA-2019-00080, attached drawings
Distance from roof to ground surface	75	ft	Maximum
Distance from floor to roof, Type I	24.5	ft	SRR-CWDA-2010-00128, Figure 3.2-2
Distance from floor to roof, Type II	27	ft	SRR-CWDA-2010-00128, Figure 3.2-16
Distance from floor to roof, Type III/IIIA	33	ft	SRR-CWDA-2010-00128, Figure 3.2-27
Distance from floor to roof, Type IV	34.3	ft	SRR-CWDA-2010-00128, Figure 3.2-45
Distance from floor to roof	24.5	ft	Minimum
Distance from WT to floor, Type I	0	ft	SRR-CWDA-2010-00128, Table 4.2-15
Distance from WT to floor, Type II	0	ft	SRR-CWDA-2010-00128, Table 4.2-15
Distance from WT to floor, Type III/IIIA	18.2	ft	SRR-CWDA-2010-00128, Table 4.2-15 (38-43)
Distance from WT to floor, Type IV	7.1	ft	SRR-CWDA-2010-00128, Table 4.2-15
Distance from water table to floor	18.2	ft	Maximum
Pressure head at roof	75	ft	
Elevation of roof	24.5	ft	Reference is floor
Head at roof	99.5	ft	
Pressure head at floor	-18.2	ft	
Elevation of floor	0	ft	Reference is floor
Head at floor	-18.2	ft	
Head difference	117.7	ft	
Gradient	**4.8**	**ft/ft**	

6.2 Decalcification Rate Coefficient Calculations

Table 6.2-1 through Table 6.2-3 summarize rate coefficient (A_U) calculations for the Realistic, Compliance, and Pessimistic Cases. Calcium solubility in grouts considered herein will be controlled by incongruent dissolution of $C\text{-}S\text{-}H$ gel (Figure 4.1-1, Figure 4.1-4, Figure 4.1-7) and average around 0.002 mol/L (SIMCO 2012, Clodic and Meike 1997, Figure 6.2-1 noting that molal ≈ mol/L). The Realistic Case assumes this value. Calcium solubility in cementitious materials is practically bounded by equilibrium with Portlandite. Although Portlandite is not predicted for grouts, the mineral is initially present in concrete (Figure 4.1-10) and calcium solubility observed in simulations is approximately 0.02 molal ≈ 0.02 mol/L (Figure 6.2-2). This bounding high value is assigned to the Pessimistic Case. The geometric mean of the Realistic and Pessimistic Cases is used in the Compliance Case.

Saturated hydraulic conductivities (K_{sat}) for the Realistic Case are characteristic of initial material states and drawn from SRR-CWDA-2020-00045, Tables 10 and 12, and SRR-CWDA-2018-00004

(saltstone grout). These values are increased an order of magnitude for the Pessimistic Case. Although no specific mechanism is invoked in making these assumptions, increased K_{sat} could be attributed to microcracking due to another mechanism or a feedback mechanism where early decalcification affects K_{sat} throughout the grout monolith. The geometric mean of the Realistic and Pessimistic Cases is assumed for the Compliance Case.

Table 6.2-1: Rate Coefficient Calculations for the Realistic Case.

Parameter	Realistic Case			Units
	LP#8-16	ZB-FF-8-D	Clean Cap	
$[Ca^{2+}]_{liquid}$ (a)	0.002	0.002	0.002	mol/L liquid
	2.00E-06	2.00E-06	2.00E-06	mol/cm^3 liquid
$[Ca]_{solid}$ (b)	1.49E-03	1.07E-03	1.40E-03	mol/cm^3 total
Ksat (c)	2.1E-09	2.1E-08	5.0E-10	cm/s
	0.066	0.662	0.016	cm/yr
dh/dz (d)	1	1	1	-
U	2.1E-09	2.1E-08	5.0E-10	cm^3 liquid / cm^2 total-s
	0.07	0.66	0.02	cm^3 liquid / cm^2 total-yr
$1/A_U = [Ca]_{solid}/([Ca^{2+}]_{liquid}*U)$	1.1E+04	8.1E+02	4.4E+04	yr/cm
A_U	8.9E-05	1.2E-03	2.3E-05	cm/yr

(a) Approximate solubility of C-S-H (SIMCO 2012, Clodic and Meike 1997, Figure 6.2-1)
(b) Equal to CaO concentration (Section 3.5, Appendix B)
(c) SRR-CWDA-2020-00045 Table 10, Table 12, and SRR-CWDA-2018-00004, respectively.
(d) Unit gradient typical of vadose zone

Table 6.2-2: Rate Coefficient Calculations for the Compliance Case.

Parameter	Compliance Case			Units
	LP#8-16	ZB-FF-8-D	Clean Cap	
$[Ca^{2+}]_{liquid}$ (a)	0.006325	0.006325	0.006325	mol/L liquid
	6.32E-06	6.32E-06	6.32E-06	mol/cm^3 liquid
$[Ca]_{solid}$ (b)	1.49E-03	1.07E-03	1.40E-03	mol/cm^3 total
Ksat (c)	6.64E-09	6.64E-08	1.58E-09	cm/s
	0.209	2.094	0.050	cm/yr
dh/dz (d)	3	3	3	-
U	2.0E-08	2.0E-07	4.7E-09	cm^3 liquid / cm^2 total-s
	0.63	6.28	0.15	cm^3 liquid / cm^2 total-yr
$1/A_U = [Ca]_{solid}/([Ca^{2+}]_{liquid}*U)$	3.8E+02	2.7E+01	1.5E+03	yr/cm
A_U	2.7E-03	3.7E-02	6.8E-04	cm/yr

(a) Geometric mean of Realistic and Pessimistic Cases
(b) Equal to CaO concentration (Section 3.5, Appendix B)
(c) Geometric mean of Realistic and Pessimistic Cases
(d) Intermediate gradient, midway between Realistic and Pessimistic Cases

Table 6.2-3: Rate Coefficient Calculations for the Pessimistic Case.

Parameter	Pessimistic Case			Units
	LP#8-16	ZB-FF-8-D	Clean Cap	
$[Ca^{2+}]_{liquid}$ (a)	0.02	0.02	0.02	mol/L liquid
	2.00E-05	2.00E-05	2.00E-05	mol/cm^3 liquid
$[Ca]_{solid}$ (b)	1.49E-03	1.07E-03	1.40E-03	mol/cm^3 total
Ksat (c)	2.1E-08	2.1E-07	5.0E-09	cm/s
	0.662	6.623	0.158	cm/yr
dh/dz (d)	5	5	5	-
U	1.1E-07	1.1E-06	2.5E-08	cm^3 liquid / cm^2 total-s
	3.31	33.11	0.79	cm^3 liquid / cm^2 total-yr
$1/A_U = [Ca]_{solid}/([Ca^{2+}]_{liquid}*U)$	2.3E+01	1.6E+00	8.8E+01	yr/cm
A_U	4.4E-02	6.2E-01	1.1E-02	cm/yr

(a) Approximate solubility of Portlandite (Figure 6.2-2)
(b) Equal to CaO concentration (Section 3.5, Appendix B)
(c) 10 times Realistic Case
(d) Bounding gradient (Table 6.1-1)

Figure 6.2-1: Calcium in Pore Solution from LP#8-16 Evolution Simulation.

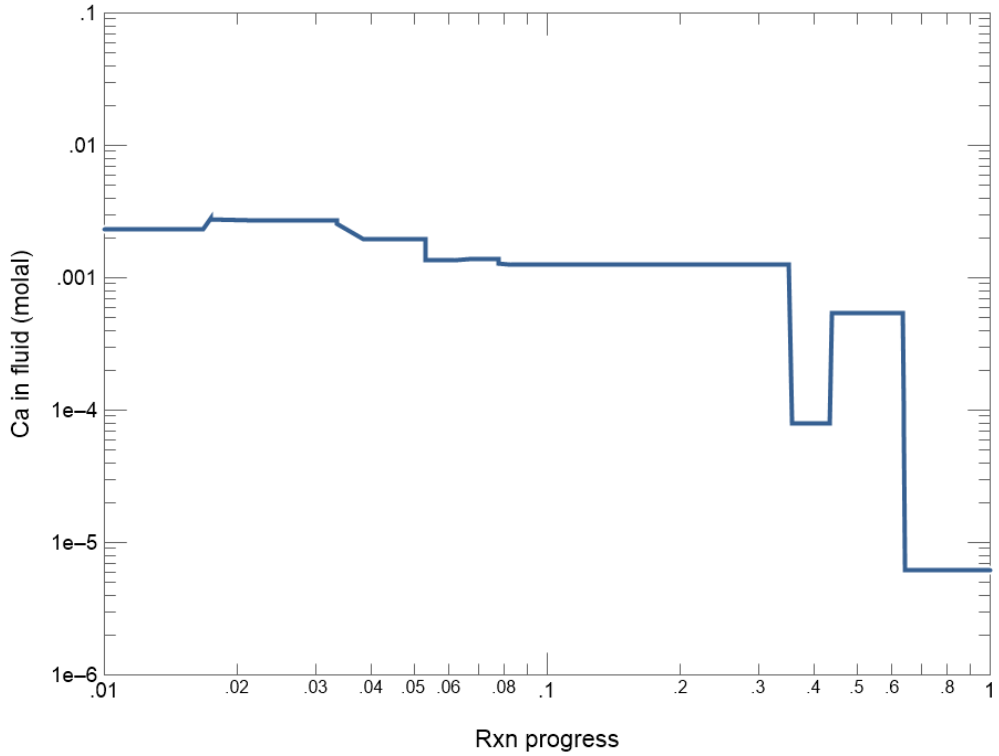

Figure 6.2-2: Calcium in Pore Solution from Concrete Evolution Simulation.

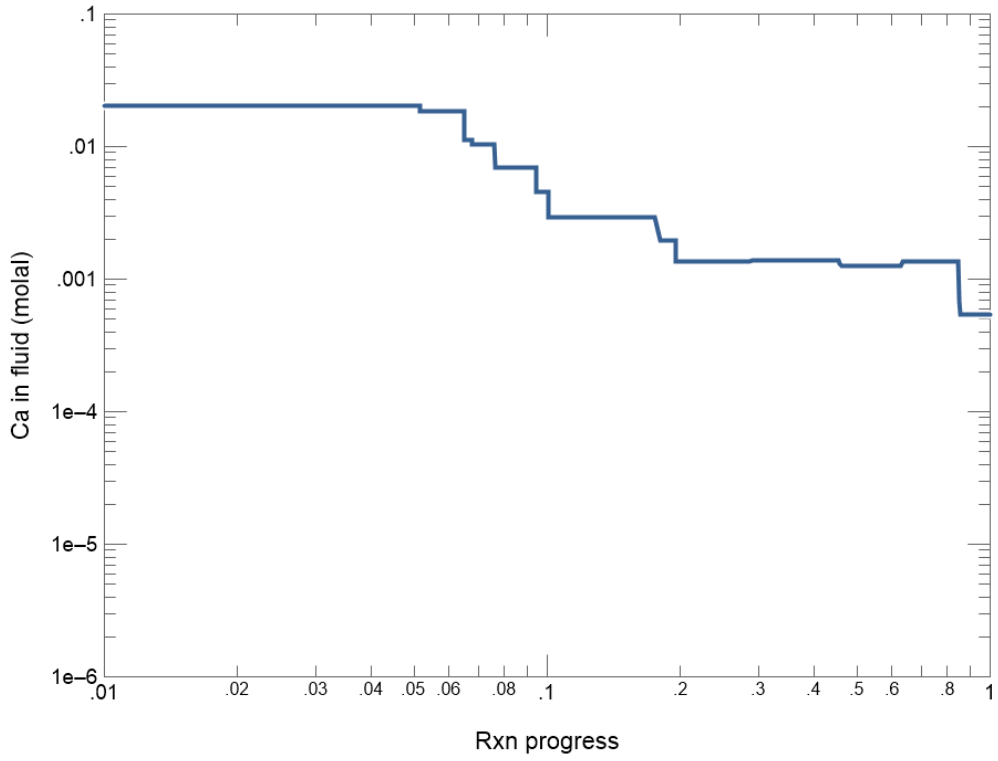

6.3 Decalcification Degradation Times

Table 6.3-1 summarizes grout degradation times computed for tank dimensions reported in SRR-CWDA-2010-00128 (Figures 3.2-2, 16, 27, 45) and the rate coefficients from Table 6.2-1 through Table 6.2-3. Degradation is assumed to start after upstream (e.g., roof) concrete has become chemically aged (low dissolved calcium) or physically degraded (e.g., cracked), such that chemical equilibrium between concrete and infiltrate no longer occurs.

Table 6.3-1: Physical Degradation Times Based On Grout Decalcification.

Tank	Approximate Height		LP#8-16	ZB-FF-8-D	CleanCap
	ft	cm	yr		
Realistic Case					
Type I	24.5	747	8.4E+06	6.0E+05	3.3E+07
Type II	27	823	9.3E+06	6.7E+05	3.6E+07
Type III/IIIA	33	1006	1.1E+07	8.1E+05	4.4E+07
Type IV	34.3	1045	1.2E+07	8.5E+05	4.6E+07
Compliance Case					
Type I	24.5	747	2.8E+05	2.0E+04	1.1E+06
Type II	27	823	3.1E+05	2.2E+04	1.2E+06
Type III/IIIA	33	1006	3.8E+05	2.7E+04	1.5E+06
Type IV	34.3	1045	3.9E+05	2.8E+04	1.5E+06
Pessimistic Case					
Type I	24.5	747	1.7E+04	1.2E+03	6.6E+04
Type II	27	823	1.9E+04	1.3E+03	7.3E+04
Type III/IIIA	33	1006	2.3E+04	1.6E+03	8.9E+04
Type IV	34.3	1045	2.4E+04	1.7E+03	9.3E+04

6.4 Corrosion of Cooling Coils

Another potential mechanism altering the hydraulic properties of grout is corrosion of any steel components embedded in grout, notably cooling coils where present. Corrosion products (rust) are expansive and could exert sufficient internal stress to crack grout depending on cooling coil size and spacing, grout strength, external confining pressures, etc. Corroded-thru cooling coils could also form vertical fast flow paths through tank-fill grout depending on the system modeling scenario. Either phenomena would increase the effective (spatial average) hydraulic conductivity of tank-fill grout.

Corrosion of cooling coil steel has been analyzed in SRNL-STI-2021-00187 under various exposure conditions and Table 6.4-1 summarizes the resulting corrosion rates and times. These through-wall corrosion times are based on a nominal wall thickness of 0.154 inches for two-inch schedule 40 pipe characteristic of cooling coils. The “Grout” condition refers to a high-pH grout being in intimate contact with the indicated surface. “Indoor Air” refers to a cooling coil filled with air that has no connection to the external environment. “Humid Air” refers a cooling coil filled with air that is connected in some manner to soil moisture/gas in backfilled soil surrounding

a closed waste tank. Closure plans call for grouting the inside of cooling coils so "Grout" is the planned closure condition. Un-grouted, air-filled, cooling coils are a postulated condition that could reflect grout shrinkage gaps inside cooling coils, poor execution of the current closure plan, an alternative closure plan, or similar non-baseline condition.

Table 6.4-1: Through-Wall Corrosion of Cooling Coils (SRNL-STI-2021-00187).

Exposure Condition and Corrosion Rate		Corrosion Time (yr)
Outside Pipe	Inside Pipe	
Grout 0.04 mil/yr	Grout 0.04 mil/yr	1,925
Grout 0.04 mil/yr	Indoor Air 0.4 mil/yr	350
Grout 0.04 mil/yr	Humid Air 2.03 mil/yr	74†
Humid Air 2.03 mil/yr	Humid Air 2.03 mil/yr	38

† calculated herein from 0.154 inch wall thickness and indicated corrosion rates

Stress-cracking of tank-fill grout is more likely to occur when cooling coils are filled with grout, preventing corrosion products from otherwise expanding unconstrained into an interior void. Beyond this assertion, no attempt is made to predict whether or when stress-cracking might occur using mechanistic analysis. Nonetheless, the through-wall corrosion times presented in Table 6.4-1 may be useful for constructing postulated grout degradation scenarios on a more heuristic basis.

7.0 PHYSICAL EVOLUTION OF CONCRETE

While concrete is physically affected by decalcification like grout, additional phenomena are more significant: corrosion of steel reinforcing bars, internal stress created by the expansive rust, and physical damage in the form of cracking. Rebar corrosion initiation and rates are affected by pH, oxygen transport rates, and chloride concentration. pH is affected by carbonation rates. The physical evolution/degradation of concrete is analyzed in this section using enhancements of methods developed for the Saltstone Disposal Facility PA described in SRNL-STI-2018-00077. As with grout, degradation times are estimated for Realistic, Compliance, and Pessimistic Cases in order of increasing conservatism.

7.1 Conceptual Models and Overview

Figure 7.1-1 illustrates conceptual models for carbon dioxide, calcium, oxygen, and chloride diffusion through a concrete thickness adjoining an impermeable steel liner. Also depicted is a physical damage front that lags a carbonation/decalcification front. These conceptual models can be used to predict concrete degradation due to reinforcing bar corrosion and help predict steel liner corrosion by defining at the concrete-liner interface 1) the arrival time of a carbonation/decalcification front, 2) oxygen flux and cumulative mass, and 3) chloride concentration. An overview of the various conceptual models is presented first followed by detailed mathematical derivations.

Initially, embedded steel reinforcing bars in concrete are assumed to experience insignificant corrosion, due to the high pH of portlandite and calcium-silicate-hydrate ($C\text{-}S\text{-}H$) gel passivating steel surfaces. Subsequently, dissolved carbon dioxide diffuses into the concrete and reacts with calcium in concrete binders to form calcium carbonate, a process referred to as carbonation. Carbonation lowers pH causing loss of passivation and much higher corrosion rates. The corrosion products (rust) are expansive and assumed to damage concrete via stress cracking sometime after the carbonation front passes. The damage front is assumed to lag the carbonation front at x_c by a fixed distance δ. Damage to concrete is assumed to take the form of cracks (fractures) that allow gaseous CO_2 to easily migrate to the damage front. Contact with gaseous CO_2 there is assumed to saturate aqueous CO_2, effectively creating a moving exposure boundary at $x_c(t) - \delta$. The carbonation front advances at a much slower timescale than that of dissolved CO_2 diffusion between the exposure surface and carbonation front, because the reaction capacity of the solid phase (Ca content) is large compared to the $CO_2(aq)$ mass in the domain at any moment. Therefore, diffusion is quasi-steady and the $CO_2(aq)$ concentration profile is practically linear between $x_c(t) - \delta$ and $x_c(t)$ as shown in Figure 7.1-1. Coincident with carbonation is decalcification where leaching of aqueous calcium and replenishment of Ca in the pore solution by mineral dissolution consumes $Ca(OH)_2$ and $C\text{-}S\text{-}H$ gel and lowers pH. The carbonation and decalcification fronts are aligned.

At some time to be defined by separate analysis, the steel liner is assumed to undergo corrosion at a rate that consumes all dissolved oxygen at the concrete-liner interface, that is, the liner corrosion rate is controlled by oxygen diffusion. Because the iron (Fe^{II}) content in steel is large compared to the amount of dissolved oxygen in concrete at any time, the $O_2(aq)$ profile will become practically linear between the damage front and liner, reflecting quasi-steady diffusion analogous to dissolved CO_2.

Chloride concentrations above a certain threshold will cause loss of passivation at the concrete-liner interface. Therefore, an estimate of chloride concentration at thickness L is of interest. Chloride is not consumed by corrosion reactions so the shape of the Cl^- concentration profile is different from those of $CO_2(aq)$ and $O_2(aq)$. Conceptually, the environmental chloride concentration is expected to either be fixed at $x = 0$ or move with $x_c(t) - \delta$, depending on the influence of concrete cracks/fractures on Cl^- diffusion. One possibility is that the cracks/fractures are unsaturated due to matric tension (effectively dewatered) and have little impact on matrix diffusion, such that the exposure surface lies at $x = 0$ for all time. Another possibility is that cracks/fractures constitute high-diffusion pathways between $x = 0$ and the damage front, such that the effective exposure surface lies at $x_c(t) - \delta$. The conservative assumption that the Cl^- exposure surface moves with the carbonation front at $x_c(t)$ in front of both $x = 0$ and $x_c(t) - \delta$ is adopted to enable a simple analytic solution for chloride ingress. To further facilitate an analytic solution, two additional approximations are adopted: 1) the concrete domain is assumed semi-infinite ($0 \leq x < \infty$) rather than finite ($0 \leq x \leq L$), and 2) the approximate position of the carbonation front has the form $A\sqrt{t}$ where A is a constant.

Figure 7.1-1: Conceptual Models for Diffusion of Carbon Dioxide, Calcium, Oxygen, and Chloride through Concrete.

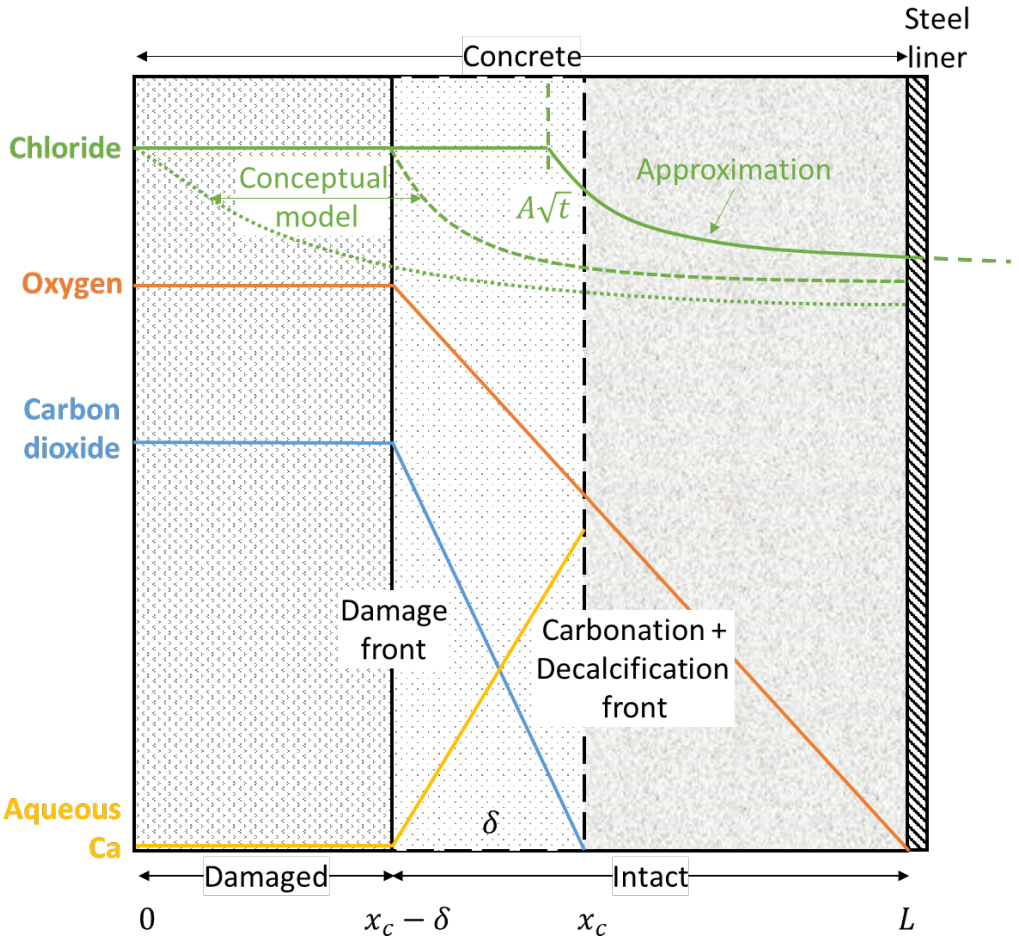

7.2 General Moving Reaction Front

Figure 7.2-1 depicts a general reaction front that moves through a porous-medium and is controlled by the dissolved reactant diffusion rate. The reaction capacity of the solid is implicitly assumed to be large compared to the mass of dissolved reactant in the system at any time, causing the aqueous concentration profile to be effectively linear. In the context of carbonation, the dissolved reactant is $CO_2(aq)$ and the solid-phase reactant is Ca. For decalcification, aqueous Ca diffuses away from a dissolution front and the solid-phase reaction capacity is again Ca content.

Figure 7.2-1: Generic Moving Reaction Front Controlled by Diffusion.

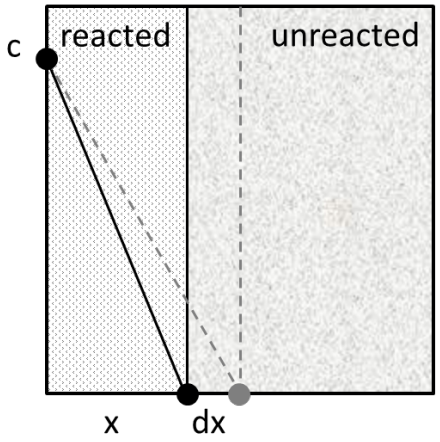

The differential molar balance for this generic moving front system is

$$Sn\tau D_m \frac{c}{x} dt = R(1-n)\rho_s dx \tag{7-1}$$

where

S = saturation of fluid phase delivering reactant to the moving front [cm^3 phase / cm^3 void]

n = porosity [cm^3 void / cm^3 total]

τ = tortuosity/constrictivity, defined here as the ratio of effective to molecular diffusion coefficient (< 1), unitless

D_m = molecular diffusion coefficient for fluid phase [cm^2/yr]

x = penetration depth [cm]

t = elapsed time [yr]

c = concentration of fluid phase reactant at the exposure surface [mol / cm^3 phase]

R = reaction capacity of solid [mol / g solid], i.e., moles of fluid phase reactant consumed per mass of solid

ρ_s = solid / mineral density [g/cm^3 solid].

Assuming a constant diffusion coefficient, integration of Equation (7-1) yields the following analytic expression for penetration depth:

$$x = \left[\frac{2Sn\tau D_m ct}{(1-n)\rho_s R}\right]^{1/2} = \left[\frac{2D_i ct}{\rho_b R}\right]^{1/2} \tag{7-2}$$

where

ρ_b = bulk density, $(1-n)\rho_s$ [g/cm^3]

D_i = intrinsic diffusion coefficient, $Sn\tau D_m$ [cm^2/yr].

Equation (7-2) can be abbreviated as

$$x = At^{1/2} \tag{7-3}$$

where the rate constant A is defined by

$$A \equiv \left[\frac{2Sn\tau D_m c}{(1-n)\rho_s R}\right]^{1/2} = \left[\frac{2D_i c}{\rho_b R}\right]^{1/2} \tag{7-4}$$

Equations (7-2) through (7-4) assume the intrinsic diffusion coefficient, D_i, is a constant. When the chemical reaction front leads to subsequent physical damage, as depicted in Figure 7.1-1, the intrinsic diffusion coefficient will be larger in the damaged region and no longer a constant. In this study, physical damage is assumed to occur when the chemical reaction front has penetrated to a depth δ. The damage front is assumed to then follow the reaction front maintaining the initial separation distance of δ. This assumption is desirable from a mathematical perspective because it yields a tractable analytic solution. A physical rationale for this assumption in the context of carbonation-influenced rebar corrosion is provided in the next section.

The time of initial damage is defined by

$$t_\delta = \left(\frac{\delta}{A}\right)^2 \tag{7-5}$$

and Equation (7-3) can be alternatively be written

$$x = \delta\left(\frac{t}{t_\delta}\right)^{1/2} \tag{7-6}$$

Through t_δ the diffusion distance between the exposure surface and reaction front grows with time, reducing the flux of the dissolved reactant to the reaction front. This effect causes the $\sqrt{t}$ dependence of the penetration depth. However, after t_δ the diffusion distance is fixed at δ because the exposure surface, coincident with the damage front, follows the reaction front. Thus, the reaction front moves at a fixed rate after t_δ and is defined for all times by the composite function

$$x = \begin{cases} \delta\left(\frac{t}{t_\delta}\right)^{1/2} & t \le t_\delta \\ \delta + (t - t_\delta)\left.\frac{dx}{dt}\right|_{t=t_\delta} = \frac{\delta}{2}\left(1 + \frac{t}{t_\delta}\right) & t \ge t_\delta \end{cases} \tag{7-7}$$

7.3 Carbonation and Damage Fronts

Carbonation commonly refers to the reaction of aqueous carbon dioxide with calcium hydroxide (Portlandite) to form calcium carbonate (calcite):

$$Ca(OH)_2 + H_2O + CO_2 \rightarrow CaCO_3 + 2H_2O \tag{7-8}$$

or in cement chemist shorthand notation

$$CH + H + \overline{C} \rightarrow C\overline{C} + 2H \tag{9}$$

where $C \equiv CaO$, $H \equiv H_2O$, and $\bar{C} \equiv CO_2$. More generally, carbonation may include other reactions of dissolved carbon dioxide with certain other high-pH calcium-bearing minerals, such as calcium-silicate-hydrate and calcium-aluminum-silicate-hydrate gels. Carbonation generally increases mechanical strength (https://precast.org/2015/07/understanding-carbonation/) and decreases alkalinity to a pH around 8.5 (https://www.cement.org/learn/concrete-technology/durability/corrosion-of-embedded-materials) in cementitious materials. While the former is beneficial, corrosion of embedded steel accelerates as pH approaches carbonated conditions, approximately $pH < 10$. The volume of the corrosion products far exceeds that of the uncorroded steel, which typically introduces enough internal pressure to cause cracking and spalling of the surrounding concrete. Going forward "carbonation" is used as shorthand for "carbonation-influenced corrosion of steel", keeping in mind that carbonation itself does not appreciably degrade the hydraulic and transport properties on cementitious materials. Rather, carbonation only leads to physical damage in the presence of embedded steel, notably reinforcing bars. Most concrete structures contain reinforcing steel, including the concrete basemat, walls, and roof surrounding waste steel liners.

Papadakis et al. (1989) developed an analytical solution for carbonation penetration depth with the same basic form as Equation (7-2). Using the nomenclature of this report, the expression is

$$x_c = \left[\frac{2\theta D_e c_{CO_2} t}{c_{Ca(OH)_2} + 3c_{CSH}}\right]^{1/2} \tag{7-10}$$

where

x_c = carbonation penetration depth [cm]

θ = gas content, Sn [cm^3 phase / cm^3 total]

D_e = effective diffusion coefficient for gas phase, τD_m [cm^2/yr]

c_{CO_2} = carbon dioxide concentration [mol / cm^3 gas]

t = elapsed time [yr]

$c_{Ca(OH)_2}$ = Portlandite concentration [mol / cm^3 total]

c_{CSH}= CSH concentration, $CSH \equiv 3CaO \cdot 2SiO_2 \cdot 3H_2O$ [mol / cm^3 total].

In the context of Equation (7-4), $c_{Ca(OH)_2} + 3c_{CSH} = (1-n)\rho_s R = \rho_b R$. Equation (7-10) considers only transport of carbon dioxide through the gas phase, which is appropriate for unsaturated concrete in typical applications. However, fully saturated conditions are also of interest for concrete in the subsurface and Equation (7-10) can be generalized to include delivery of dissolved carbon dioxide to the reaction front as

$$x_c = \left[\frac{2\left(\theta_g D_{e,g} c_{CO_2,g} + \theta_\ell D_{e,\ell} c_{CO_2,\ell}\right)t}{c_{Ca}}\right]^{1/2} = At^{1/2} \tag{7-11}$$

where the subscripts g and ℓ denote the gas and liquid phases, respectively, and

$$A \equiv \left[\frac{2\left(\theta_g D_{e,g} c_{CO_2,g} + \theta_\ell D_{e,\ell} c_{CO_2,\ell}\right)}{c_{Ca}}\right]^{1/2} \tag{7-12}$$

Also, the denominator of Equation (7-10) is equivalent to the cumulative molar concentration of Ca in $Ca(OH)_2$ and CSH (more generally C-S-H gel), and denoted by c_{Ca} in these equations. Equation (7-11) is used as the basis for predicting carbonation depth under saturated and unsaturated conditions in this study. However, to account for a damage front following the carbonation front by distance δ, Equations (7-5) and (7-7) with A defined by Equation (7-12) then supersede Equation (7-11).

The assumption of a damage front that trails the carbonation front by a fixed distance δ can be qualitatively justified by invoking two concepts. One idea is that accelerated corrosion starts when the low-pH front reaches rebar and time will elapse before enough corrosion products are created to produce damage. During that time the low-pH front will continue forward, creating a δ between the low-pH and damage fronts. Another concept is that rebar resides at a few discrete depths, so the low-pH front will often be advancing through local material without rebar, such that no damage can occur until the next set of rebar is reached. This second concept suggests the δ between the low-pH and damage fronts should be correlated to rebar spacing, and furthermore be of similar magnitude. A plausible setting for δ is the average spacing of rebar or the depth of near-surface rebar beneath concrete cover. Concrete cover over rebar is typically one inch or more, so $\delta \geq 2.54$ cm can be justified based on a typical surface to first-layer rebar thickness.

A potential vulnerability with the constant-δ concept is that expanding rebar may generate cracks in all directions, including in the direction of the low-pH front, and those cracks could even extend past the low-pH front. A potential mitigating factor is that material on the exposure surface side of rebar is already damaged and thus weaker, making more likely the scenario that damage will take the form of one-sided spalling in the direction of the exposure surface. While the current damage model has not been rigorously vetted and is undoubtedly biased, it is certainly more conservative than ignoring damage altogether and useful from that perspective.

7.4 Decalcification

Leaching of aqueous calcium and replenishment of Ca in the pore solution by mineral dissolution is another process that consumes $Ca(OH)_2$ and $C\text{-}S\text{-}H$ gel and lowers pH. The process is termed decalcification in this study. For decalcification Equation (7-4) becomes

$$A = \left[\frac{2\theta_\ell D_{e,\ell} c_{Ca,\ell}}{c_{Ca}}\right]^{1/2} \tag{7-13}$$

where c_{Ca} is the total molar concentration of Ca in $Ca(OH)_2$ and $C\text{-}S\text{-}H$ gel, as in Equations (7-11) and (7-12).

7.5 Combined Carbonation and Decalcification

Carbonation and decalcification are be expected to occur together, with $Ca(OH)_2$ and/or $C\text{-}S\text{-}H$ gel being simultaneously consumed by leaching and reaction. The rate coefficient for combined carbonation and decalcification is gotten by combining Equations (7-12) and (7-13) as

$$A \equiv \left[\frac{2\left[\theta_g D_{e,g} c_{CO_2,g} + \theta_\ell D_{e,\ell}\left(c_{CO_2,\ell} + c_{Ca,\ell}\right)\right]}{c_{Ca}}\right]^{1/2} \tag{7-14}$$

For the special case of fully saturated concrete, Equation (7-14) reduces to

$$A \equiv \left[\frac{2n D_{e,\ell}\left(c_{CO_2,\ell} + c_{Ca,\ell}\right)}{c_{Ca}}\right]^{1/2} \tag{7-15}$$

where n is porosity.

7.6 Oxygen Diffusion Rate and Amount

Gaseous oxygen is assumed to readily migrate through cracks to the damage front and fully saturate aqueous oxygen at that location. Thus, the oxygen exposure surface coincides with the moving damage front, as with dissolved carbon dioxide. However, $O_2(aq)$ is consumed at the steel liner due by corrosion rather than the carbonation front as with $CO_2(aq)$. The flux of $O_2(aq)$ controlling corrosion of the steel liner is a composite function defined in terms of the carbonation penetration depth $x_c(t)$

$$f = \begin{cases} \dfrac{D_i c}{L} & t \le t_\delta \\ \dfrac{D_i c}{L - (x_c - \delta)} & t \ge t_\delta \end{cases} \tag{7-16}$$

Similarly, the cumulative mass of $O_2(aq)$ delivered to the corroding steel surface is the composite function

$$m = \begin{cases} \dfrac{D_i c}{L} t & t \le t_\delta \\ \dfrac{D_i c}{L} t_\delta + \dfrac{D_i c}{L} \displaystyle\int_{t_\delta}^{t} \frac{1}{1 - \left(\frac{x_c - \delta}{L}\right)} dt & t \ge t_\delta \end{cases} \tag{7-17}$$

defined by integrating Equation (7-16). After straightforward but lengthy evaluation and simplification of the integral term, Equation (7-17) becomes

$$m = \begin{cases} \dfrac{D_i c}{L} t & t \le t_\delta \\ \dfrac{D_i c}{L} t_\delta \left[1 - \dfrac{2L}{\delta} ln\left(1 + \dfrac{\delta}{2L} - \dfrac{\delta}{2L} \cdot \dfrac{t}{t_\delta}\right)\right] & t \ge t_\delta \end{cases} \tag{7-18}$$

If corrosion at the steel liner is not active starting at time zero (likely), the cumulative mass of oxygen consumed by corrosion can be accurately approximated by

$$\Delta m = m(t) - m(t_0) \tag{7-19}$$

where t_0 is starting time for active corrosion. Equation (7-16) can be expanded to account for partially saturated concrete, such that oxygen can also migrate through the gas phase, by replacing D_i with and effective aqueous diffusion coefficient defined as

$$D_{i,eff} = D_i + D_{i,gas} \frac{c_{gas}}{c} \tag{7-20}$$

where the un-subscripted parameters implicitly describe the liquid phase.

7.7 Chloride Concentration

Chloride concentration at the steel liner surface may also be of interest from a passivation perspective. Because chloride is not consumed at a reaction front like carbon dioxide and oxygen, its concentration profile has a much different character and simplifying assumptions are required to readily achieve a closed-from expression. Also, because the chloride source is aqueous, the location of the effective exposure surface is not obvious under unsaturated conditions, as noted earlier. The following conditions are assumed to facilitate a closed-form analytic solution:

- The concrete domain is semi-infinite rather than finite thickness L (non-conservative).
- The effective exposure surface resides at the carbonation front not either the damage front or $x = 0$ (conservative).
- The carbonation front is located at $A\sqrt{t}$ for all time not just $t \le t_\delta$ (non-conservative).

On the balance these assumptions are expected to overpredict chloride concentration at the steel liner if the conceptual model has the exposure surface fixed at $x = 0$. If the conceptual model has the exposure surface coinciding with the damage, these assumptions are generally expected to overpredict chloride concentrations at early times and underpredict at later times. The governing equations corresponding to these assumptions are

$$\frac{\partial c}{\partial t} = D_e \frac{\partial^2 c}{\partial x^2} \tag{7-21}$$

$$c = c_0 \quad @\, x = x_c(t) = At^{1/2} \tag{7-22}$$

$$c = 0 \quad @\, x = \infty, t = 0 \tag{7-23}$$

where $D_e \equiv \tau D_m = D_i / Sn$ is the effective diffusion coefficient. The following expression can be shown to satisfy Equations (7-21) through (7-23) by substitution of the function and its derivatives

$$c = \frac{c_0}{erfc\left(\frac{A}{2\sqrt{D_e}}\right)} \cdot erfc\left(\frac{x}{2\sqrt{D_e t}}\right) \tag{7-24}$$

The degree of approximation associated with Equation (7-24) will depend on each specific case analyzed. In comparison, for the conceptual model with the exposure surface fixed at $x = 0$,

$$c = c_0 \cdot erfc\left(\frac{x}{2\sqrt{D_e t}}\right) \tag{7-25}$$

Thus, the assumption that the chloride exposure surface moves as $A\sqrt{t}$ increases Cl^- concentration by the constant

$$\frac{1}{erfc\left(\frac{A}{2\sqrt{D_e}}\right)} \tag{7-26}$$

7.8 Rate Coefficient and Penetration Depth Calculations

Table 7.8-1 summarizes rate coefficient calculations for concrete under the Realistic, Compliance, and Pessimistic Cases for carbonation (Section 7.3), decalcification (Section 7.4), and combined carbonation + decalcification (Section 7.5), except for floor concrete in the Pessimistic Case where a 3x higher diffusion coefficient is assumed to reflect postulated cracks (SRNL-STI-2021-00187). The carbonation + decalcification rate coefficients for Pessimistic Case floor concrete are A = 0.197 and 1.050 cm/√yr under saturated and vadose zone conditions, respectively. Additional calculations for oxygen diffusion rate and chloride concentration are not pursued herein because steel liner service life estimates are outside the scope of this study.

The air-entry pressure of concrete is expected to far exceed suction heads surrounding waste tanks; see SRNL-STI-2018-00077 for example calculations. Therefore 0% gas saturation is expected for intact concrete and adopted for the Realistic Case and any tank that is submerged. Following SRNL-STI-2018-00077, two additional values are assumed for the Compliance and Realistic Cases, 2% and 5% gas saturation, respectively. Although no specific cause is invoked in postulating these more conservative values, increased gas saturation could be associated with concrete that has degraded by becoming more porous and/or cracked through various underlying mechanisms.

The distance δ by which the damage front lags the carbonation+decalcification front is needed to compute penetration depth as a function of time using rate coefficients from Table 7.8-1. As discussed in Section 7.3, this lag distance can be reasonably associated with the thickness of concrete cover over rebar. Inspection of SRS tank drawings and duPont Engineering Standard B-14-L indicates the minimum rebar cover ranges from 1.5 to 2.0 inches. The lower value, 1.5 inches = 3.81 cm, is assumed for all concrete components in the Realistic and Compliance Cases. For the Pessimistic Case δ = 1.0 inches = 2.54 cm is assumed for all components.

Figure 7.8-1 through Figure 7.8-3 illustrate penetration depths through time for the Realistic, Compliance, and Pessimistic Cases, respectively (except floor concrete in the Pessimistic Case).

The carbonation + decalcification (dissolution) front initially advances in proportion to $\sqrt{t}$, prior to physical damage altering the spatial-average diffusion coefficient. After damage initiation at $x = \delta$, penetration is linear with time. The damage front lags by $x = \delta$ and advances linearly after initiation. The position of the carbonation + decalcification front when the diffusion coefficient is assumed to be constant ($\delta = \infty$) is also plotted to show the effect of the damage feedback model (finite δ).

Table 7.8-2 summarizes the physical degradation times for each tank type, concrete component, and modeling case. Damage "Start" times coincide with the carbonation + decalcification front reaching $x = \delta$, which are the same value for each tank type and component within a modeling case. "Damage time" is the time when the damage front fully penetrates the designated thickness, that is, the time for complete physical degradation. The carbonation + decalcification front moves ahead of the damage front and its times for complete penetration are also listed for reference.

Table 7.8-1: Rate Coefficient Calculations for Concrete.

Parameter	Realistic and Submerged Tank Cases	Compliance Case	Pessimistic Case	Units
Carbonation				
p_{CO_2} (a)	0.01	0.01	0.01	atm
$c_{CO_2,g}$ (b)	4.16e-07	4.16e-07	4.16e-07	mol/cm^3 gas
$c_{CO_2,\ell}$ (c)	3.41e-06	3.41e-06	3.41e-06	mol/cm^3 liquid
n (d)	0.168	0.168	0.168	cm^3 void / cm^3 total
ρ_b (d)	2.06	2.06	2.06	g/cm^3 total
$D_{m,g}$ (e)	0.165	0.165	0.165	cm^2/s
τ (f)	3.48E-02	3.48E-02	3.48E-02	-
$D_{e,g}$ (g)	5.74E-03	5.74E-03	5.74E-03	cm^2/s
$D_{e,\ell}$ (d)	8.0E-07	8.0E-07	8.0E-07	cm^2/s
c_{Ca} (h)	3.56e-03	3.56e-03	3.56e-03	mol/cm^3 total
S_g (i)	0	0.02	0.05	cm^3 gas / cm^3 void
S_ℓ (j)	1	0.98	0.95	cm^3 liquid / cm^3 void
θ_g (j)	0	0.00336	0.0084	cm^3 gas / cm^3 total
θ_ℓ (j)	0.168	0.16464	0.1596	cm^3 liquid / cm^3 total
A (k)	**0.090**	**0.387**	**0.603**	cm/√yr
Decalcification				
$c_{Ca^{2+}}$ (l)	2.0e-06	2.0e-06	2.0e-06	mol/cm^3 liquid
A (m)	**0.069**	**0.068**	**0.067**	cm/√yr
Carbonation + Decalcification				
A (n)	**0.114**	**0.393**	**0.606**	cm/√yr

(a) SRNL-L3200-2012-00017
(b) p_{CO_2} and ideal gas law at 20C
(c) SRNL-STI-2018-00077 Rev. 1 Table 4-1
(d) SRR-CWDA-2010-00128, Rev. 1, Table 4.2-28
(e) Marrero and Mason (1972), Table 13 and Equation (4.3-2), air-CO_2 system at 298°K
(f) Calculated from liquid-phase effective diffusion coefficient assuming a molecular diffusion coefficient of 2.3e-05 cm^2/s (Holz et al. 2000)
(g) $D_{e,g} = \tau D_{m,g}$
(h) Equal to CaO concentration (Section 3.5, Appendix B)
(i) Expected condition for Realistic Case; postulated conditions for Compliance and Pessimistic Cases
(j) $S_g + S_\ell = 1$, $\theta_g = S_g n$ and $\theta_\ell = S_\ell n$
(k) Equation (7-12)
(l) Approximate solubility of CSH (SIMCO 2012, Clodic and Meike 1997, Figure 6.2-1)
(m) Equation (7-13)
(n) Equation (7-15)

Figure 7.8-1: Carbonation+Decalcification and Damage Front Penetration for Vadose Zone Tanks and the Realistic Case.

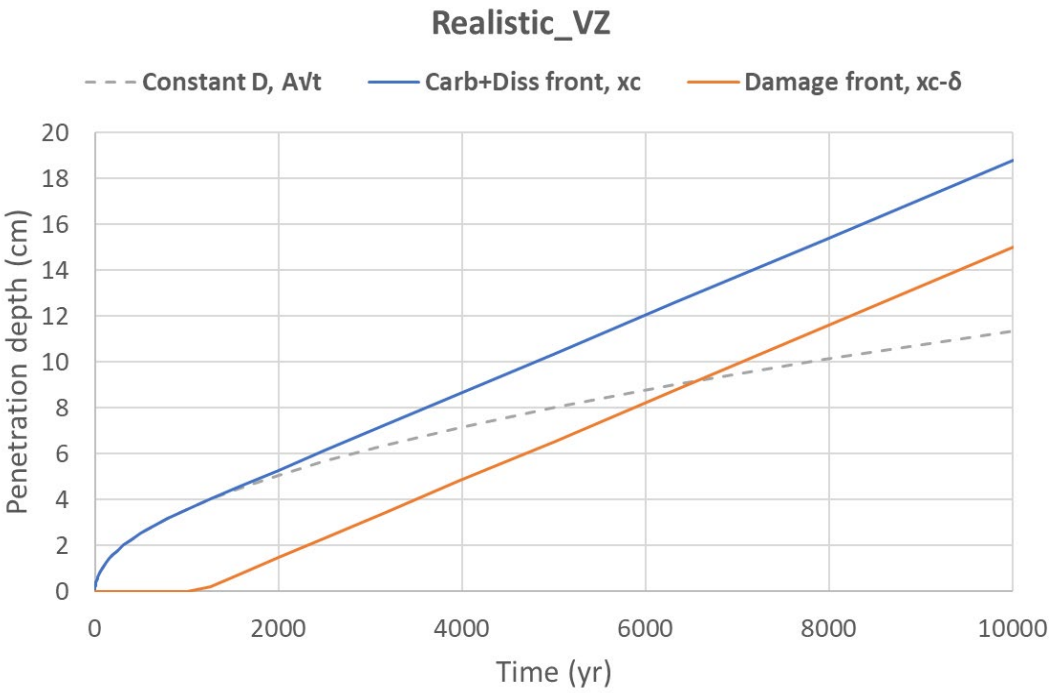

Figure 7.8-2: Carbonation+Decalcification and Damage Front Penetration for Vadose Zone Tanks and the Compliance Case.

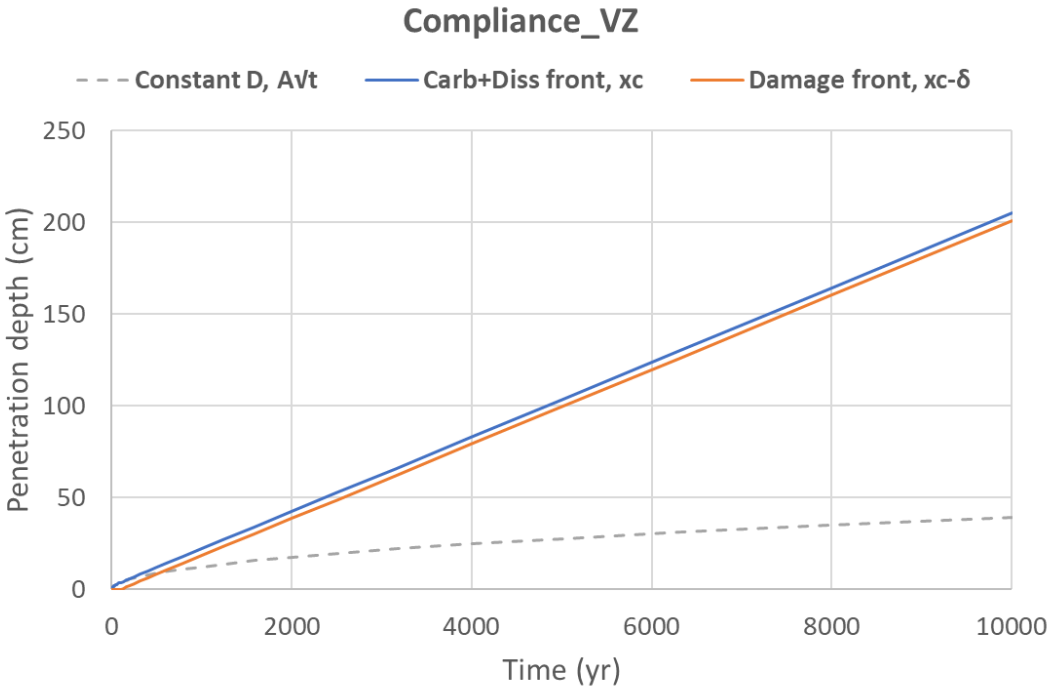

Figure 7.8-3: Carbonation+Decalcification and Damage Front Penetration for Vadose Zone Tanks the Pessimistic Case.

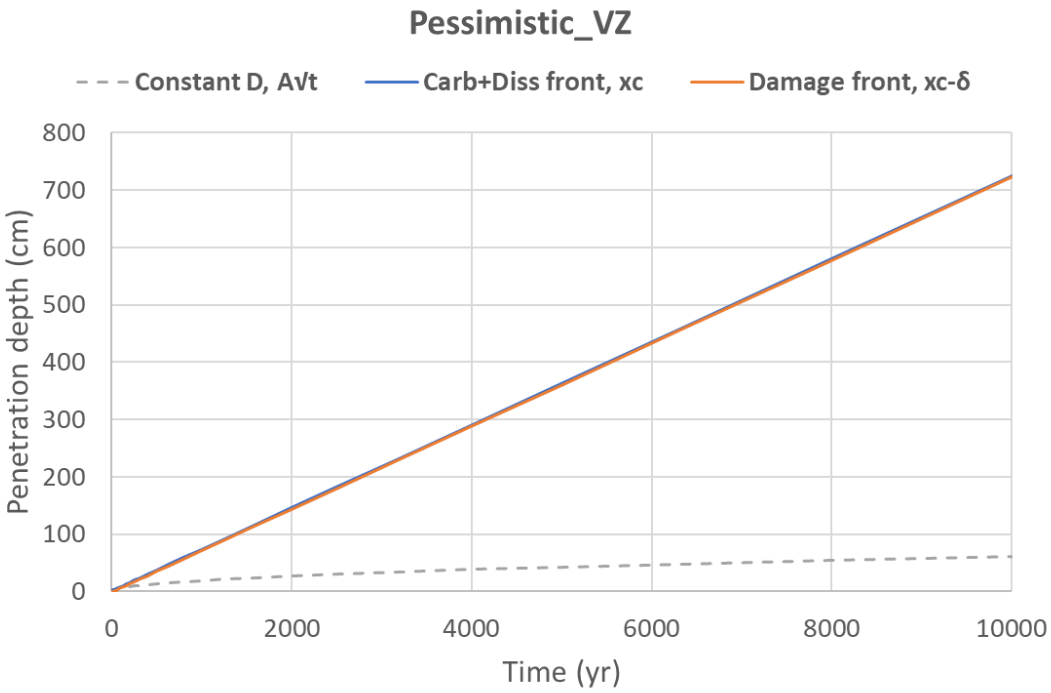

Table 7.8-2: Physical Degradation Times for Concrete Based on Rebar Corrosion Controlled by Carbonation and Decalcification.

Tank	Component	Thickness		Saturated Zone		Vadose Zone	
		(cm)	(in)	Carb+Diss (yr)	Damage (yr)	Carb+Diss (yr)	Damage (yr)
Realistic Case				Start:	1,126	Start:	1,126
Type I	Roof	55.9	22.0	31,928	34,181	31,928	34,181
Type I	Wall	55.9	22.0	31,928	34,181	31,928	34,181
Type I	Floor	76.2	30.0	43,932	46,185	43,932	46,185
Type II	Roof	114.3	45.0	66,461	68,714	66,461	68,714
Type II	Wall	83.8	33.0	48,426	50,679	48,426	50,679
Type II	Floor	106.7	42.0	61,967	64,220	61,967	64,220
Type III/IIIA	Roof	121.9	48.0	70,955	73,208	70,955	73,208
Type III/IIIA	Wall	76.2	30.0	43,932	46,185	43,932	46,185
Type III/IIIA	Floor	106.7	42.0	61,967	64,220	61,967	64,220
Type IV	Roof	17.8	7.0	9,399	11,652	9,399	11,652
Type IV	Wall	17.8	7.0	9,399	11,652	9,399	11,652
Type IV	Floor	17.5	6.9	9,222	11,474	9,222	11,474
Compliance Case				Start:	1,126	Start:	94
Type I	Roof	55.9	22.0	31,928	34,181	2,658	2,845
Type I	Wall	55.9	22.0	31,928	34,181	2,658	2,845
Type I	Floor	76.2	30.0	43,932	46,185	3,657	3,844
Type II	Roof	114.3	45.0	66,461	68,714	5,532	5,720
Type II	Wall	83.8	33.0	48,426	50,679	4,031	4,218
Type II	Floor	106.7	42.0	61,967	64,220	5,158	5,346
Type III/IIIA	Roof	121.9	48.0	70,955	73,208	5,906	6,094
Type III/IIIA	Wall	76.2	30.0	43,932	46,185	3,657	3,844
Type III/IIIA	Floor	106.7	42.0	61,967	64,220	5,158	5,346
Type IV	Roof	17.8	7.0	9,399	11,652	782	970
Type IV	Wall	17.8	7.0	9,399	11,652	782	970
Type IV	Floor	17.5	6.9	9,222	11,474	768	955
Pessimistic Case				Start:	501	Start:	18
Type I	Roof	55.9	22.0	21,536	22,537	755	790
Type I	Wall	55.9	22.0	21,536	22,537	755	790
Type I	Floor	76.2	30.0	29,538	30,539	1,035	1,070
Type II	Roof	114.3	45.0	44,558	45,559	1,562	1,597
Type II	Wall	83.8	33.0	32,534	33,535	1,140	1,175
Type II	Floor	106.7	42.0	41,562	42,563	1,457	1,492
Type III/IIIA	Roof	121.9	48.0	47,554	48,555	1,667	1,702
Type III/IIIA	Wall	76.2	30.0	29,538	30,539	1,035	1,070
Type III/IIIA	Floor	106.7	42.0	41,562	42,563	1,457	1,492
Type IV	Roof	17.8	7.0	6,516	7,518	228	263
Type IV	Wall	17.8	7.0	6,516	7,518	228	263
Type IV	Floor	17.5	6.9	6,398	7,399	224	259

7.9 Anoxic Rebar Corrosion

The conceptual model described in Section 7.1 assumes that rebar corrosion can be neglected prior to arrival of the carbonation + decalcification front. Although corrosion of passivated steel is much slower than that of un-passivated steel, the rate is not zero and could become limiting over long periods. Anoxic corrosion of rebar has been analyzed in SRNL-STI-2021-00187 and Table 7.9-1 summarizes the results.

Table 7.9-1: Physical Degradation Times for Concrete Based on Anoxic Rebar Corrosion (SRNL-STI-2021-00187).

Tank	Component	Damage Time (yr)
Type I	Roof	11,002
Type I	Wall	10,809
Type I	Floor	9,178
Type II	Roof	21,341
Type II	Wall	16,373
Type II	Floor	22,983
Type III/IIIA	Roof	20,884
Type III/IIIA	Wall	20,393
Type III/IIIA	Floor	17,228
Type IV	Roof	4,742
Type IV	Wall	8,021
Type IV	Floor	5,418

7.10 Limiting Physical Degradation Times

Because the carbonation + decalcification and anoxic corrosion phenomena can be treated as independent and operating in parallel, the limiting physical degradation time is the minimum of the two times from those corrosion processes. Table 7.10-1 compares the physical degradation times arising from carbonation + decalcification and anoxic rebar corrosion and lists the more limiting time. Anoxic corrosion is the limiting process for the Realistic Case and vadose zone concrete, and for all cases involving saturated concrete.

Table 7.10-1: Physical Degradation Times for Concrete.

				Saturated Zone Concrete			Vadose Zone Concrete		
Tank	Compo-nent	Thick-ness (cm)	(in)	Carb + Decal (yr)	Anoxic (yr)	Limiting Time (yr)	Carb + Decal (yr)	Anoxic (yr)	Limiting Time (yr)
Realistic case			start:	1,126	-		1,126	-	
Type I	Roof	55.9	22.0	34,181	11,002	11,002	34,181	11,002	11,002
Type I	Wall	55.9	22.0	34,181	10,809	10,809	34,181	10,809	10,809
Type I	Floor	76.2	30.0	46,185	9,178	9,178	46,185	9,178	9,178
Type II	Roof	114.3	45.0	68,714	21,341	21,341	68,714	21,341	21,341
Type II	Wall	83.8	33.0	50,679	16,373	16,373	50,679	16,373	16,373
Type II	Floor	106.7	42.0	64,220	22,983	22,983	64,220	22,983	22,983
Type III/IIIA	Roof	121.9	48.0	73,208	20,884	20,884	73,208	20,884	20,884
Type III/IIIA	Wall	76.2	30.0	46,185	20,393	20,393	46,185	20,393	20,393
Type III/IIIA	Floor	106.7	42.0	64,220	17,228	17,228	64,220	17,228	17,228
Type IV	Roof	17.8	7.0	11,652	4,742	4,742	11,652	4,742	4,742
Type IV	Wall	17.8	7.0	11,652	8,021	8,021	11,652	8,021	8,021
Type IV	Floor	17.5	6.9	11,474	5,418	5,418	11,474	5,418	5,418
Compliance case			start:	1,126	-		94	-	
Type I	Roof	55.9	22.0	34,181	11,002	11,002	2,845	11,002	2,845
Type I	Wall	55.9	22.0	34,181	10,809	10,809	2,845	10,809	2,845
Type I	Floor	76.2	30.0	46,185	9,178	9,178	3,844	9,178	3,844
Type II	Roof	114.3	45.0	68,714	21,341	21,341	5,720	21,341	5,720
Type II	Wall	83.8	33.0	50,679	16,373	16,373	4,218	16,373	4,218
Type II	Floor	106.7	42.0	64,220	22,983	22,983	5,346	22,983	5,346
Type III/IIIA	Roof	121.9	48.0	73,208	20,884	20,884	6,094	20,884	6,094
Type III/IIIA	Wall	76.2	30.0	46,185	20,393	20,393	3,844	20,393	3,844
Type III/IIIA	Floor	106.7	42.0	64,220	17,228	17,228	5,346	17,228	5,346
Type IV	Roof	17.8	7.0	11,652	4,742	4,742	970	4,742	970
Type IV	Wall	17.8	7.0	11,652	8,021	8,021	970	8,021	970
Type IV	Floor	17.5	6.9	11,474	5,418	5,418	955	5,418	955
Pessimistic case			start:	501	-		18	-	
Type I	Roof	55.9	22.0	22,537	11,002	11,002	790	11,002	790
Type I	Wall	55.9	22.0	22,537	10,809	10,809	790	10,809	790
Type I	Floor	76.2	30.0	10,180	9,178	9,178	357	9,178	357
Type II	Roof	114.3	45.0	45,559	21,341	21,341	1,597	21,341	1,597
Type II	Wall	83.8	33.0	33,535	16,373	16,373	1,175	16,373	1,175
Type II	Floor	106.7	42.0	14,188	22,983	14,188	497	22,983	497
Type III/IIIA	Roof	121.9	48.0	48,555	20,884	20,884	1,702	20,884	1,702
Type III/IIIA	Wall	76.2	30.0	30,539	20,393	20,393	1,070	20,393	1,070
Type III/IIIA	Floor	106.7	42.0	14,188	17,228	14,188	497	17,228	497
Type IV	Roof	17.8	7.0	7,518	4,742	4,742	263	4,742	263
Type IV	Wall	17.8	7.0	7,518	8,021	7,518	263	8,021	263
Type IV	Floor	17.5	6.9	2,466	5,418	2,466	86	5,418	86

8.0 DISCUSSION

This section compares chemical evolution simulations to SRNL-STI-2012-00404, discusses potential implications to radionuclide solubilities, and summarizes how to use physical degradation times to compute hydraulic properties as a function of time.

8.1 Chemical Evolution and Solubility Implications

The simulated pH evolutions provided in Section 4.1 have a stair-step nature that results from approximating C-S-H gel with a solid solution model comprising a few distinct minerals. In contrast, C-S-H gel dissolves incongruently, its stoichiometry varies more continuously, and a smoother pH variation is expected. Figure 8.1-1 illustrates this concept with a semi-transparent thick gold line overlaying the pH evolution simulated for LP#8-16 from initial curing to pH = 8.3, when C-S-H gel is exhausted and calcite is the buffer. Figure 8.1-2 adds the base and sensitivity cases from SRNL-STI-2012-00404 with axis ranges modified to match Figure 11 in that report. The simulated pH variation from this study ("SRR-CWDA-2021-00034") is comparable to the various SRNL-STI-2012-00404 cases. All simulations approximately follow the gold trendline, albeit in a stair-step fashion. In that sense each simulation is a credible approximation to expected reality, including the original SRNL-STI-2012-00404 base case.

The updated C-S-H solid solution model and CEMDATA18.1 thermodynamic database are evidently less important than degree of hydration and silica mineralogy assumptions ("disposition of silica" in SRNL-STI-2012-00404 parlance) to pH evolution. The inherent challenge is that cement mineralogy evolves with ongoing hydration reactions and even "long-term" experiments lasting years are far shorter than PA timeframes of hundreds, thousands, to tens of thousands of years. In this study, degrees of hydration assumptions are based on short-term experimental observations that minimize reaction capacity, thus pessimistically biasing predictions toward faster chemical aging.

Figure 8.1-2 also depicts the pH regions defined for subsequent radionuclide and chemical waste solubility analyses. Considering the brevity of Region I, only Regions II and III from the base case were used in SRNL-STI-2012-00404 for solubility analysis. If the gold line amalgamating model results is divided at pH = 10 into two regions, the pore volume breakpoint is 1968, which is close to the 2119 pore volumes dividing Regions II and III. On average Region III is representative of the 10 > pH > 8.3 portion of the gold line. Within the pH > 10 window, Region II is biased high but more representative of early (Region b) pore volumes that may drive compliance with PA performance objectives. Thus, the pore solutions associated with Regions II and III still appear to be a reasonable binary approximation to the physical system, and solubility recommendations based on these regions are deemed still valid.

However, the present "SRR-CWDA-2021-00034" simulation exhibits an extended "Region c" period at pH 10.0, midway between Region II at pH 11.1 and Region III at 9.2. These intermediate pore solution conditions described in Section 5.1 (or more generally Regions a through e) could be further examined with respect to key radionuclide solubilities to provide added confidence in PA predictions. Similarly, Section 5.2 offers alternative groundwater solutions that could be analyzed in relation to trace species solubility for added PA confidence. Finally, the vadose and saturated zone solutions derived in this study are based on P_{CO_2} = 0.01 atm, which results in

elevated dissolved inorganic carbon (DIC) concentrations and could impact solubility recommendations.

Figure 8.1-1: pH Evolution Simulated for LP#8-16 Compared to Expected Variation.

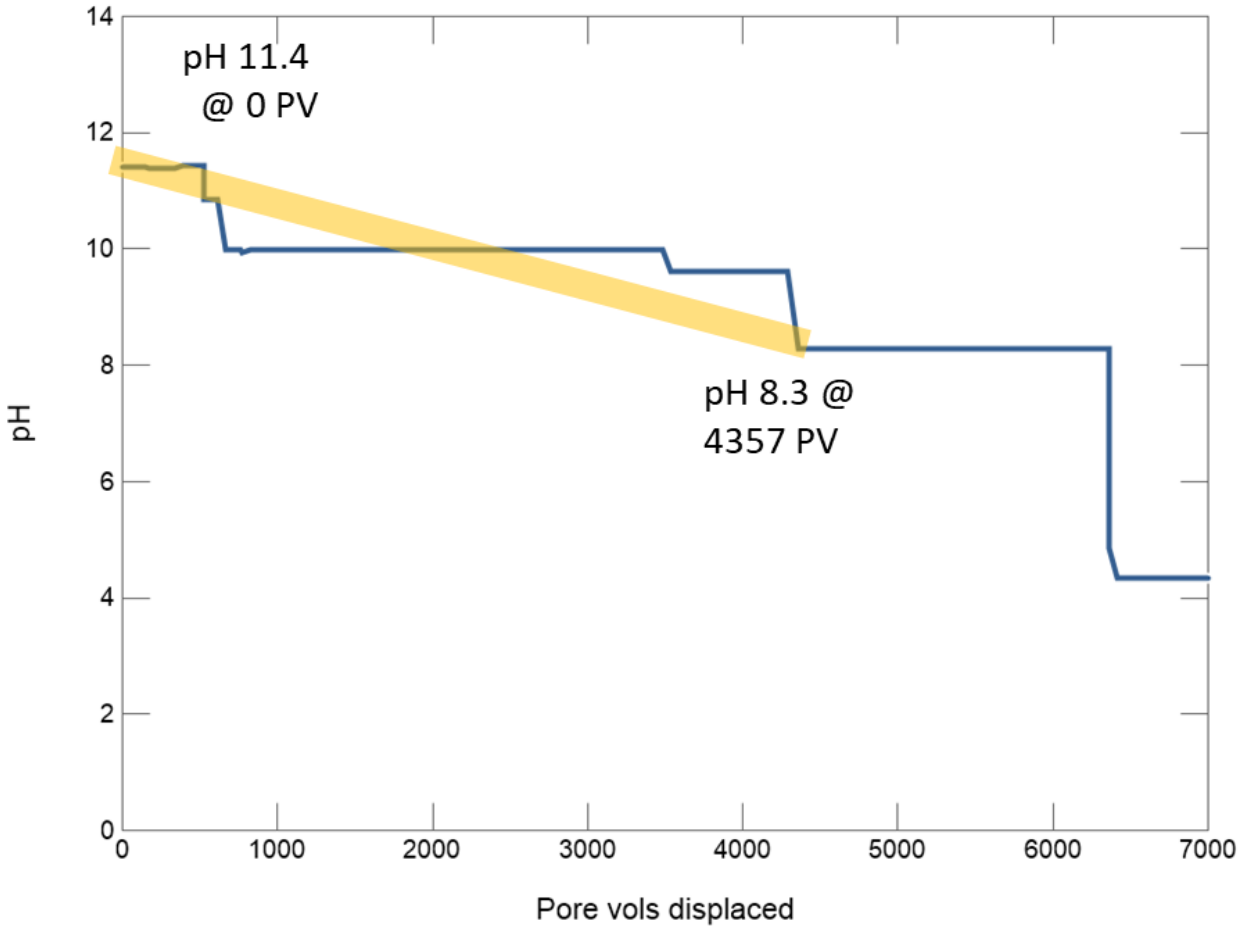

Figure 8.1-2: SRNL-STI-2012-00404 pH Evolutions and Solubility Regions.

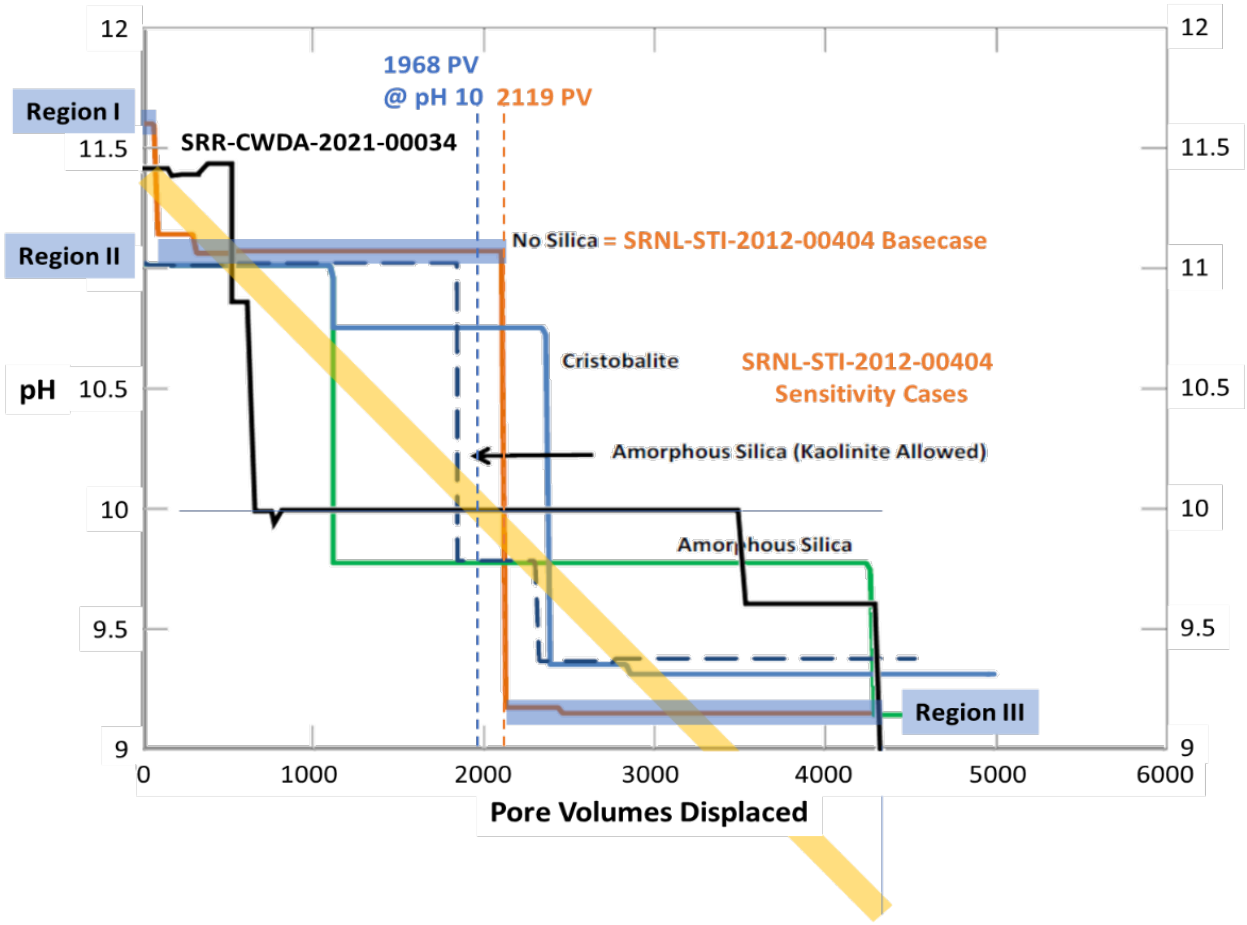

8.2 Physical Degradation

The physical degradation times provided in Table 6.3-1 and Table 7.10-1 for grouts and concrete, respectively, reflect a comprehensive reanalysis of tank cementitious materials using new methods and coordination with the steel corrosion analyses recently conducted by Savannah River National Laboratory (SRNL) (SRNL-STI-2021-00187). Although Realistic Cases use inputs that tend to be best-estimate values, the simplified analytic method for combined carbonation and decalcification conservatively assumes the penetration front advances linearly with time after 1.5 inches. The coupled equilibrium chemistry and diffusive transport simulations in Section 4.2 are a more rigorous and realistic simulation of these processes for early times, that is, before significant rebar damage occurs and alters the effective diffusion coefficient of the system. Figure 4.2-8 indicates the pH = 10 front in concrete at approximately 2.5 cm (1 in), which is less than the thickness of rebar cover and suggests low rebar corrosion rates through 20,000 years. In contrast, the analytic method indicates significant corrosion and damage at 20,000 years. This comparison is an indication of the pessimism embedded in the analytic technique. The Compliance and Pessimistic Cases reflect additional bias via more conservative input values.

The updated physical degradation times in Table 6.3-1 and Table 7.10-1 can be associated with degradation fractions and equivalent property models to predict transient variations of hydraulic properties following SRNL-STI-2018-00077 and SRNL-STI-2017-00525. A degradation fraction (f) can defined in terms of the start (t_0) and end (t_1) times for degradation as

$$f(t) \equiv \frac{min[max(t_0, t_1)] - t_0}{t_1 - t_0} \tag{8-1}$$

Then, assuming geometric averaging for example, the time-variation of saturated hydraulic conductivity can be written as

$$K_{sat}(t) = exp[f(t) \cdot lnK_1 + (1 - f(t)) \cdot lnK_0] \tag{8-2}$$

where K_0 and K_1 are the initial and fully degraded values, respectively. SRNL-STI-2018-00077 discusses alternatives to Equation (8-2) including arithmetic, harmonic, and generalized p-norm averages.

9.0 REFERENCES

B-14-L, du Pont, *Concrete Engineering Standard*, issued July 1946, revised and reaffirmed December 1983.

C-DCF-G-00397, *Populate Mix Design Tables, Attachment 5.5*, Savannah River Site, Aiken, SC, Rev. 0, November 2015.

C-DCF-G-00400, *Revise "Designing, Furnishing and Delivery of Ready Mixed Concrete, Grout and CLSM (U)" Specification*, Savannah River Site, Aiken, SC, Rev. 0, February 2018.

C-SPP-F-00055, *Furnishing and Delivery of Tank Closure Grout*, Savannah River Site, Aiken, SC, Rev. 6, October 2016.

C-SPP-Z-00012, *Vault 4 Clean Cap Grout*, Savannah River Site, Aiken, SC, Rev. 1, March 2014.

C-SPS-G-00096, *Designing, Furnishing and Delivery of Ready Mixed Concrete, Grout and CLSM (GS & PS)*, Savannah River Site, Aiken, SC, Rev. 3, September 2015.

Clodic, L. and A. Meike, *Development of a Database to Model Concrete Dissolution at 25°C Using the EQ3/6 Geochemical Modeling Code*, Lawrence Livermore National Laboratory report UCRL-ID-132088, August 1997.

Denham, M.E., *Opportunities to Update the Model of Tank Closure Grout Aging (SRNL-STI-2012-00404) Based on Experimental Results by the Savannah River Ecology Laboratory*, Inspection Experts Inc. report IEI 2024-001, developed by Panoramic Environmental Consulting LLC, Aiken, SC, November 2020.

DPST-85-958, Hubbard, J.E., *An Update on the SRP Burial Ground Area Water Balance and Hydrology*, Savannah River Site, Aiken, SC, Rev. 0, January 9, 1986.

DPST-86-658, Parizek, R.R., and R.W. Root, Jr., *Development of a Ground-Water Velocity Model for the Radioactive Waste Management Facility Savannah River Plant, South Carolina*, Savannah River Site, Aiken, SC, Rev. 0, June 1986.

Giffaut, E., M. Grivé, P. Blanc, P. Vieillard, E. Colàs, H. Gailhanou, S. Gaboreau, N. Marty, B. Madé, L. Duro, *Andra thermodynamic database for performance assessment: ThermoChimie*, Applied Geochemistry, 49, 225-236, 2014.

Holz, M., S.R. Heil and A. Sacco, *Temperature-dependent self-diffusion coefficients of water and six selected molecular liquids for calibration in accurate 1H NMR PFG Measurements*, Phys. Chem. Chem. Phys. 2, 4740–4742, 2000.

Kulik, D.A., *Improving the structural consistency of C-S-H solid solution thermodynamic models*, Cement and Concrete Research, 41, 477-495, 2011.

Lothenbach, B. and F. Winnefeld, *Thermodynamic modeling of the hydration of Portland cement*, Cement and Concrete Research, 36, 209-226, 2006.

Lothenbach, B., D.A. Kulik, T. Matschei, M. Balonis, L. Baquerizo, B. Dilnesa, G.D. Miron, and R.J. Myers, *Cemdata18: A chemical thermodynamic database for hydrated Portland cements and alkali-activated materials*, Cement and Concrete Research, 115, 472–506, 2019.

Manual 1Q, Procedure 20-1, *Software Quality Assurance*, Revision 21, 9/30/2020.

Manual E7, Procedure 5.01, *Software Engineering and Control*, Revision 5, 9/30/2020.

Manual E7, Procedure 2.31A, *LW Engineering Calculations*, Revision 11, 2/18/2021.

Marrero, T.R., and E.A. Mason, *Gaseous Diffusion Coefficients*, J. Phys. Chem. Ref. Data, Vol. 1, No. 1, https://srd.nist.gov/JPCRD/jpcrd1.pdf.

Nuclear Energy Agency (NEA), https://www.oecd-nea.org/jcms/pl_37223/electronic-database-of-the-tdb-project, downloaded 1/12/2021, December 2020.

Nimmo, J.R., J.A. Deason, J.A. Izbicki and P. Martin, *Evaluation of unsaturated zone water fluxes in heterogeneous alluvium at a Mojave Basin Site*, Water Resources Research 38, 1215, doi:10.1029/2001WR000735, 2002.

Papadakis, V.G., C.G. Vayenas, and M.N. Fardis, *A Reaction Engineering Approach to the Problem of Concrete Carbonation*, AIChE Journal, 35:1639-1650, 1989.

Pilar, F.L., *Chemistry: The Universal Science*, Addison-Wesley, Reading MA, 1979.

R-21-0001, Seaman, J.C., S.P. Simner, and C. Logan, *Aqueous and Solid Phase Characterization of Potential Tank Fill Materials*, Savannah River Ecology Laboratory, Aiken, SC, Rev. 0, 2020.

Railsback, L.B., *Some Fundamentals of Mineralogy and Geochemistry*, http://railsback.org/Fundamentals/1121WeatheringCO207.pdf, accessed 3/29/21, January 2009.

Rumble, J.R., ed., *CRC Handbook of Chemistry and Physics*, 101st Edition (Internet Version 2020), CRC Press/Taylor & Francis, Boca Raton, FL.

SIMCO Technologies Inc., *Washington Savannah River Company Subcontract AC81850N Report – Vault Concrete Characterization*, March 2012.

SRNL-L3200-2012-00017, *Summary Carbon Dioxide in Water Table Wells and the Vadose Zone at SRS*, Savannah River Site, Aiken, SC, Rev. 0, May 2012.

SRNL-L3200-2012-00022, *Background Water Table Chemistry in the General Separations Area*, Savannah River Site, Aiken, SC, Rev. 0, August 2012.

SRNL-STI-2009-00637, Roberts, K.A., and D.I. Kaplan, *Reduction Capacity of Saltstone and Saltstone Components*, Savannah River Site, Aiken, SC, Rev. 0, November 2009.

SRNL-STI-2010-00035, Langton, C.A., *Chemical Degradation Assessment for the H-Area Tank Farm Concrete Tanks and Fill Grouts*, Savannah River Site, Aiken, SC, Rev. 0, January 29, 2010.

SRNL-STI-2010-00047, Garcia-Diaz, B.L., *Life Estimation of High Level Waste Tank Steel for H-Tank Farm Closure Performance Assessment*, Savannah River Site Aiken, SC, March 2010.

SRNL-STI-2012-00404, Denham, M.E. and M.R. Millings, *Evolution of Chemical Conditions and Estimated Solubility Controls on Radionuclides in the Residual Waste Layer during Post-Closure Aging of High-Level Waste Tanks*, Savannah River Site, Aiken, SC, Rev. 0, August 2012.

SRNL-STI-2017-00525, Flach, G.P., *Method for Modeling the Gradual Physical Degradation of a Porous Material*, Savannah River National Laboratory, Aiken, SC, Rev. 0, September 2017.

SRNL-STI-2018-00077, Flach, G.P., *Degradation of Saltstone Disposal Unit Cementitious Materials*, Savannah River National Laboratory, Aiken, SC, Rev. 1, August 2018.

SRNL-STI-2021-00017, Kaplan, D.I., *Geochemical Data Package for Performance Assessment Calculations Related to the Savannah River Site*, Savannah River National Laboratory, Aiken, SC, Rev. 0, February 2021.

SRNL-STI-2021-00187, Wiersma, B.J., *Corrosion of Steel During Long-Term Exposure to Evolving Cementitious Environments*, Savannah River National Laboratory, Aiken, SC, Rev. 0, April 2021.

SRR-CWDA-2010-00128, *Performance Assessment for the H-Tank Farm at the Savannah River Site,* Savannah River Site, Aiken, SC, Rev. 1, November 2012.

SRR-CWDA-2013-00144, *Comment Response Matrix for NRC Staff Clarification Questions on DOE Responses to Request for Additional Information on the Draft Basis for Section 3116 Determination and Associated Performance Assessment for the H-Area Tank Farm at the Savannah River Site*, Savannah River Site, Aiken, SC, Rev. 0, January 2014.

SRR-CWDA-2018-00004, Hommel, S.P., *Recommended Values for Cementitious Degradation Modeling to Support Future SDF Modeling*, Savannah River Site, Aiken, SC, Rev. 1, August 2018.

SRR-CWDA-2020-00045, *Characterization and Assessment of CLSM Grouts for Potential Use in Waste Tank Operational Closures*, Savannah River Site, Aiken, SC, Rev. 0, June 2020.

SRR-CWDA-2020-00066, *Normative Mineral Compositions of Saltstone Disposal Facility Cementitious Materials*, Savannah River Site, Aiken, SC, Rev. 0, September 2020.

SRS-REG-2007-00002, *Performance Assessment for the F-Tank Farm at the Savannah River Site,* Savannah River Site, Aiken, SC, Rev. 1, March 2010.

Walter, G.R. and C.L. Dinwiddie, *Tank Grout Water-Conditioning Tests – Status Report*, Center for Nuclear Waste Regulatory Analyses, San Antonio, TX, April 2019.

Walter, G.R. and C.L. Dinwiddie, *Final Report: Tank Grout Water-Conditioning Tests – Fiscal Year 2019 Status Report*, Center for Nuclear Waste Regulatory Analyses, San Antonio, TX, DOI: 10.13140/RG.2.2.24013.26080, 2020.

Wilson, L.G., *Monitoring in the vadose zone: A review of technical elements and methods*, Rep. No. EPA-600/7-80-134, Environmental Protection Agency, Washington, DC, 1980.

WSRC-RP-92-450, Strom, R.N., and D.S. Kaback, *SRP Baseline Hydrogeologic Investigation: Aquifer Characterization*, Savannah River Site, Aiken, SC, Rev. 0, March 1992.

WSRC-STI-2007-00061, Subramanian, K.H., *Life Estimation of High Level Waste Tank Steel for F-Tank Farm Closure Performance Assessment*, Savannah River Site, Aiken, SC, Rev. 2, June 2008.

WSRC-STI-2007-00607, Langton, C.A., *Chemical Degradation Assessment of Cementitious Materials for the HLW Tank Closure Project*, Savannah River Site, Aiken, SC, Rev. 0, September 14, 2007.

WSRC-TR-2002-00479, Millings, M.R., J.V. Noonkester, M.E. Denham, and B.P. Jackson, *Natural Strontium, Iodine, Cesium, and Cobalt in Savannah River Site Groundwater: Data Report (U)*, Savannah River Site, Aiken, SC, Rev. 0, October 2003.

APPENDIX A - DEGREE OF HYDRATION

The following table augments Section 3.5 and provides additional results from a parametric study to estimate the degree of hydration appropriate for tank-fill grouts. Simulation results enclosed by a box exhibit pH values approximately matching SREL observations. The heavy boxes highlight the 100% cement / 70% slag / 20% fly ash assumption that roughly matches observations for all three materials tested.

TFG-NBFS 100% Quartz		
Minerals	**4.83E+05**	**wt%**
Al(OH)3(mic)	1.20E+05	25%
Calcite	0.2797	0%
Ettringite	1.54E+04	3%
Ferrihydrite	4.30E+04	9%
INFCA_CNASHss	1.79E+05	37%
OH-Hydrotalcite	1.13E+04	2%
Quartz	1.15E+05	24%
pH	10.322	

TFG-NBFS 100% SiO2(a)		
Minerals	**4.79E+05**	**wt%**
Al(OH)3(mic)	1.21E+05	25%
Calcite	0.2069	0%
Ferrihydrite	4.30E+04	9%
Gypsum	6156	1%
INFCA_CNASHss	1.86E+05	39%
OH-Hydrotalcite	1.13E+04	2%
SiO2(a)	1.12E+05	23%
pH	9.532	

TFG-NBFS 50% Si 50% Al		
Minerals	**3.09E+05**	**wt%**
Al(OH)3(mic)	4.53E+04	15%
Calcite	0.1738	0%
Ferrihydrite	4.30E+04	14%
Gypsum	6070	2%
INFCA_CNASHss	1.86E+05	60%
OH-Hydrotalcite	1.13E+04	4%
SiO2(a)	1.78E+04	6%
pH	9.532	

TFG-NBFS 25% Si 25% Al		
Minerals	**2.27E+05**	**wt%**
5CA_CNASHss	1.35E+05	60%
Al(OH)3(mic)	1.44E+04	6%
C4AH13	6.93E+03	3%
Ettringite	1.62E+04	7%
Ferrihydrite	4.30E+04	19%
Monocarboalumin	2.25E+00	0%
OH-Hydrotalcite	1.13E+04	5%
pH	12.156	

TFG-NBFS 100/70/40%		
Minerals	**2.48E+05**	**wt%**
Al(OH)3(mic)	3.90E+04	16%
Calcite	1.55E-01	0%
Ferrihydrite	1.93E+04	8%
Gypsum	4.67E+03	2%
INFCA_CNASHss	1.61E+05	65%
OH-Hydrotalcite	5.91E+03	2%
SiO2(a)	1.84E+04	7%
pH	9.532	

TFG-NBFS 50% Si 50% Al Quartz		
Minerals	**3.14E+05**	**wt%**
Al(OH)3(mic)	4.42E+04	14%
Calcite	0.2587	0%
Ettringite	1.53E+04	5%
Ferrihydrite	4.30E+04	14%
INFCA_CNASHss	1.79E+05	57%
OH-Hydrotalcite	1.13E+04	4%
Quartz	2.04E+04	7%
pH	10.322	

TFG-NBFS 100/70/20%		
Minerals	**1.73E+05**	**wt%**
5CA_CNASHss	6.35E+04	37%
Al(OH)3(mic)	1.50E+04	9%
Calcite	2.16E-01	0%
Ettringite	1.18E+04	7%
Ferrihydrite	1.14E+04	7%
INFCA_CNASHss	6.73E+04	39%
OH-Hydrotalcite	4.18E+03	2%
pH	11.414	

TFG 100% Si 100% Al		
Minerals	**4.89E+05**	**wt%**
Al(OH)3(mic)	5.81E+04	12%
Calcite	0.2115	0%
Gypsum	1.12E+04	2%
INFCA_CNASHss	3.15E+05	64%
Magnetite	2.11E+04	4%
OH-Hydrotalcite	4.30E+04	9%
Pyrite	86.6	0%
SiO2(a)	4.09E+04	8%
pH	9.532	
Amorphous		85%

TFG 75% Si 75% Al		
Minerals	**4.20E+05**	**wt%**
Al(OH)3(mic)	2.81E+04	7%
Calcite	2.74E-01	0%
Ettringite	9465	2%
Gypsum	7.28E+03	2%
INFCA_CNASHss	3.11E+05	74%
Magnetite	2.11E+04	5%
OH-Hydrotalcite	4.31E+04	10%
Pyrite	86.6	0%
pH	10.172	
Amorphous		81%

TFG 50% Si 50% Al		
Minerals	**3.48E+05**	**wt%**
5CA_CNASHss	2.33E+05	67%
Al(OH)3(mic)	1.24E+04	4%
Calcite	0.2505	0%
Ettringite	2.83E+04	8%
INFCA_CNASHss	9335	3%
Magnetite	2.11E+04	6%
OH-Hydrotalcite	4.31E+04	12%
Pyrite	86.59	0.0%
pH	11.414	
Amorphous		73%

TFG 25% Si 25% Al		
Minerals	**2.95E+05**	**wt%**
C4AH13	3.83E+04	13%
Ettringite	2.83E+04	10%
Magnetite	2.11E+04	7%
Monocarboalumin	2.248	0%
OH-Hydrotalcite	4.31E+04	15%
Portlandite	3.01E+04	10%
Pyrite	86.13	0%
T2C_CNASHss	1.34E+05	46%
pH	12.464	
Amorphous		46%

TFG 100% Si 100% Al Quartz		
Minerals	**4.97E+05**	**wt%**
Al(OH)3(mic)	5.63E+04	11%
Calcite	0.2853	0%
Ettringite	2.76E+04	6%
INFCA_CNASHss	3.03E+05	61%
Magnetite	2.11E+04	4%
OH-Hydrotalcite	4.31E+04	9%
Pyrite	86.6	0%
Quartz	4.57E+04	9%
pH	10.322	
Amorphous		72%

TFG 100/70/40%		
Minerals	**3.04E+05**	**wt%**
5CA_CNASHss	6.43E+04	19%
Al(OH)3(mic)	1.29E+04	4%
Calcite	0.241	0%
Ettringite	2.08E+04	6%
INFCA_CNASHss	1.66E+05	48%
Magnetite	9.97E+03	3%
OH-Hydrotalcite	2.92E+04	8%
Pyrite	225.1	0.1%
pH	11.414	
Amorphous		70%

TFG 100% Si 100% Al Quartz+Gibbsite		
Minerals	**4.97E+05**	**wt%**
Calcite	2.91E-01	0%
Ettringite	2.73E+04	6%
Gibbsite	5.63E+04	11%
INFCA_CNASHss	3.03E+05	61%
Magnetite	2.11E+04	4%
OH-Hydrotalcite	4.31E+04	9%
Pyrite	86.6	0%
Quartz	4.57E+04	9%
pH	10.354	
Amorphous		61%

TFG 100/70/20%		
Minerals	**2.53E+05**	**wt%**
5CA_CNASHss	1.84E+05	53%
Al(OH)3(mic)	3.29E+03	1%
Calcite	0.2314	0%
Ettringite	1.92E+04	6%
INFCA_CNASHss	1.19E+04	3%
Magnetite	6.27E+03	2%
OH-Hydrotalcite	2.80E+04	8%
Pyrite	352.9	0.1%
pH	11.414	
Amorphous		57%

CLSM 25% Si 25% Al		
Minerals	**1.83E+05**	**wt%**
Al(OH)3(mic)	2.07E+04	11%
Calcite	0.1766	0%
Ferrihydrite	4.28E+04	23%
Gypsum	3165	2%
INFCA_CNASHss	1.01E+05	55%
OH-Hydrotalcite	1.02E+04	6%
SiO2(a)	5.16E+03	3%
pH	9.532	

CLSM 25% Si 25% Al Quartz		
Minerals	**1.86E+05**	**wt%**
Al(OH)3(mic)	2.01E+04	11%
Calcite	0.3113	0%
Ettringite	8.56E+03	5%
Ferrihydrite	4.28E+04	23%
INFCA_CNASHss	9.76E+04	52%
OH-Hydrotalcite	1.03E+04	6%
Quartz	6.71E+03	4%
pH	10.322	

CLSM 100/70/20%		
Minerals	**1.17E+05**	**wt%**
Al(OH)3(mic)	2.23E+04	19%
Calcite	0.1547	0%
Ferrihydrite	9.67E+03	8%
Gypsum	1231	1%
INFCA_CNASHss	6.63E+04	57%
OH-Hydrotalcite	2.75E+03	2%
SiO2(a)	1.50E+04	13%
pH	9.532	

CLSM 100/70/20% Quartz		
Minerals	**1.19E+05**	**wt%**
Al(OH)3(mic)	2.21E+04	19%
Calcite	0.2964	0%
Ettringite	3.90E+03	3%
Ferrihydrite	9674	8%
INFCA_CNASHss	6.45E+04	54%
OH-Hydrotalcite	2.82E+03	2%
Quartz	1.58E+04	13%
pH	10.322	

APPENDIX B - INITIALLY CURED CEMENTITIOUS MATERIALS

The following information is provided herein for mixes LP#8-16, ZB-FF-8-D, Vault 4 Clean Cap, and B3000-6-0-2-A:

- Dry/unreacted composition
- Simulated cured composition when hydrated with the prescribed mix water
- Simulated cured composition when hydrated with sufficient water to produce 100% saturation

LP#8-16 Grout: Dry/Unreacted Composition

Tanks 5, 6, 12, 16, 18, 19 Grout (Mix LP#8-16)

Parameter	Cement	Slag	Fly Ash	Silica Fume	Metakaolin	Inert B	Dry mix	Water	w/c (weight) ratio	w/dry mix	Notes:
Mix (lbs/yd3)	125	210	363			2590	3288	404.0	0.579	0.123	-- C-SPP-F-00055 Rev. 6
(kg/m3)	74	125	215	0	0	1537	1951	239.7			2190
All ingredients fraction	0.034	0.057	0.098	0.000	0.000	0.702	0.891	0.109			
Dry ingredients fraction	0.038	0.064	0.110	0.000	0.000	0.788	1				
Binders fraction	0.18	0.30	0.52	0.00	0.00		1				

Parameter	Cement	Slag	Fly Ash	Silica Fume	Metakaolin	Inert B	Binders	Dry Mix	MW	mol/	GWB / PHREEQC	mol/m3
Proportions	g/100g	g/100g	g/100g	g/100g	g/100g		g/100g	g/100g	g/mol	kg dry mix		
Reactive ingredients	97.4	98.8	93.0	96.3	98.5							
C (CaO)	64.6	39.0	4.2	0.6	0.2		20.2	4.29	56	0.766	C (CaO)	1494
S (SiO2)	20.4	36.5	50.9	95.0	53.1		16.6	3.53	60	0.589	S (SiO2)	1148
A (Al2O3)	5.0	10.5	27.9	0.2	43.6		6.0	1.27	102	0.125	A (Al2O3)	243.7
F (Fe2O3)	3.5	0.4	8.7	0.1	1.6		1.6	0.35	160	0.022	F (Fe2O3)	42.11
Sbar (SO3)	2.8	2.3	0.3	0.2	0.0		1.0	0.21	80	0.027	Sbar (SO3)	51.87
M (MgO)	1.2	10.1	0.9	0.2	0.1		2.4	0.52	40	0.130	M (MgO)	252.9
Inert A	2.6	1.2	7.0	3.8	1.5	100.0	52.1	11.06		110.6		
Inert B								78.77		787.7		
Water								12.29	18	122.9	H (H2O)	13316
checks	100	100	100	100	100	100	100	100		1000		
Degree of rxn/hydration	100%	70%	20%	20%	20%			0.579		0.579		

Parameter	Cement	Slag	Fly Ash	Silica Fume	Metakaolin	Total			
Reducing capacity (µeq/g)		819					Fe	84.2	
Reducing capacity (eq/m3)	0.0	71.4	0.0	0.0	0.0	71.43	FeO (FeII)	71.43	
							Fe2O3 (FeIII)	6.40	
Unreacted dry mix (kg/m3)	0	37.376	172.29	0	0	209.66			

LP#8-16 Grout: Hydrated with Mix Water

LP#8-16 GWB hydration -- initial				Mass (g)	Volume (mL)	Density (g/mL)	Volume Fraction	Porosity	Water Content	Water Saturation	Water Addition (g)	Water Addition (mol)	Water Comments
pH	11.414		Inert:	1.747E+06	6.641E+05	2.63	66.4%						Inert B + unreacted binders
pe	-8.347		Minerals:	2.528E+05	9.251E+04	2.73	9.3%						Hydrated minerals
Eh (V)	-0.49	Water (unreacted):		1.851E+05	1.851E+05	1.00	18.5%	24.3%	18.5%	76.0%	5.83E+04	3239	Compared to measured n=21%
Water mass	185.07	kg	Air:		5.830E+04		5.8%						
			Total:	2.185E+06	1.000E+06	2.18	100.0%						
Phase	MW (g/mol)	MV (mL/mol)	Moles	Mass (g)	Volume (mL)	Density (g/mL)							
5CA	172.20567	57.3	1.067E+03	1.837E+05	6.114E+04	3.01							
AlOHmic	78.0055	31.956	4.217E+01	3.289E+03	1.348E+03	2.44							
Brc	58.328	24.63		0	0	0							
C4AH13	560.491	274.47001		0	0	0							
Cal	100.0911	36.934	2.312E-03	2.314E-01	8.539E-02	2.71							
Fe-ettringite	1312.878	717.55997		0	0	0							
Ferrihydrite	106.8677	106.8677		0	0	0							
Gp	172.176	74.69		0	0	0							
INFCA	173.20825	59.31	6.855E+01	1.187E+04	4.066E+03	2.92							
M4A-OH-LDH	443.371	219.1	6.322E+01	2.803E+04	1.385E+04	2.02							
Mag	231.5386	44.524	2.710E+01	6.275E+03	1.207E+03	5.20							
Maghemite	159.691	29.087		0	0	0							
Portlandite	74.096	33.06		0	0	0							
Py	119.975	23.94	2.941E+00	3.528E+02	7.041E+01	5.01							
Qtz	60.0843	22.688		0	0	0							
T2C-CNASHss	189.2443	80.6		0	0	0							
T5C-CNASHss	190.245375	79.3		0	0	0							
TobH-CNASHss	191.24645	85		0	0	0							
ettringite	1255.147	707.03003	1.531E+01	1.922E+04	1.082E+04	1.78							
hemicarbonat10.5	537.45655	261.264		0	0	0							
monocarbonate	568.4701	261.95801		0	0	0							

LP#8-16 Grout: Hydrated with Sufficient Water to Produce 100% Saturation

LP#8-16															
GWB hydration -- water add to achieve 100% sat.				**Mass (g)**	**Volume (mL)**	**Density (g/mL)**	**Volume Fraction**	**Porosity**	**Water Content**	**Water Saturation**	**Water Addition (g)**	**Water Addition (mol)**	**Water Comments**
pH	11.414		Inert:	1.747E+06	6.641E+05	2.63	66.4%						Inert B + unreacted binders
pe	-8.347		Minerals:	2.526E+05	9.245E+04	2.73	9.2%						Hydrated minerals
Eh (V)	-0.49	Water (unreacted):		2.434E+05	2.434E+05	1.00	24.3%	**24.3%**	**24.3%**	**100.0%**	1.24E+00	**0**	Compared to measured n=21%
Water mass	243.42	kg	Air:		1.244E+00		0.0%						
3x	**730.3**	kg	Total:	2.243E+06	1.000E+06	**2.24**	100.0%						
-2x	**-486.8**	kg											
halite	**6.5723**	mmol		9.000E-03	mmol								
Phase	**MW (g/mol)**	**MV (mL/mol)**		**Moles**	**Mass (g)**	**Volume (mL)**	**Density (g/mL)**						
5CA	172.205675	57.3		1.066E+03	1.836E+05	6.108E+04	3.01						
AlOHmic	78.0055	31.956		4.215E+01	3.288E+03	1.347E+03	2.44						
Brc	58.328	24.63			0	0	0						
C4AH13	560.491	274.47001			0	0	0						
Cal	100.0911	36.934		1.794E-03	1.796E-01	6.626E-02	2.71						
Fe-ettringite	1312.878	717.55997			0	0	0						
Ferrihydrite	106.8677	106.8677			0	0	0						
Gp	172.176	74.69			0	0	0						
INFCA	173.200825	59.31		6.870E+01	1.190E+04	4.075E+03	2.92						
M4A-OH-LDH	443.371	219.1		6.322E+01	2.803E+04	1.385E+04	2.02						
Mag	231.5386	44.524		2.710E+01	6.275E+03	1.207E+03	5.20						
Maghemite	159.691	29.087			0	0	0						
Portlandite	74.096	33.06			0	0	0						
Py	119.975	23.94		2.941E+00	3.528E+02	7.041E+01	5.01						
Qtz	60.0843	22.688			0	0	0						
T2C-CNASHss	189.2443	80.6			0	0	0						
T5C-CNASHss	190.245375	79.3			0	0	0						
TobH-CNASHss	191.24645	85			0	0	0						
ettringite	1255.147	707.03003		1.530E+01	1.920E+04	1.082E+04	1.78						
hemicarbonat10.5	537.45655	261.264			0	0	0						
monocarbonate	568.4701	261.95801			0	0	0						

ZB-FF-8-D Grout: Dry/Unreacted Composition

Zero-Bleed Flowable Fill / CLSM (Mix ZB-FF-8-D)																			
Parameter	Cement	Slag	Fly Ash	Silica Fume	Metakaolin	Inert B	Dry mix	Water	w/c (weight) ratio	w/dry mix		Notes:							
Mix (lbs/yd3)	150	500				2650	3300	416.5	0.641	0.126		-- C-DCF-G-00400, C-SPS-G-00096 Re							
(kg/m3)	89	0	297	0	0	1572	1958	247.1				2205							
All ingredients fraction	0.040	0.000	0.135	0.000	0.000	0.713	0.888	0.112											
Dry ingredients fraction	0.045	0.000	0.152	0.000	0.000	0.803	1												
Binders fraction	0.23	0.00	0.77	0.00	0.00		1												
Parameter	Cement	Slag	Fly Ash	Silica Fume	Metakaolin	Inert B		Binders	Dry Mix		MW	mol/	GWB / PHREEQC						mol/m3
Proportions	g/100g	g/100g	g/100g	g/100g	g/100g			g/100g	g/100g	g/kg	g/mol	kg dry mix							
Reactive ingredients	97.4	98.8	93.0	96.3	98.5														
C (CaO)	64.6	39.0	4.2	0.6	0.2			15.5	3.06	30.6	56	0.547	C (CaO)	1071					
S (SiO2)	20.4	36.5	50.9	95.0	53.1			12.6	2.47	24.7	60	0.412	S (SiO2)	807					
A (Al2O3)	5.0	10.5	27.9	0.2	43.6			5.4	1.07	10.7	102	0.105	A (Al2O3)	205.6					
F (Fe2O3)	3.5	0.4	8.7	0.1	1.6			2.2	0.42	4.2	160	0.026	F (Fe2O3)	51.86					
Sbar (SO3)	2.8	2.3	0.3	0.2	0.0			0.7	0.13	1.3	80	0.017	Sbar (SO3)	32.99					
M (MgO)	1.2	10.1	0.9	0.2	0.1			0.4	0.08	0.8	40	0.020	M (MgO)	39.94					
Inert A	2.6	1.2	7.0	3.8	1.5	100.0		63.2	12.45	124.5									
Inert B									80.30	803.0									
Water									12.62	126.2	18	7.012	H (H2O)	13728					
checks	100	100	100	100	100	100		100	100	1000									
Degree of rxn/hydration	100%	70%	20%	20%	20%				0.641	0.641									
Parameter	Cement	Slag	Fly Ash	Silica Fume	Metakaolin	Total											Fe	103.7	
Reducing capacity (µeq/g)		819											FeO (FeII)	0.00					
Reducing capacity (eq/m3)	0.0	0.0	0.0	0.0	0.0	0.0							Fe2O3 (FeIII)	51.86					
Unreacted dry mix (kg/m3)	0	0	237.31	0	0	237.31													

ZB-FF-8-D Grout: Hydrated with Mix Water

ZB-FF-8-D GWB hydration -- initial				Mass (g)	Volume (mL)	Density (g/mL)	Volume Fraction	Porosity	Water Content	Water Saturation	Water Addition (g)	Water Addition (mol)	Water Comments
pH	11.414		Inert:	1.809E+06	6.880E+05	2.63	68.8%						Inert B + unreacted binders
pe	9.236		Minerals:	1.810E+05	7.254E+04	2.50	7.3%						Hydrated minerals
Eh (V)	0.54	Water (unreacted):		2.081E+05	2.081E+05	1.00	20.8%	24.0%	20.8%	86.9%	3.14E+04	1747	
Water mass	208.06	kg	Air:		3.145E+04		3.1%						
			Total:	2.198E+06	1.000E+06	2.20	100.0%						
Phase	MW (g/mol)	MV (mL/mol)	Moles	Mass (g)	Volume (mL)	Density (g/mL)							
5CA	172.20567	57.3	7.972E+02	1.373E+05	4.568E+04	3.01							
AlOHmic	78.0055	31.956	1.673E+02	1.305E+04	5.346E+03	2.44							
Brc	58.328	24.63		0	0	0							
C4AH13	560.491	274.47001		0	0	0							
Cal	100.0911	36.934	2.230E-03	2.232E-01	8.236E-02	2.71							
Fe-ettringite	1312.878	717.55997		0	0	0							
Ferrihydrite	106.8677	106.8677	1.037E+02	1.108E+04	1.108E+04	1.00							
Gp	172.176	74.69		0	0	0							
INFCA	173.20825	59.31	8.234E+00	1.426E+03	4.884E+02	2.92							
M4A-OH-LDH	443.371	219.1	9.985E+00	4.427E+03	2.188E+03	2.02							
Mag	231.5386	44.524		0	0	0							
Maghemite	159.691	29.087		0	0	0							
Portlandite	74.096	33.06		0	0	0							
Py	119.975	23.94		0	0	0							
Qtz	60.0843	22.688		0	0	0							
T2C-CNASHss	189.2443	80.6		0	0	0							
T5C-CNASHss	190.245375	79.3		0	0	0							
TobH-CNASHss	191.24645	85		0	0	0							
ettringite	1255.147	707.03003	1.097E+01	1.377E+04	7.756E+03	1.78							
hemicarbonat10.5	537.45655	261.264		0	0	0							
monocarbonate	568.4701	261.95801		0	0	0							

ZB-FF-8-D Grout: Hydrated with Sufficient Water to Produce 100% Saturation

ZB-FF-8-D															
GWB hydration -- water add to achieve 100% sat.				Mass (g)	Volume (mL)	Density (g/mL)	Volume Fraction	Porosity	Water Content	Water Saturation	Water Addition (g)	Water Addition (mol)	Comments		
pH	11.414		Inert:	1.809E+06	6.880E+05	2.63	68.8%						Inert B + unreacted binders		
pe	9.220		Minerals:	1.810E+05	7.254E+04	2.50	7.3%						Hydrated minerals		
Eh (V)	0.54	Water (unreacted):		2.395E+05	2.395E+05	1.00	24.0%	24.0%	24.0%	100.0%	-1.98E+01	-1			
Water mass	239.53	kg	Air:		-1.977E+01		0.0%								
3x	718.6	kg	Total:	2.230E+06	1.000E+06	2.23	100.0%								
-2x	-479.1	kg													
halite	6.4673	mmol		9.000E-03	mmol										
Phase	MW (g/mol)	MV (mL/mol)	Moles	Mass (g)	Volume (mL)	Density (g/mL)	mol e-/mol	mol e-							
5CA	172.205675	57.3	7.971E+02	1.373E+05	4.567E+04	3.01									
AlOHmic	78.0055	31.956	1.673E+02	1.305E+04	5.346E+03	2.44									
Brc	58.328	24.63		0	0	0									
C4AH13	560.491	274.47001		0	0	0									
Cal	100.0911	36.934	1.950E-03	1.952E-01	7.202E-02	2.71									
Fe-ettringite	1312.878	717.55997		0	0	0									
Ferrihydrite	106.8677	106.8677	1.037E+02	1.108E+04	1.108E+04	1.00									
Gp	172.176	74.69		0	0	0									
INFCA	173.200825	59.31	8.313E+00	1.440E+03	4.930E+02	2.92									
M4A-OH-LDH	443.371	219.1	9.985E+00	4.427E+03	2.188E+03	2.02									
Mag	231.5386	44.524		0	0	0	1	0							
Maghemite	159.691	29.087		0	0	0									
Portlandite	74.096	33.06		0	0	0									
Py	119.975	23.94		0	0	0	15	0							
Qtz	60.0843	22.688		0	0	0									
T2C-CNASHss	189.2443	80.6		0	0	0									
T5C-CNASHss	190.245375	79.3		0	0	0									
TobH-CNASHss	191.24645	85		0	0	0									
ettringite	1255.147	707.03003	1.097E+01	1.377E+04	7.756E+03	1.78									
hemicarbonat10.5	537.45655	261.264		0	0	0									
monocarbonate	568.4701	261.95801		0	0	0									

Vault 4 Clean Cap Grout: Dry/Unreacted Composition

Vault 4 Clean Cap 1 Grout	157.6	709.4	709.4			350.6	1927	967.3	0.614	0.502	-- SRR-CWDA-2020-00040 for saltsto	
Parameter	Cement	Slag	Fly Ash	Silica Fume	Metakaolin	Inert B	Dry mix	Water	w/c (weight) ratio	w/dry mix	Notes:	
Mix (lbs/yd3)	192.7	867.2	867.2				1927	967.3	0.502	0.502	-- Rescaled cementitious materials	
(kg/m3)	114	514	514	0	0	0	1143	573.9			1717	
All ingredients fraction	0.067	0.300	0.300	0.000	0.000	0.000	0.666	0.334	-- ... hoping to approximately preserve 1.0 yd3 volume			
Dry ingredients fraction	0.100	0.450	0.450	0.000	0.000	0.000	1		-- Result is consistent with C-SPP-Z-00012 Rev. 1 ...			
Binders fraction	0.10	0.45	0.45	0.00	0.00		1		-- ... for "Vault 4 Clean Cap 1" (w/c = 0.5)			
Parameter	Cement	Slag	Fly Ash	Silica Fume	Metakaolin	Inert B		Binders	Dry Mix	MW	mol/	GWB / PHREEQC mol/m3
Proportions	g/100g	g/100g	g/100g	g/100g	g/100g			g/100g	g/100g	g/kg	g/mol kg dry mix	
Reactive ingredients	97.4	98.8	93.0	96.3	98.5							
C (CaO)	64.6	38.0	4.2	0.6	0.2			18.8	18.79	187.9	56 3.356	C (CaO) 3837
S (SiO2)	20.4	35.5	50.9	95.0	53.1			17.8	17.82	178.2	60 2.970	S (SiO2) 3395
A (Al2O3)	5.0	10.2	27.9	0.2	43.6			6.2	6.23	62.3	102 0.611	A (Al2O3) 698.3
F (Fe2O3)	3.5	3.0	8.7	0.1	1.6			2.1	2.08	20.8	160 0.130	F (Fe2O3) 148.7
Sbar (SO3)	2.8	2.2	0.3	0.2	0.0			1.0	1.00	10.0	80 0.125	Sbar (SO3) 142.4
M (MgO)	1.2	9.9	0.9	0.2	0.1			3.3	3.31	33.1	40 0.828	M (MgO) 947.0
Inert A	2.6	1.2	7.0	3.8	1.5	100.0		50.8	50.77	507.7		
Inert B									0.00	0.0		
Water									50.20	502.0	18 27.887	H (H2O) 31882
checks	100	100	100	100	100	100		100	100	1000		
Degree of rxn/hydration	100%	70%	20%	20%	20%				0.502	0.502		
Parameter	Cement	Slag	Fly Ash	Silica Fume	Metakaolin	Total						Fe 297.3
Reducing capacity (µeq/g)		819										FeO (FeII) 294.9
Reducing capacity (eq/m3)	0.0	294.9	0.0	0.0	0.0	294.9						Fe2O3 (FeIII) 1.18
											Adjusted Fe content of slag to have enough to make required amount of FeO	
Unreacted dry mix (kg/m3)	0	154.34	411.58	0	0	565.92						

Vault 4 Clean Cap Grout: Hydrated with Mix Water

Clean Cap GWB hydration -- initial				Mass (g)	Volume (mL)	Density (g/mL)	Volume Fraction	Porosity	Water Content	Water Saturation	Water Addition (g)	Water Addition (mol)	Water Comments
pH	11.378		Inert:	5.659E+05	2.264E+05	2.50	22.6%						Inert B + unreacted binders
pe	-8.234		Minerals:	7.197E+05	2.675E+05	2.69	26.8%						Hydrated minerals
Eh (V)	-0.49	Water (unreacted):		4.154E+05	4.154E+05	1.00	41.5%	50.6%	41.5%	82.1%	9.07E+04	5041	
Water mass	415.36	kg	Air:		9.074E+04		9.1%						
			Total:	1.701E+06	1.000E+06	1.70	100.0%						
Phase	MW (g/mol)	MV (mL/mol)	Moles	Mass (g)	Volume (mL)	Density (g/mL)							
5CA	172.20567	57.3	1.795E+03	3.091E+05	1.029E+05	3.01							
AlOHmic	78.0055	31.956		0	0	0							
Brc	58.328	24.63		0	0	0							
C4AH13	560.491	274.47001		0	0	0							
Cal	100.0911	36.934	5.880E-03	5.885E-01	2.172E-01	2.71							
Fe-ettringite	1312.878	717.55997		0	0	0							
Ferrihydrite	106.8677	106.8677		0	0	0							
Gp	172.176	74.69		0	0	0							
INFCA	173.200825	59.31	1.272E+03	2.203E+05	7.544E+04	2.92							
M4A-OH-LDH	443.371	219.1	2.367E+02	1.049E+05	5.186E+04	2.02							
Mag	231.5386	44.524	9.465E+01	2.192E+04	4.214E+03	5.20							
Maghemite	159.691	29.087		0	0	0							
Portlandite	74.096	33.06		0	0	0							
Py	119.975	23.94	1.332E+01	1.598E+03	3.189E+02	5.01							
Qtz	60.0843	22.688		0	0	0							
T2C-CNASHss	189.2443	80.6		0	0	0							
T5C-CNASHss	190.245375	79.3	7.155E+01	1.361E+04	5.674E+03	2.40							
TobH-CNASHss	191.24645	85		0	0	0							
ettringite	1255.147	707.03003	3.842E+01	4.822E+04	2.716E+04	1.78							
hemicarbonat10.5	537.45655	261.264		0	0	0							
monocarbonate	568.4701	261.95801		0	0	0							

Vault 4 Clean Cap Grout: Hydrated with Sufficient Water to Produce 100% Saturation

Clean Cap GWB hydration -- water add to achieve 100% sat.			Mass (g)	Volume (mL)	Density (g/mL)	Volume Fraction	Porosity	Water Content	Water Saturation	Water Addition (g)	Water Addition (mol)	Comments
pH	11.378	Inert:	5.659E+05	2.264E+05	2.50	22.6%						Inert B + unreacted binders
pe	-8.234	Minerals:	7.196E+05	2.675E+05	2.69	26.7%						Hydrated minerals
Eh (V)	-0.49	Water (unreacted):	5.062E+05	5.062E+05	1.00	50.6%	50.6%	50.6%	100.0%	-5.66E+01	-3	
Water mass	506.2 kg	Air:		-5.661E+01		0.0%						
3x	**1518.6** kg	Total:	1.792E+06	1.000E+06	**1.79**	100.0%						
-2x	**-1012.4** kg											
halite	**13.6674** mmol		9.000E-03 mmol									

Phase	MW (g/mol)	MV (mL/mol)	Moles	Mass (g)	Volume (mL)	Density (g/mL)	mol e-/mol	mol e-
5CA	172.205675	57.3	1.795E+03	3.091E+05	1.029E+05	3.01		
AlOHmic	78.0055	31.956		0	0	0		
Brc	58.328	24.63		0	0	0		
C4AH13	560.491	274.47001		0	0	0		
Cal	100.0911	36.934	5.094E-03	5.099E-01	1.881E-01	2.71		
Fe-ettringite	1312.878	717.55997		0	0	0		
Ferrihydrite	106.8677	106.8677		0	0	0		
Gp	172.176	74.69		0	0	0		
INFCA	173.200825	59.31	1.272E+03	2.203E+05	7.544E+04	2.92		
M4A-OH-LDH	443.371	219.1	2.367E+02	1.049E+05	5.186E+04	2.02		
Mag	231.5386	44.524	9.465E+01	2.192E+04	4.214E+03	5.20	1	94.65
Maghemite	159.691	29.087		0	0	0		
Portlandite	74.096	33.06		0	0	0		
Py	119.975	23.94	1.332E+01	1.598E+03	3.189E+02	5.01	15	199.8
Qtz	60.0843	22.688		0	0	0		
T2C-CNASHss	189.2443	80.6		0	0	0		
T5C-CNASHss	190.245375	79.3	7.132E+01	1.357E+04	5.656E+03	2.40		
TobH-CNASHss	191.24645	85		0	0	0		
ettringite	1255.147	707.03003	3.839E+01	4.819E+04	2.714E+04	1.78		
hemicarbonat10.5	537.45655	261.264		0	0	0		
monocarbonate	568.4701	261.95801		0	0	0		

B3000-6-0-2-A Concrete: Dry/Unreacted Composition

3000 psi Structural Concrete (Mix B3000-6-0-2-A)														
Parameter	**Cement**	**Slag**	**Fly Ash**	**Silica Fume**	**Metakaolin**	**Inert B**	**Dry mix**	**Water**	**w/c (weight) ratio**	**w/dry mix**		**Notes:**		
Mix (lbs/yd3)	520					3015	3535	299.9	0.577	0.085		-- C-DCF-G-00397		
(kg/m3)	309	0	0	0	0	1789	2097	177.9				2275		
All ingredients fraction	0.136	0.000	0.000	0.000	0.000	0.786	0.922	0.078				-- C-SPS-G-00096 Rev. 3		
Dry ingredients fraction	0.147	0.000	0.000	0.000	0.000	0.853	1							
Binders fraction	1.00	0.00	0.00	0.00	0.00		1							
Parameter	**Cement**	**Slag**	**Fly Ash**	**Silica Fume**	**Metakaolin**	**Inert B**		**Binders**	**Dry Mix**		**MW**	mol/	**GWB / PHREEQC**	
Proportions	g/100g	g/100g	g/100g	g/100g	g/100g			g/100g	g/100g	g/kg	g/mol	kg dry mix		mol/m3
Reactive ingredients	97.4	98.8	93.0	96.3	98.5									
C (CaO)	64.6	39.0	4.2	0.6	0.2			64.6	9.50	95.0	56	1.697	C (CaO)	3558
S (SiO2)	20.4	36.5	50.9	95.0	53.1			20.4	3.01	30.1	60	0.501	S (SiO2)	1051
A (Al2O3)	5.0	10.5	27.9	0.2	43.6			5.0	0.73	7.3	102	0.072	A (Al2O3)	150.1
F (Fe2O3)	3.5	0.4	8.7	0.1	1.6			3.5	0.52	5.2	160	0.032	F (Fe2O3)	67.90
Sbar (SO3)	2.8	2.3	0.3	0.2	0.0			2.8	0.41	4.1	80	0.051	Sbar (SO3)	106.5
M (MgO)	1.2	10.1	0.9	0.2	0.1			1.2	0.17	1.7	40	0.043	M (MgO)	89.76
Inert A	2.6	1.2	7.0	3.8	1.5	100.0		2.6	0.38	3.8				
Inert B									85.29	852.9				
Water									8.48	84.8	18	4.713	H (H2O)	9884
checks	100	100	100	100	100	100		100	100	1000				
Degree of rxn/hydration	100%	100%	100%	100%	100%				0.577	0.577				
Parameter	**Cement**	**Slag**	**Fly Ash**	**Silica Fume**	**Metakaolin**	**Total**							Fe	135.8
Reducing capacity (µeq/g)		819											FeO (FeII)	0.00
Reducing capacity (eq/m3)	0.0	0.0	0.0	0.0	0.0	0.0							Fe2O3 (FeIII)	67.90
Unreacted dry mix (kg/m3)	0	0	0	0	0	0.00								

B3000-6-0-2-A Concrete: Hydrated with Mix Water

B3000-6-0-2-A GWB hydration -- initial				Mass (g)	Volume (mL)	Density (g/mL)	Volume Fraction	Porosity	Water Content	Water Saturation	Water Addition (g)	Water Addition (mol)	Water Comments
pH	12.464		Inert:	1.789E+06	6.802E+05	2.63	68.0%						Inert B + unreacted binders
pe	8.292		Minerals:	4.232E+05	2.008E+05	2.11	20.1%						Hydrated minerals
Eh (V)	0.49	Water (unreacted):		5.559E+04	5.559E+04	1.00	5.6%	11.9%	5.6%	46.7%	6.34E+04	3522	
Water mass	55.586	kg	Air:		6.340E+04		6.3%						
			Total:	2.268E+06	1.000E+06	2.27	100.0%						
Phase	MW (g/mol)	MV (mL/mol)	Moles	Mass (g)	Volume (mL)	Density (g/mL)							
5CA	172.20567	57.3		0	0	0							
AlOHmic	78.0055	31.956		0	0	0							
Brc	58.328	24.63		0	0	0							
C4AH13	560.491	274.47001	9.215E+01	5.165E+04	2.529E+04	2.04							
Cal	100.0911	36.934		0	0	0							
Fe-ettringite	1312.878	717.55997		0	0	0							
Ferrihydrite	106.8677	106.8677	1.358E+02	1.451E+04	1.451E+04	1.00							
Gp	172.176	74.69		0	0	0							
INFCA	173.20825	59.31		0	0	0							
M4A-OH-LDH	443.371	219.1	2.244E+01	9.949E+03	4.917E+03	2.02							
Mag	231.5386	44.524		0	0	0							
Maghemite	159.691	29.087		0	0	0							
Portlandite	74.096	33.06	1.399E+03	1.037E+05	4.625E+04	2.24							
Py	119.975	23.94		0	0	0							
Qtz	60.0843	22.688		0	0	0							
T2C-CNASHss	189.2443	80.6	1.051E+03	1.989E+05	8.471E+04	2.35							
T5C-CNASHss	190.245375	79.3		0	0	0							
TobH-CNASHss	191.24645	85		0	0	0							
ettringite	1255.147	707.03003	3.550E+01	4.456E+04	2.510E+04	1.78							
hemicarbonat10.5	537.45655	261.264		0	0	0							
monocarbonate	568.4701	261.95801	2.936E-03	1.669E+00	7.691E-01	2.17							

B3000-6-0-2-A Concrete: Hydrated with Sufficient Water to Produce 100% Saturation

B3000-6-0-2-A															
GWB hydration -- water add to achieve 100% sat.				Mass (g)	Volume (mL)	Density (g/mL)	Volume Fraction	Porosity	Water Content	Water Saturation	Water Addition (g)		Water Addition (mol)	Comments	
pH	12.464		Inert:	1.789E+06	6.802E+05	2.63	68.0%							Inert B + unreacted binders	
pe	8.208		Minerals:	4.231E+05	2.007E+05	2.11	20.1%							Hydrated minerals	
Eh (V)	0.48	Water (unreacted):		1.190E+05	1.190E+05	1.00	11.9%	11.9%	11.9%	100.0%	1.72E+01		1		
Water mass	119.04	kg	Air:		1.720E+01		0.0%								
3x	**357.1**	kg	Total:	2.331E+06	1.000E+06	**2.33**	100.0%								
-2x	**-238.1**	kg													
halite	**3.2141**	mmol		9.000E-03	mmol										
Phase	**MW (g/mol)**	**MV (mL/mol)**		**Moles**	**Mass (g)**	**Volume (mL)**	**Density (g/mL)**								
5CA	172.205675	57.3			0	0	0								
AlOHmic	78.0055	31.956			0	0	0								
Brc	58.328	24.63			0	0	0								
C4AH13	560.491	274.47001		9.214E+01	5.164E+04	2.529E+04	2.04								
Cal	100.0911	36.934			0	0	0								
Fe-ettringite	1312.878	717.55997			0	0	0								
Ferrihydrite	106.8677	106.8677		1.358E+02	1.451E+04	1.451E+04	1.00								
Gp	172.176	74.69			0	0	0								
INFCA	173.200825	59.31			0	0	0								
M4A-OH-LDH	443.371	219.1		2.244E+01	9.949E+03	4.917E+03	2.02								
Mag	231.5386	44.524			0	0	0								
Maghemite	159.691	29.087			0	0	0								
Portlandite	74.096	33.06		1.397E+03	1.035E+05	4.618E+04	2.24								
Py	119.975	23.94			0	0	0								
Qtz	60.0843	22.688			0	0	0								
T2C-CNASHss	189.2443	80.6		1.051E+03	1.989E+05	8.471E+04	2.35								
T5C-CNASHss	190.245375	79.3			0	0	0								
TobH-CNASHss	191.24645	85			0	0	0								
ettringite	1255.147	707.03003		3.550E+01	4.456E+04	2.510E+04	1.78								
hemicarbonat10.5	537.45655	261.264			0	0	0								
monocarbonate	568.4701	261.95801		2.935E-03	1.668E+00	7.688E-01	2.17								

APPENDIX C - VERIFICATION OF A REPRESENTATIVE PHREEQC CARBONATION, DISSOLUTION, AND DIFFUSION SIMULATION

The PHREEQC simulations in Section 4.2 involve carbonation of calcium-bearing minerals, dissolution and precipitation of minerals, diffusion of calcium and other aqueous species from the system, and diffusion of dissolved carbon dioxide and other aqueous species into the system. To provide confidence in these simulations, a simplified verification problem is considered to facilitate an independent analytic solution in lieu of a code-to-code comparison. The simplified mineral system involves only portlandite dissolution and calcite precipitation, but otherwise includes the key elements of Section 4.2 simulations (dissolution, carbonation, and diffusive transport):

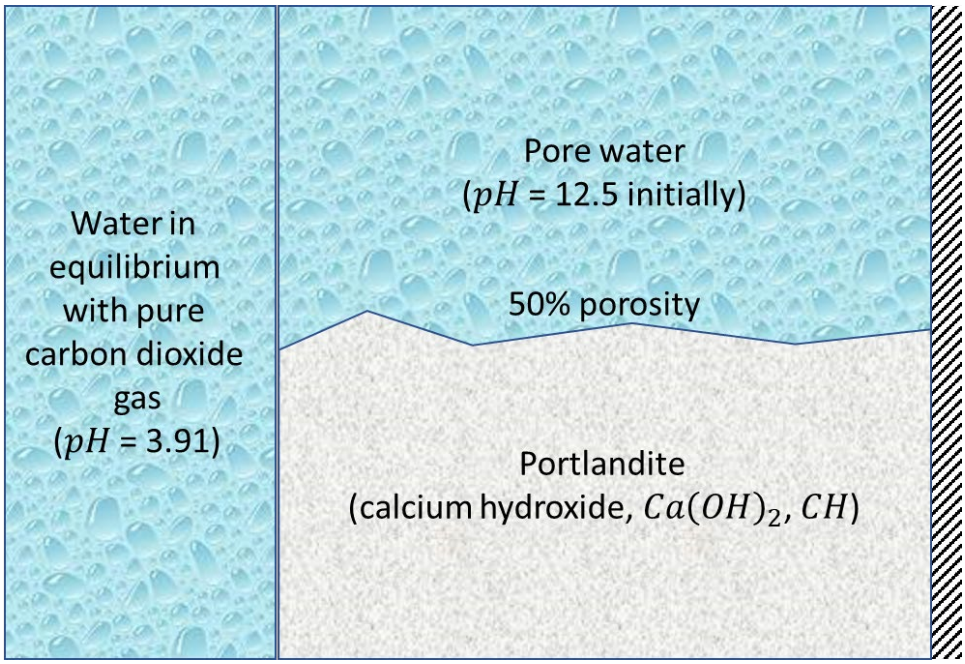

At the right side of the domain is a no-flux boundary. The left boundary is exposed to water in equilibrium with pure carbon dioxide gas (to maximize the dissolved CO_2 concentration). Dissolved CO_2 diffuses in and reacts with portlandite to form calcite. Portlandite dissolves and Ca^{++} ions are leached from the system by diffusion. Dissolution and carbonation are assumed to take place at a distinct reaction front:

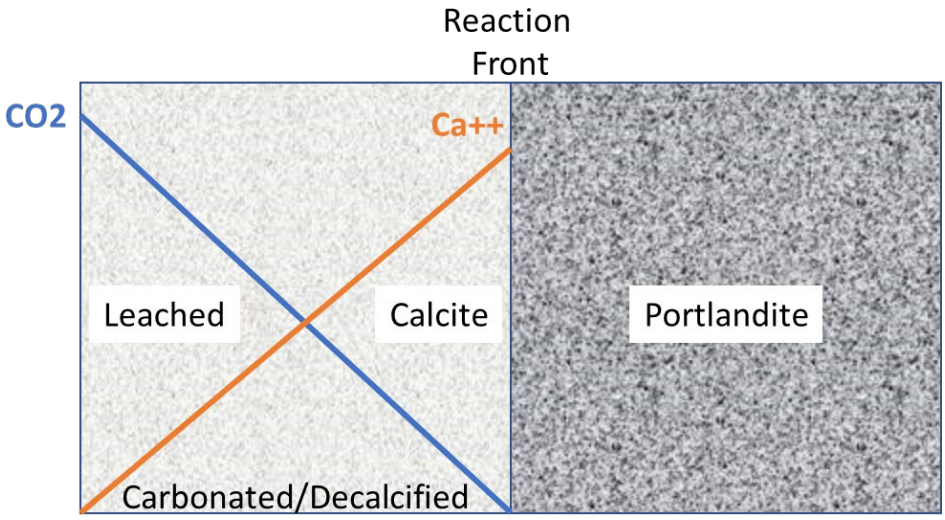

The carbonation reaction is

$$Ca(OH)_2 + CO_2 \rightarrow CaCO_3 + H_2O$$

The dissolution and ionization reaction is

$$Ca(OH)_2 \rightarrow Ca^{++} + 2OH^-$$

Note that one mole of portlandite reacts with one mole of CO_2 or dissolves into one mole of Ca^{++}. The position of the reaction front from the left boundary (x) can be derived from the following differential molar balance per unit area:

$$SnD_e \frac{[CO_2]}{x} dt + SnD_e \frac{[Ca^{++}]}{x} dt = \rho_b R dx$$

$$CO_2 \text{ reacted} + Ca^{++} \text{ leached} = Ca(OH)_2 \text{ depleted}$$

where [·] = molar concentration, S = saturation, n = porosity, t = time, ρ_b = dry bulk density, and R = molar reaction capacity of the solid. Integration of the differential molar balance yields

$$x = \left[\frac{2SnD_e([CO_2] + [Ca^{++}])}{\rho_b R}\right]^{1/2} t^{1/2} \equiv At^{1/2}$$

where A is the rate coefficient for a given system. The below table summarizes the results of a representative test problem. The PHREEQC simulation agrees closely with the analytic result.

Parameter	Value	Units	Comments
Volume	0.001	m^3	Problem definition
Length	1	m	Problem definition
Area	0.001	m^2	Problem definition
Porosity	0.5	m^3 void/m^3	Problem definition
Saturation	1	m^3 water/m^3 void	Problem definition
Water mass	0.5	kg	Problem definition
Effective diffusion coefficient	1.00E-09	m^2/s	Problem definition
Water density	1000	kg/m^3	Problem definition
$Ca(OH)_2$ density	2.65	g/cm^3	Problem definition
$Ca(OH)_2$ molecular weight	74.093	g/mol	
$Ca(OH)_2$ mass	1.325	kg	Calculated
$Ca(OH)_2$ moles	17.88	mol	Calculated
(Bulk density)(Rxn capacity)	1.788E+04	mol/m^3	Calculated
Ca^{++} concentration	1.495E-02	mol/kg water	As simulated by PHREEQC
	1.495E+01	mol/m^3 water	
CO_2 concentration	3.454E-02	mol/kg water	As simulated by PHREEQC
	3.454E+01	mol/m^3 water	
"A" coefficient	1.66356E-06	$m/\sqrt{s}$	See analytic solution
Time to penetrate length	11458.15355	yr	Calculated time of portlandite depletion based on analytic solution
PHREEQC time step	2	yr	Simulation input
Predicted STEP_NO	5729		Calculated Step No. when portlandite is expected to be depleted
PHREEQC STEP_NO	5727		Actual Step No. when portlandite is depleted in PHREEQC simulation
PHREEQC time	11454	yr	Actual time when portlandite is depleted in PHREEQC simulation
Relative difference	-0.04%		Difference between calculated and observed times for portlandite depletion